Doctoral Thesis

Reversible Cross-links in Polymer Chains

The influence of sacrificial bonds on the mechanical behavior of polymeric system investigated using Monte Carlo simulations

S. Soran Nabavi

November 2014

Montanuniversität Leoben
Institute of Physics

Affidavit

I declare in lieu of oath, that I wrote this thesis and performed the associated research myself, using only literature cited in this volume.

Abstract

Natural materials are a constant source of inspiration for material scientists in manufacturing materials with new and desired mechanical properties. However, this requires a thorough understanding of the structure and the mechanisms that make biological materials achieve their outstanding mechanical properties. One strategy to improve the mechanical performance of natural materials is sacrificial bonding that can be found in bone, wood, and in some softer biological materials like silk, mussel byssus threads and whelk egg capsules. Sacrificial bonds (SBs) are weaker than the covalent bonds that hold the structure together. Thus, upon loading SBs break before the covalent bonds rupture. The rupture of SBs reveals hidden length providing a very efficient energy dissipation significantly toughening the structure. Furthermore, SBs can form and open reversibly. Thus, they can reform after release of the load providing molecular repair and self-healing.

In this thesis Monte Caro simulations are used to examine the role of SBs on the mechanical properties of single polymeric chains and chain bundles. The polymers are modeled as a string of hard spheres that are covalently connected to their two neighbors. Additionally some of the beads are defined as "sticky". These so called "sticky sites" are allowed to form a SB. The SBs are assumed to be a factor of 4 weaker than the covalent bonds. The influence of SB topology and thermal backbone fluctuations on the mechanical behavior of the chains is investigated by computationally mimicking tensile loading tests. It is shown that the topology of the bonds determines the position and spacing of the force peaks due to SBs in the load-displacement curves. The height of these peaks (i.e. the effective strength of SBs) is intimately tied to the magnitude of thermal fluctuations in the chain that are dependent on the effective chain length. This large influence of thermal fluctuations is surprising, because the lowest energy in the system is still a factor 50 larger than $k_B T$. Furthermore, the effect of different density and arrangements of SBs on the work to fracture and dissipating energy is investigated in a (computational) cyclic loading test. The results show that increasing the density of SBs increases the work to fracture as well as the dissipation of energy. The arrangement of SBs has a strong influence on the work to fracture as well as on the strength and apparent stiffness of the single polymeric chain.

The second part of this thesis investigates the role of reversible cross-links on the mechanical properties of a chain-bundle system. The biggest topological difference between a single chain and a chain bundle is the possibility of the cross-links to connect two different chains (i.e. forming an interchain cross-link), while for a single chain naturally only intrachain cross-links can be formed. This bears some surprising consequences, like that only two interchain cross-links (each having the strength of a quarter of a covalent bond) are necessary to provide backbone rupture of the chain. Load-displacement curves are simulated to investigate the influence of grafting density and cross-link density on the mechanical response of the system.

Special emphasis is put on the interplay of inter- and intrachain cross-links. It is shown that the possibility of backbone failure reduces the strength of the bundle but increases the work to elongate the molecule. The results show that the most important factor influencing the ratio of intra- to interchain cross-links is the grafting density (i.e. the distance of the different chains).

These results bear important implications for the understanding of natural systems and for the generation of strong and ductile biomimetic polymers.

Zusammenfassung

In dieser Arbeit wird der Einfluss von reversiblen Querverbindungen auf die mechanischen Eigenschaften polymerer Systeme untersucht. Die Motivation für diese Arbeit findet sich in der Vielzahl von quervernetzten Systemen in biologischen Systemen. Die Natur verwendet solche Querverbindungen, um die mechanischen Eigenschaften von Proteinnetzwerken gezielt zu steuern und einzustellen. Diese Querverbindungen sind schwächer als die kovalenten Bindungen der Hauptkette und brechen daher früher unter Belastung. Dieses frühzeitige Brechen der zusätzlichen Bindungen öffnet Schleifen im Protein, deren Auseinanderziehen Energie sehr effizient dissipiert. Deshalb spricht man im Englischen auch von „Sacrificial Bonds" und „Hidden Length". In der vorliegenden Arbeit wurde ein einfaches Modell entwickelt, um solche Prozesse im Computer nachstellen zu können. In diesem Modell werden Polymere als Ketten von Massenpunkten beschrieben, die über kovalente Bindungen zusammengehalten werden. Weiters wurden manche der Monomere als „klebrig" definiert. Jeweils zwei solcher klebrigen Monomere konnten eine Querverbindung schaffen, die als Sacrificial Bond wirkt. Das Verhalten dieses einfachen Modells wurde mittels Monte Carlo Simulationstechniken untersucht. Zunächst wurde das Verhalten von einzelnen Polymerketten untersucht. Es konnte gezeigt werden, dass die Topologie der Querverbindungen einen großen Einfluss auf die mechanischen Eigenschaften der Kette hat. Überraschenderweise ist auch die zusätzliche Kraft, die durch die Sacrificial Bonds ausgeübt wird, rein entropischen Ursprungs. Das ist vor allem deshalb überraschend, weil die kleinsten Energien im System einen Faktor 50 größer als kT sind und somit eigentlich zu erwarten wäre, dass der Einfluss der Temperatur eher gering ist. In weiterer Folge konnte auch gezeigt werden, dass die Verteilung der klebrigen Monomere einen großen Einfluss auf die Mechanik des Systems hat. Eine regelmäßige Verteilung erhöht die Festigkeit des Systems und eine zufällige Verteilung erniedrigt diese. Weiters konnte durch zyklische Belastungstest gezeigt werden, dass die Systeme Energie dissipieren. Die Menge der dissipierten Energie hängt von der Anzahl der Sacrificial Bonds im System ab. Es konnte auch gezeigt werden, dass die Geschwindigkeit der Entlastung einen großen Einfluss auf die Topologie der wieder geformten Bindungen hat und somit das Verhalten des zweiten Belastungszyklus stark bestimmt. Zusätzlich wurden auch Faserbündel untersucht. Hier können sich Querverbindungen auch zwischen einzelnen Ketten ausbilden. Das überraschendste Resultat in diesen Systemen ist, dass schon zwei Sacrificial Bonds ausreichen, um zu einem Aufbrechen der Hauptkette zu führen. Und das obwohl eine Querverbindung einen Faktor 4 schwächer als die Bindung entlang der Hauptkette ist. Gleichzeitig erhöht sich allerdings die Steifigkeit dieser Systeme beträchtlich.

Contents

1 Motivation

Computational science has become an essential and indispensable branch to solve and analyze complicated problems and complex systems in every sector of science ranging from economic innovation to the natural and engineering sciences. In particular, computer simulations are a reliable and powerful tool to investigate systems of many different scales ranging from the atomic scale to macroscopic and even astronomic scales. Astrophysics, climate and earth system research, fluid dynamics, polymer physics, genomics, condensed and soft matter physics and particle physics are examples where computational approaches play a tremendous role on progressing these fields. One advantage of computational approaches is that the system is known in every detail [1]. This can be especially helpful in interpreting experiments on biological systems that are characterized by a tremendous complexity. Reducing this complexity by developing simple, computationally tractable models of the processes and structures in these systems and testing these models by computer simulations is one strategy in identifying the most important mechanism underlying the biological function. Understanding these mechanisms from a fundamental point of view is of utmost importance to be able to transfer some of the concepts that nature has developed to technology. Of special interest is to understand how natural materials achieve their outstanding performance and which were the demands that gave the biological constraints they were optimized for.

This thesis follows exactly this strategy. Computational tractable models are built to simplify the situation faced when dealing with real experimental systems. The systems studied are motivated by the enormous amount of polymers used as structural load bearing materials in biological and technological applications. The work of this thesis focuses on a very important aspect of these materials: the influence of (reversible) cross-linking of the polymer chains on the mechanical behavior of these systems.

As the name suggests "polymers" can be seen as macromolecules consisting of a long chain composed as a sequence of many repeating "monomers". In the most simple case all these monomers are the same. One example would be Polyethylene, where the monomer is simply one C_2H_4 group. Natural polymers, so called biopolymers, are of course much more complex. Examples include DNA, RNA, cellulose or proteins. The monomers building the latter ones are taken out of an "alphabet" of about twenty different amino acids that are all characterized by different side-groups [2]. It is the subtle interplay of the mutual interaction of the side-groups and of the side-groups with the solvent that are responsible for the enormous diversity of pro-

tein structures. The motivation of this thesis is found in load-bearing proteins like collagen (that is found in e.g. bone or tendon) or the proteins making the byssus of marine mussels. Mostly the mechanical behavior of the polymeric structures is not determined by the properties of the bare protein, but the mechanical properties are carefully tailored to meet specific demands by introducing cross-links in the system. A cross-link is an additional bond that connects two monomers that are not (directly) covalently bonded along the chain. Such cross-links can either be reversible or irreversible, whereas the focus of this thesis lies on reversible cross-links.

This thesis is organized as follows: in the remaining sections of this chapter some examples from biology and technology are introduced to highlight the importance and the fascinating and unexpected properties of cross-linked systems.

The second chapter explains some fundamentals of theoretical polymer science. The concepts of ideal and real chains are introduced. Then existing theoretical approaches from literature are presented to describe permanent and reversible cross-links as well as the effect of cross-link topology.

In the third chapter the method and models used in this thesis are presented. First the bead-spring model as well as the potential functions used to describe the interactions in the polymeric system are explained. Then a short review of the Monte Carlo method is given. Then the simulation procedure is explained in detail. Finally some aspects of the difference of load and displacement controlled experiments are discussed and basic mechanical parameters used to describe the obtained load-displacement curves are introduced.

Chapter 4 presents and discusses the results obtained for a single cross-linked chain, while chapter 5 deals with a system composed of a bundle of chains.

Finally in chapter 6 some concluding remarks and an outlook on how this work could be possibly extended in future work are given.

In the following section, some examples of biological and technological materials containing reversible cross-links are introduced and explained how these cross-links improve the mechanical properties of material.

1.1 Reversible cross-links in biological materials

Although nature uses a very limited number of base elements to built its structures, these structures show an enormous diversity in shape and properties [3]. An effective strategy used by nature to specifically tailor the mechanical properties of load-bearing polymeric structures is to reversibly cross-link the polymers. Different to covalent cross-links these reversible cross-links can open and close reversibly [4]. Such reversible cross-links can be found in a large variety of biological materials such as some hard tissues like wood [5], bone [6, 7], abalone shell [4] and in some softer fibers like silk [8, 9, 10], mussel byssus threads [11, 12, 13, 14], their cuticle

[12] and whelk egg capsules [15, 16]. These bonds are weaker than the covalent bonds that hold the structure and , thus, upon loading break before the backbone ruptures. Because they are reversible, unlike typical covalent cross-links, they can reform during unloading the structure. Consequently after some time the material may recover its initial mechanical performance providing some type of self-healing behavior[17, 18, 19, 20]. Typically such a cross-link constrains a part of the molecule from stretching. The shielded length of this part unravels due to SB rupture and is called "hidden length". The combination of hidden length unraveling and self-repair capability provides a very effective energy dissipation mechanism that increases the toughness of the material dramatically [6, 21]. Because the cross-links rupture "sacrificially" to provide the hidden length, such cross-links are called sacrificial bonds (SBs).

Different kind of bonds are known as sacrificial bonds such as ionic bonds [22], hydrogen bonds [23, 24, 25, 26, 27, 28], hydrophobic interaction [29, 30, 31], Van der Waals interaction [32] and metal-coordination bonds [33]. This large variety of types of SBs results also in a large variety of the strength of individual SBs. The strength can differ from several $100\,meV$ for hydrogen bridges to a value close to the strength of covalent bonds of about few eV for metal coordination bonds [34, 20]. One example of such a strong metal-coordination bond can be found in the histidine-rich domain and in 3,4-dihydroxyphenylalanine (DOPA)-Fe proteins found in the mussel byssus. The strength of these bonds strongly depend on the environmental conditions like the pH value [35, 36, 37, 38, 39] but they are always much stronger than hydrogen bonds.

One of the most important experimental tools in deciphering the secrets of SBs is the Atomic Force Microscope (AFM). The AFM consists of a sharp tip on a cantilever that can be scanned over the surface of a sample. By monitoring the deflection of the cantilever, the loads experienced on the tip can be monitored. Additionally, by tethering single molecules to the tip the AFM can be used to study the unfolding of single molecules and proteins (Figure 1.1.1 shows a sketch of the measuring principle) [40]. One prominent example of such a single molecule stretching experiment using the AFM was to study the unfolding and refolding of globular domains of titin. It could be shown that some domains of this molecules could reversibly unfold. Each unfolding event was seen as a peak in the recorded force-displacement curve. When the structure was unloaded and subsequently reloaded, peaks in the force-displacement curves indicated that some of these domains had refolded [23, 41].

In the following sections, the influence of SBs on the mechanical properties of some biological materials such as abalone shell, bone and the mussel byssus is described. Finally, also the effect of cross-linking in man-made materials is discussed.
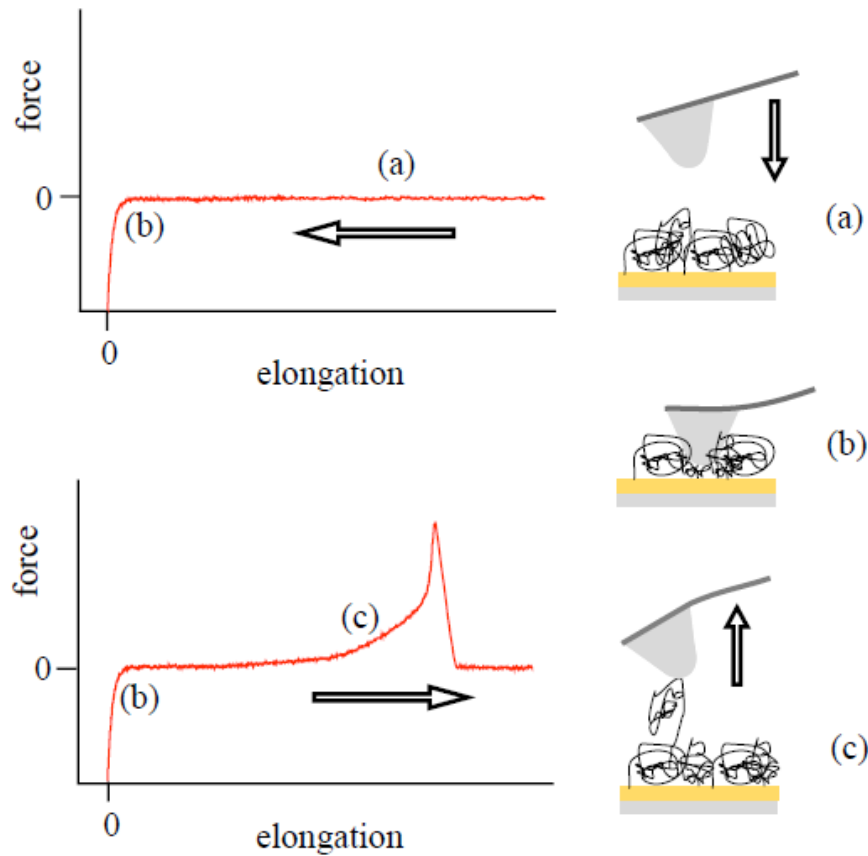
Figure 1.1.1: Atomic force microscopy (AFM) experiment, (a) the cantilever is brought to the surface making a contact between the grafted polymer and the molecule, (b) when the tip is too close to the grafted film, the repulsion force between tip and the surface, bends the cantilever and (c) retraction of the cantilever stretches the molecule. For the three steps, the force and the elongation are recorded (figure taken from [40])

1.1.1 SBs in abalone and bone

Nacre is a composite of the mineral calcium carbonate that is sandwiched between a thin layer of organic material. Due to this special structure the material is approximately 3000 times more fracture resistant than the pure brittle mineral [4]. Cyclic loading tests on nacre done with the AFM produced load-displacement curves showing the characteristic (reversible) saw-tooth patterns of SBs reminiscent of the unfolding of single molecular domains. The strength of these cross-links was found to be in the order of a few hundred piconewton which is lower than the amount of force required to break a single covalent bond. Furthermore, cyclic loading curves revealed an asymmetry between loading and unloading providing a hysteresis loop as a measure of the dissipated energy per cycle [4]. Interestingly, it could be shown that the saw-tooth pattern sustains even for the second and third loading cycle indicating that the bonds can reform.

A similar mechanism could also be found in bone [42, 43]. Bone is a nanocomposite of an organic matrix and hydroxyapatite crystals. The organic matrix mainly consisting of collagen (a triple helical load-bearing protein) contains reversible cross-links as could be shown by cyclic loading test on bone. Using the AFM and nanoindentation techniques it could be shown that the sacrificial bonds in bone protect the polymer backbone and dissipate energy [43]. Experiments with different waiting times between successive loading cycles showed that longer waiting times increased the amount of dissipated energy due to the larger number of reformed SBs. Furthermore, it was shown that indenting the bone surface by $50\,nm$ does not produce any permanent deformation due to the SB reversibility [42]. A sketch of the situation that was motivated by the experimental findings is shown Figure 1.1.2.
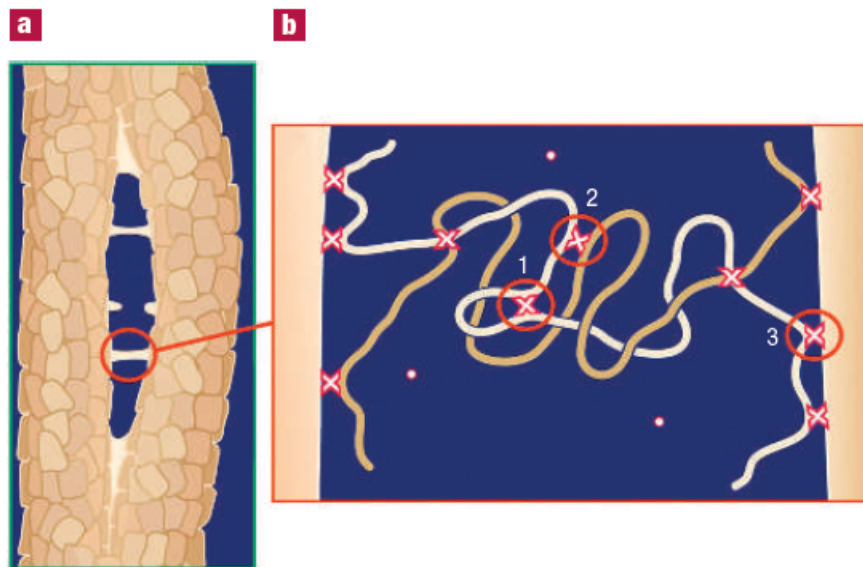
Figure 1.1.2: (A) The organic matrix acts as a glue resisting the separation of the mineralized collagen fibrils,(B) a hypothesized structure of polymers between two mineralized fibril plates containing three types of SBs. The first type of SB is linking two segments from the same polymer (intrachain SB), the second SB is cross-linking two segments of different chains (interchain SB) and the third is a bond between the polymer chains and the surface. The figure is taken with permission from [6].

In this model three possible kinds of SBs have been proposed (see Figure 1.1.2B): (1) The SBs could link two regions of the same polymer i.e. forming intrachain SB, (2) it could cross-link two different polymer chains i.e. forming an interchain SB and (3) the SB may form between the polymer chain and the mineralized plate. In this thesis SBs of the first and second kind will be investigated [33]. Using a simple model based on the worm-like chain model it could be shown that the SBs increase the stiffness as well as the fracture toughness of these systems [33].

1.1.2 Mussel byssus threads

The mussel byssus is produced by marine mussels to adhere to rocky substrates. Not only that the byssus has to stick in wet environments, it also sustains strains up to 100 % without breaking and after release of the load, it recovers its original mechanical properties. The mussel byssus combines a high strength with a large extensibility. In Figure 1.1.3(A) the strength of these threads is indicated by showing that only three threads can hold three mussels and a piece of mica [44]. Byssus threads consist of two parts with different morphological and mechanical properties: the proximal (closer to the organism) and the distal part (closer to the substrate connected to surface by plaque). One of the main functions of the proximal part is decelerating the mussel speed in a very short time to balance the large accelerations the mussel experiences by high speed detachment from or collisions with rocks [45, 46, 47].

In [11] the distal part of the byssus was investigated, showing that its low-strain behavior was similar to tendon, but that the ultimate strain it can bear was up to 100% compared to only 10 % to 15 % for tendon. The distal part consists of collagen-like domains, flanking domains and histidine rich end-domains [48, 49]. The collagen-like domains are triple helical, stiff motifs. The flanking domains surrounding the collagen-like domains resemble load-bearing motifs in e.g. silk-dragline. The histidine rich end-domains are known to coordinate with metal ions and are able to cross-link reversibly shown as is in Figure 1.1.3(C). It is these end-domains that include metal-coordination bonds as SBs and that the model investigated in this thesis is based on.

Figure 1.1.3(D) shows a typical stress-strain curve of the distal region of a byssal thread [11]. For low strains ($< 15\%$) the distal thread behaves elastically. For intermediate strains (15 to 45 %) the thread shows a pronounced yield behavior, where no increase in stress can be observed. For larger strains, stress rises significantly (post-yield stiffening) and the thread fails catastrophically for strains larger than 100 %. An interesting behavior could be observed for cyclic loading with different waiting times between successive loading cycles (see Figure 1.1.3E). While there is a large deterioration of mechanical properties when there is no waiting time between the first and second cycle, the mechanical properties recover when there is a 1 h lag between different loading cycles (see Figure 1.1.3E). During unloading, the cross-links need some time to find their partners and to reform. Therefore, if the second stretching is immediately started after unloading, the energy dissipation (i.e. the area of the hysteresis loop) as well as the stiffness of the material are strongly reduced. Nevertheless, for longer waiting times the SBs reform and the system recovers its initial mechanical properties [17]. Furthermore, it was shown that the recovery process is thermally induced, i.e. recovery is faster at elevated temperatures [11].

Using in-situ x-ray diffraction further evidence of the validity of the concept of "hidden length" could be found. It could be shown that the collagen-like domains

stretched not more than 2 %, even when the thread strain was as high as 70 % [11]. These results motivate the following model (see also Figure 1.1.3C): Some part of the molecule has to provide hidden length to the system that allow for large thread strains, while the corresponding strain in the collagen-like domains remains small. The best candidate are the histidine-rich end-domains that allow to form reversible SB cross-linking. These SBs start opening at intermediate strains allowing for unfolding of the polymer chain and providing hidden length for efficient energy dissipation. After release of the load and upon re-folding of the polymer chain these bonds can close reversibly [11]. As indicated by the temperature dependence of the refolding this process is thermally activated where increasing temperature from $4\,°C$ to $37\,°C$ associates the faster recovery of mechanical performance [11].

1.1.3 The byssal thread cuticle

The extensible byssal threads are covered with a hard coating providing wear resistance when they are in contact with hard rocks during the natural occurring tides. This proteinous cover has remarkable mechanical properties combining high hardness ($100 - 150\,MPa$ which is almost five times harder than the thread core) and extensibility (70 % strain) [50]. The cuticle contains granules which are rich in DOPA and inorganic ions like Fe forming metal-coordination bonds and a surrounding matrix with a lower amount of cross-links [51]. The mechanical properties of different mussels strongly depend on the structure of the granules i.e. their diameter, their volume fraction and their homogeneity [50, 52]. In this structure the densely cross-linked granules provide the high hardness, while the less densely cross-linked matrix is responsible for the large extensibility [12]. Nanoindentation experiments confirmed the importance of the metals (Ca and Fe) for the integrity of the structure. Removal of the metal ions resulted in a 50 % reduction of the hardness as well as in disrupting the cuticle [51].

1.2 Cross-links in man-made materials

Reversible and irreversible (covalent) cross-linking are also used in polymer science to create materials with unique mechanical properties. The most famous example is probably the vulcanization process invented by Charles Goodyear in 1839 to make natural rubber harder and more durable. In this process rubber is (permanently) cross-linked with sulfur bridges. The vulcanization process is introducing permanent cross-links in the system that result in hard material, but make the material also very difficult to recycle by devulcanization [53].

More recent examples of covalent cross-linking are found in double network gels. In these materials the aim is to manufacture materials having a high water content and high mechanical strength and toughness at the same time. Typically these gels

consist of two types of polymers with opposing physical properties; a rigid network containing a large number of covalent cross-links and a ductile part including few cross-links. This combination is similar to bone and dentin containing organic-inorganic composites where the organic part is usually very soft and the inorganic part is very brittle [54, 6]. During tensile loading of the double networks, first the rigid part ruptures serving as some kind of sacrificial bond at a relatively low strain, while the soft network effectively acts as the hidden length making the material tougher [54, 55]. In these hydrogels, non-reversible cross-links have been used, they show negligible self-recovery and fatigue resistance regarding.

Most recent approaches try replacing the brittle network of covalent bonds with a material composed of physical reversible bonds making a "super tough". Upon cyclic loading, the internal reversible bonds break and reform and thus, they serve as reversible sacrificial bonds [56, 57, 31]. Cyclic loading experiments of such structures showed that these materials show a large dissipation of energy as well as a recovery of their initial mechanical properties [58, 59, 55].
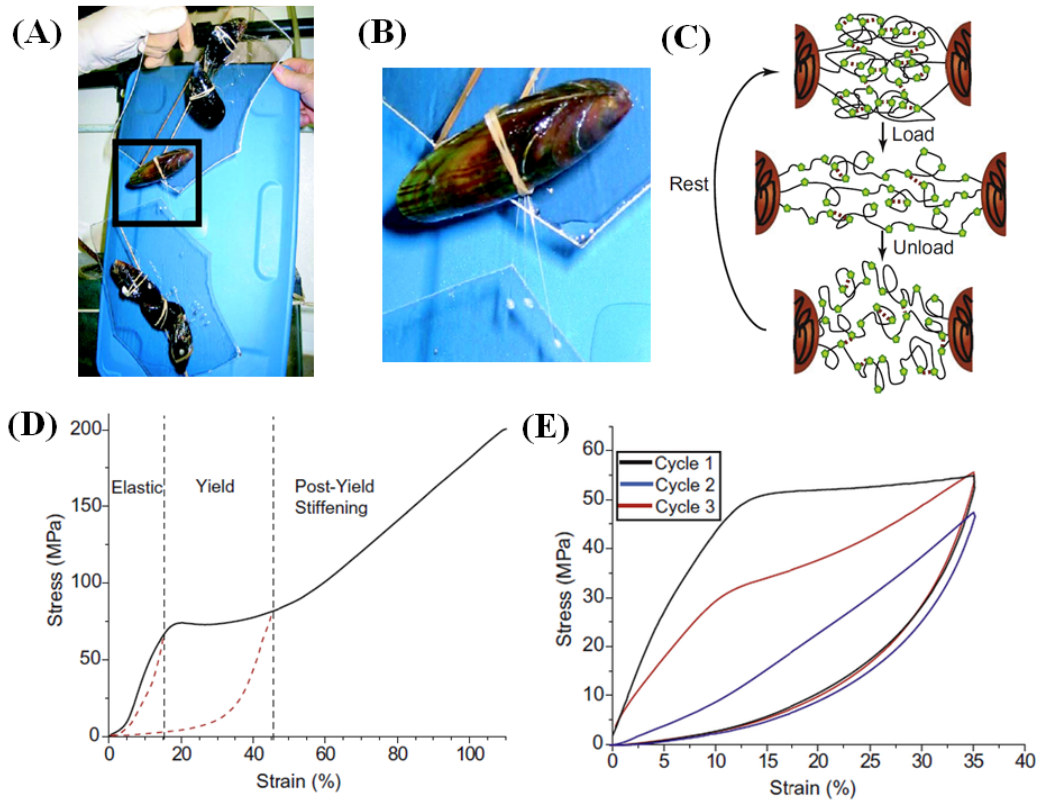
Figure 1.1.3: (A) shows one mussel holding three other mussels plus a piece of mica (B) enlargement of the square area in (A) showing the mussel holds the others with only three threads indicating the high strength of the threads [44] (C) shows a sketch of the histidine rich end-domains that are able to coordinate with metal ions and to form reversible cross-links. Green pentagons indicate so called sticky sites that may form a cross-link. Upon stretching these sacrificial bonds open revealing hidden length. When the load is released the domain returns to its initial length and after some time due to thermal fluctuations the sacrificial bonds may reform. (D) An experimental stress-strain curve of a byssus thread in tension. The deformation behavior can be divided into three distinct regimes. First, an elastic, tendon like behavior for strains up to 15 %. Then a pronounced yield regime where the strain increases at constant load (15 to 45 % of strain). Lastly the regime of post-yield stiffening, where the stress increases again until thread ruptures. (E) Cyclic loading of such a thread with different waiting times between different cycles (cycle 1: first loading, cycle 2: no waiting time and cycle 3: one hour waiting time) shows partial recovery of the initial stiffness and energy dissipation of the thread for longer waiting times (Figure reproduced from [44, 11]).

2 Fundamentals

The systems this thesis deals with are polymeric in nature. To put the models used in this thesis into the context of existing concepts used in polymer science this chapter introduces very shortly basic concepts of polymer science. All shown results of this chapter are used from the standard textbooks such as [60, 61, 62] otherwise it will have the corresponding reference.

A polymer is a macromolecule that is made of several repeating units called monomers. These monomers are connected via covalent bonds providing the backbone of the structure. Polymers are heavily used in technology like Polyethylen and also in nature (DNA, RNA, proteins, cellulose). Polymers exist in a broad range of configurations and show a remarkable variety of properties. Their characteristics are related to their degree of polymerization (the number of monomers), the polymer architecture, the location of the monomer in the polymer (polymer configuration) and the spatial location of the monomers (polymer conformation). Different connections between the polymer segments provide different architectures of the polymers such as linear, ring, star, H, comb, ladder dendrimer and randomly branched polymers [60] (see Figure 2.0.1).
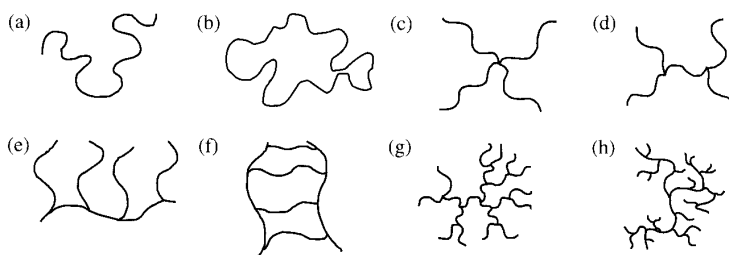
Figure 2.0.1: Examples of different polymer architectures; (a) linear, (b) ring, (c) star, (d) H, (e) comb, (f) ladder, (g) dendrimer which is a repeatedly branched molecule and (h) randomly branched (Figure taken from [60]).

In addition to the bonds in the backbone that hold the structure together, many polymers may also form a bond between non-neighboring monomers or segments. These bond can be formed between two segments of one polymer chain or two different polymer chains. Though not as strong as the backbone, these *"cross-links"* have important effects on the polymer characteristics. One famous example is the sol-gel transition.

Upon adding cross-links to the system first branched polymers form and the polymer remains soluble, which is known as the sol stage. Increasing the number of cross-links leads to the formation of clusters that increase their size upon further increase in the cross-link density. Eventually at a certain point, the structure changes and the polymer chains link to each other at multi points such that the whole system acts as a big covalently bonded molecule known as the gel stage [63].

In this chapter, some basic theoretical physical models available to describe polymeric system will be discussed. Essentially these models can be classified in two different groups: mesoscopic models where the single monomers are averaged out and the polymer is described as a continuous contour and microscopic models that keep the monomer as the basic unit of the polymer.

2.1 Theoretical approaches to describe polymers

As already discussed in the introduction, a polymer is a macromolecule made of a sequence of many repeating units, the monomers. When the monomers are effectively averaged out the polymer may be described as a continuous contour, whose behavior is determined by a bending rigidity. The standard model in this framework is the worm like chain model of a stretched chain described by the following hamiltonian,

$$H = H_{bending} + H_{external} = \frac{\kappa}{2} \int_0^{L_C} (\frac{d^2\vec{r}(s)}{ds^2})^2 ds - F \int_0^{L_C} \frac{dz}{ds} ds$$

where the first term describes the resistance of the chain to bending which is proportional to the inverse square of curvature of the of the continuous chain. Here κ denotes the bending rigidity. The second term is the stretching energy of an external force on the chain [64, 65, 66].

$\vec{r}_S$ is the position vector along the chain at point s, F the puling force along z direction and L_C the effective contour length. One essential parameter in describing the WLC is the so called persistence length L_P. The persistence length is a measure over which length orientational correlations decay. For a chain with constant bond-length between the monomers, it is found via

$$L_P = l \sum_{i=1}^{n} \sum_{j=1}^{n} \cos \theta_{ij} \tag{2.1.1}$$

where θ_{ij} shows the angle between bond vectors $\vec{r_i}$ and $\vec{r_j}$ in the chain with n bonds. It can be shown that the bending rigidity and the persistence length are related via $Lp = 2\kappa/k_B T$ [64]. Thus, the WLC model as formulated above includes the limit

of rigid rods for $L_C \ll L_P$, the limit of flexible chains for $L_C \gg L_P$ and the very important subclass of semiflexible polymers for $L_P \approx L_C$ [60].

Using the theoretical framework of the WLC model in [67] a formula for the force as a function of elongation was derived. The force on the chain upon stretching is

$$F = \frac{k_B T}{L_P} \left[\frac{L}{L_C} + \frac{1}{4} \frac{1}{(1 - L/L_C)^2} - \frac{1}{4} \right] \tag{2.1.2}$$

Equation 2.1.2 is heavily used to derive the persistence length by fitting this expression to experimentally derived load-displacement curves [65].

The total energy of a polymer chain can be divided in to covalent and non-covalent contributions

$$E_{tot} = E_{covalent} + E_{non-covalent} \tag{2.1.3}$$

The covalent term is the energy contribution due to the backbone bonds of covalently linked neighbors. In general this covalent interaction is split into a sum of bond stretching, bending and torsion terms [68]. The non-covalent bonds are between non-neighboring particles. Among others non-covalent interactions include van der Waals, electrostatic and excluded volume interactions.

$$E_{covalent} = E_{Stretching} + E_{bending} + E_{torsion}$$
$$E_{non-covalent} = E_{van\,der\,Waals} + E_{electrostatic} + E_{excluded-V} \tag{2.1.4}$$

In the following two important groups of models will be shortly introduced that are widely used in describing polymeric configurations. Ideal chain models take only the covalent interactions into account and totally neglect the non-covalent interactions. One famous example of such a model is the WLC model mentioned above. There the only interaction is due to local bending of the contour. The second group are the real chain models. Here covalent as well as non-covalent interactions are considered. Excluded volume interactions effectively forbid self intersections of the chain, while van der Waals and coulombic interactions also allow to describe the interaction of monomers with the solvent as well as mutual interactions of the different side groups [60].

2.1.1 Ideal chains

The ideal chain model is based on two assumptions; first, the monomers which occupy no space i.e. the volume is zero (which essentially means to neglect excluded

volume interactions), and second, there is no long interaction between the monomers i.e. if the monomers are not covalently bound neighbors, then they do not interact at all, $E_{non-covalent} = 0$ [60]. Suppose now a linear chain with N similar monomers ($n = N - 1$ bonds) where atom $i - 1$ is connected to atom i by a bond vector $\vec{r_i}$ as shown in Figure 2.1.1.
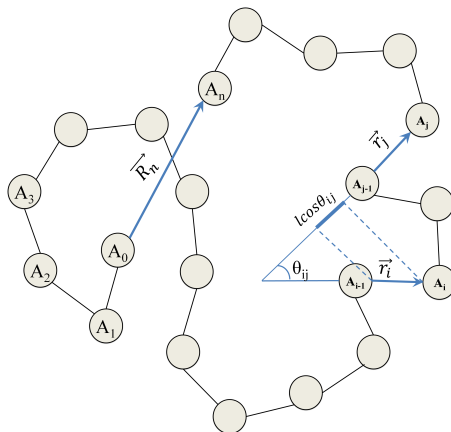
Figure 2.1.1: Typical conformation of a flexible chain: A_i denotes the i-th monomer in the chain. θ_{ij} shows the angle between bond vectors $\vec{r_i}$ and $\vec{r_j}$ and $\vec{R_n}$ indicates the end-to-end vector (figure is reproduced from [60]).

Since there is no preferred direction, the average end-to-end vector $\vec{R_n}$ of the chain is zero; $< \vec{R_n} >= 0$. The simplest non-zero average is the mean square of the end-to-end distance;

$$< R^2 >= \left\langle \left(\sum_{i=1}^{n} \vec{r_i} \right) . \left(\sum_{j=1}^{n} \vec{r_j} \right) \right\rangle = \sum_{i=1}^{n}\sum_{j=1}^{n} \langle \vec{r_i}.\vec{r_j} \rangle \qquad (2.1.5)$$

If all bond vectors are of similar length l, then we can write (see Figure 2.1.1).

$$< R^2 >= l^2 \sum_{i=1}^{n}\sum_{j=1}^{n} \langle \cos \theta_{ij} \rangle \qquad (2.1.6)$$

with θ_{ij} the angle between the bonds $\vec{r_i}$ and $\vec{r_j}$.

One of the most simple models for ideal chains is the *"freely jointed chain model"* where all bonds are identical and there is no correlation between the direction of different bond vectors. In other words $E_{bending} = E_{torsion} = 0$ and all bond-lengths are constrained to their equilibrium length l. Thus we find for the mean square of the end-to-end distance of the freely jointed chain

$$\begin{aligned} &< cos\theta_{ij} >= 0 \quad if : i \neq j \\ &< cos\theta_{ij} >= 1 \quad if : i = j \end{aligned} \implies < R^2 >= nl^2 \qquad (2.1.7)$$

This theoretical framework is completely analogous the concept of a random walk. Thus, one of the simplest models for a polymer is a random walk or self avoiding walk on a lattice [62, 69]. By modeling the interaction of monomers by assigning nearest neighbor energies this model can be refined to (also) describe the sol-gel transition [70].

One generalization of the freely jointed chain model is the freely rotating chain. Here bond lengths and bond angles are fixed, but all torsional angles are equally probable and independent from each other.

The *worm like chain model* (some times called Katky-Porod model) which has been discussed at the beginning of this chapter can be seen as a special case of the freely rotating chain model for very small bond angles and is usually used for very stiff chains.

Finally, the hindered rotation model also includes the description of torsional angles in the model. Here the bond length and angles are fixed and the torsion potential is restricting the torsional angle to the configurations corresponding to the trans and gauche states [60].

2.1.2 Real chains

In contrast to ideal chain models, real chain models also contain non-covalent interactions ($E_{non-covalent} \neq 0$). The additional short and long-range interactions between the monomers and the monomers and the solvent largely influence the conformation of the polymer. The conformation of the polymer mainly depends on three characteristics; the flexibility of the chain, the interactions between the monomers in the chain and the interactions between the monomer and the environment (especially the solvent) [60].

The effective interaction between monomers depends on the difference between the monomer-monomer interaction and the interaction between the monomers with the surroundings [60]. An attractive effective interaction means that the monomer-monomer energy is lower than the corresponding monomer-solvent interaction energy. As a consequence the monomers would rather be near each other than to expose themselves to the solvent leading to a rather condensed structure. In contrast, effective repulsive interactions mean that the monomers prefer to interact with the surrounding molecules rather than the other monomers resulting in rather open structures. The required energy to bring two monomers from ∞ to a distance r is characterized by first an attractive interaction for large distances and a very strong repulsive interaction for shorter distances. The reason for this strong repulsive interaction is the beginning overlap of two monomers is the beginning overlap of two monomers i.e. the steric repulsion of overlapping monomers the so called excluded volume interaction. For the system with hard spheres, the excluded volume interaction is 8 times larger than the volume of the monomer. This interaction plays a very important role for an isolated chain and has a large influence on the long-range

structure of the chain because it essentially forbids self-intersection of the chain [71]. Moreover if the monomers are identical to the solvent and there is no energy difference between monomer-monomer and monomer-solvent interaction, then the energy contains only the steric repulsion and the solvent is known as athermal.

Real chains models show a collapse of the chain due to the large attraction compared to the repulsion, for low temperatures while for high temperatures, the repulsion between the monomers overcomes the attraction and the chains swell. At a special intermediate temperature the so called "θ-temperature", the repulsive and attractive interactions between the monomers exactly cancel and the chain behaves nearly like an ideal chain [60].

Another interaction strongly influencing the conformation of polymers are additional bonds between monomers that are not directly covalently linked. These cross-links can be either very strong bonds similar to the covalent bond of the backbone acting as permanent cross-links or weaker, reversible physical bonds like ionic , Van der Waals or hydrogen bonds.

2.2 Permanent cross-links

In this part theoretical approaches are presented to describe polymers containing permanent cross-links modeled as stable covalent bonds that are not allowed to break. Thus, there will be no bond rupture and the main influence of the cross-links is on the structure of the polymer network.

The topology and density of permanent cross-links determine the polymer configurations [72]. For instance, suppose a network containing a number of semiflexible chains that are randomly distributed. Adding random permanent cross-links changes the alignment and direction of the segments and fix their orientation of with respect to the other polymer chains. When the density of cross-links increases a fluid-gel transition may occur and since the cross-links are randomly distributed in the network, the small regions containing high density of cross-links get localized at the random positions. The random distribution of the localized regions together with the similar orientation of the chains result in an isotropic to nematic phase transition for stiff enough polymers. As the stiffness of the polymer decreases, the transition shifts to higher cross-link densities and results in an amorphous structure with randomly frozen chains [72].

Furthermore, it could be shown that if the polymer chains are grafted between two planes with the ending points free to slide along the planes, then the localization length is larger for regions close to the boundaries where the polymers are free to move. As a consequence, the gelation transition upon increasing the cross-link density provides also an in-plane shear modulus of the system [73]. The force-extension curve for parallel-stretched polymer chains with permanent random cross-links shows that the contribution of the cross-links is inversely proportional to the force. This is

because a higher number of cross-links increases the differential stretching stiffness of the network by reducing thermal fluctuations [66, 74]. It has also been shown that the reduction of thermal fluctuations is because a single cross-link between two chains grafted onto a rigid planar surface reduces the fluctuations of the free endings of the chains i.e. reducing the number of allowed configurations [75].

2.3 Reversible cross-links

This section introduces some theoretical approaches to study the influence of reversible cross-links on the mechanical properties of polymeric chains. In particular these approaches are based on the SB model to describe deformations in bone proposed by Fantner et. al. [6]. In this model the polymers are described in the framework of the WLC model and the polymers between two mineralized fibril plates may form three different types of SBs as shown in Figure 1.1.2. These are, first, intrachain SB (the cross-link is between two particles located at the same polymer chain), second, interchain SB (the cross-link is between two particles located at two different polymer chains) and, third, the SB may form between the polymer chain and the plate. The topology of intrachain cross-links strongly influences the entropy contributions of the chain [76, 77]. Three different cross-link configurations may form: the independent, pseudoknotted and nested structure [77, 78]. These three different topologies will be discussed in detail in chapter 4.

A numerical analysis of the model presented by Fantner et al. shows that the topologies of SBs and the SB strength provide different mechanical properties. It can also be shown that for a constant contour length there is an optimal number of cross-links, while for a higher number of cross-links no further benefit on the toughness can be gained and the force-extension curves become indistinguishable from each other [79].

In order to have a higher mechanical performance of the system with three types of SB having different strengths, SB cross-link between the polymer chain and the plates should be strongest (type 3 in Figure 1.1.2(B)). Upon loading, the weaker SBs rupture earlier and then the SBs with higher strength start to rupture. Thus, the force extension curve shows a stepwise decrease of the experienced load [79] due to breaking of connected segments of polymer from the plates (see Figure 2.3.1A and B). Experimental results showed that the supported force by a fibril is in the order of a few micronewton while the strength of a single polymer chain is in the order of a few hundred piconewton. Therefore it is necessary to have more than thousand polymer chains to sustain the force [79]. Elbanna et. al. performed an analytical calculation for multiple chains up to $N = 200$. The results for the system with 200 chains showed that increasing the number of chains in the system increases the toughness as well as the stiffness of the system significantly as can be seen in Figure 2.3.1(B). The results for 200 polymer chains is in good qualitative agreement with the experimental results in terms of the shape of the load-displacement curve
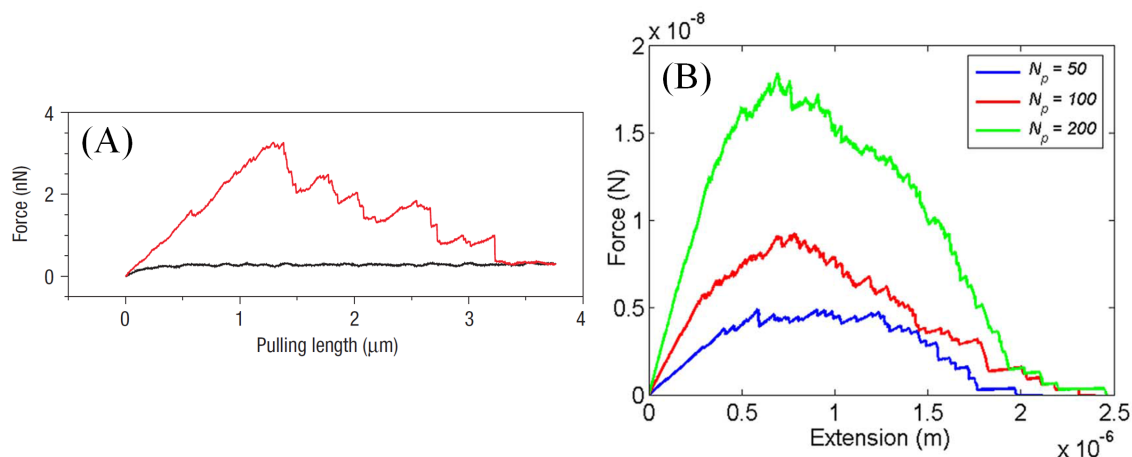
Figure 2.3.1: (A) Experimental curve of pulling a dentin molecule with the AFM where all filaments are broken [6]. (B) The analytical results of force-extension curve for a different number of chains using the model presented in [79]. The small force drops show the sacrificial bond rupture while the larger force drops indicate the detachment of the polymer from the plate. The figures are reproduced with permission from [6, 79].

as shown in Figure 2.3.1(A). In particular, increasing the number of polymers does not influence the maximum displacement. In the force-extension curve two different regions can be observed (see Figure 2.3.1(B)). First, for small extensions the force increases resisting against crack initiation and second for larger extensions the force decreases stepwise due to detachments of SBs from the plates [79]. The analytical results of the kinetic model show that the height of the peaks depends on the pulling rate where increasing the stretching rate increases the height of the peaks. After each stretching cycle when all end bonds have ruptured, the time till the next stretching has considerable impact on the mechanical response since increasing the time delay increases the amount of work to fracture [80].

2.4 Cross-links topology

The topology of cross-links in single polymer chain is a key factor determining the influence of these cross-links on the stability and mechanical properties of the chain [77]. If cross-links form a loop such that the applied force is distributed over all the cross-links, then the strength of the chains is directly related to the number of cross-links [81]. Figure 2.4.1 shows such configurations maximizing the strength for a chain with 51 beads and a different number of cross-links along the chain. The numbers shown in Figure 2.4.1(A) are the number of the bead along the chain, e.g. for the chain with two cross-links, the two cross-links are formed between beads $(22, 47)$ and $(23, 48)$. When the chain is stretched, a shear force acts on the two cross-links simultaneously, such that both cross-links experience a similar amount of

force. Finally the two cross-links break. The required force to break the cross-links gets larger by increasing the number of cross-links in this configuration. As a further consequence, the amount of work to fracture for the chain increases, considerably(see Figure 2.4.1(B)).
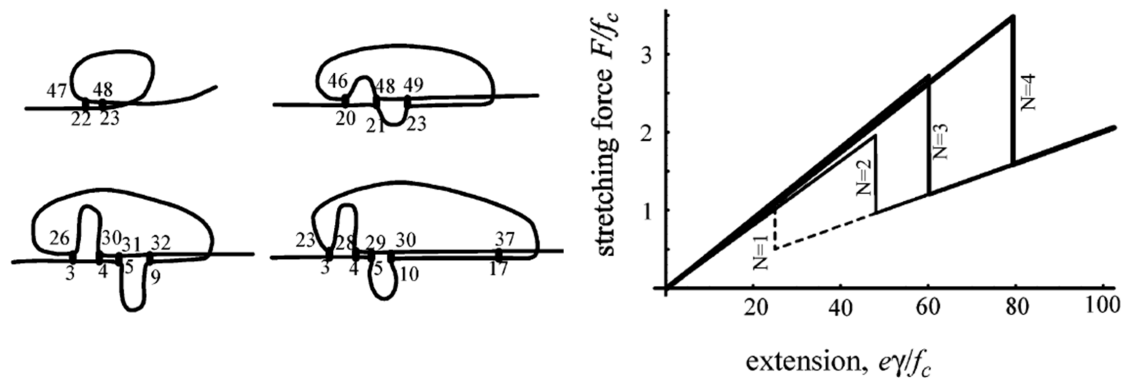
Figure 2.4.1: The optimum polymer configuration to make a strong material. For a different number of cross-links (A) shows the cross-links configuration along the chain with 2 to 5 cross-links. The shown number denote the position of the bead along the chain e.g. for the chain with two cross-links the beads $(22, 47)$ and $(23, 48)$ form a loop. (B) shows the corresponding force-extension curves. The force is measured in units of f_c i.e. the critical force to rupture one cross-link and the extension in units of f_c/γ where γ is the effective force constant (Figure taken from [81]).

Comparing the results for the chain with a cross-link topology that is maximizing strength (shown in Figure 2.4.1(A)) and a random topology of four cross-links shows that the work done on the chain in the first configuration is five times larger than for a chain with random cross-link configuration [81, 82]. In biological materials, a configuration of cross-links maximizing strength can be found e.g. in in the muscle protein titin that is making parallel β sheets providing a material with a high mechanical performance [83].

3 Method and Models

In this chapter the model investigated throughout this thesis is presented. This model is motivated by the experimental results obtained in [11]. The model was built to describe a situation as shown in Figure 1.1.3C to study the influence of reversible cross-linking on the mechanical properties of the polymeric chains. Then the Monte Carlo method is shortly introduced and the simulation procedure is explained in detail. Finally, some basic mechanical parameters are described that are used throughout this thesis to characterize the mechanical behavior of the investigated structures. These include displacement (strain), load (stress), stiffness, strength, work to fracture and dissipated energy.

3.1 The model

The model consists of a (linear) polymeric chain modeled as a covalently linked chain of N hard spheres with diameter R (to avoid self-intersecting phantom chains) oriented along the Z-axis. In the following the hard sphere radius will serve as the unit of length. The covalent binding energy between neighboring beads is described by a Morse potential since this potential is known to provide an accurate description of covalent bonds (see Figure 3.1.1B). All (inner) beads are covalently linked to their two neighbors (bead $i - 1$ and $i + 1$) and are allowed to move freely during the simulation, while the first and the last bead ($i = 0$ and $i = N - 1$, respectively) have only one neighbor and are held fixed. Thus, the excluded volume and covalent interactions between two beads i and j separated a distance r can be described via

$$E_{ij}(r) = \begin{cases} \infty & r \leq 2R \\ E_0[(1 - e^{-\beta(r-r_0)})^2 - 1] & r > 2R \quad \text{and} \ |i - j| = 1 \\ 0 & \text{else} \end{cases} \qquad (3.1.1)$$

where E_0 is the depth of the energy minimum and about 5eV for a covalent bond, $\beta^{-1} = 0.5 \ R$, is a measure for the width of the potential that is set to 2 in the simulations (i.e. the width of the potential is given by half of the hard sphere radius). $r_0 = 3 \ R$ is the equilibrium distance of a covalent bond (i.e. the position of the energy minimum) in the following. Consequently, the contour length of the
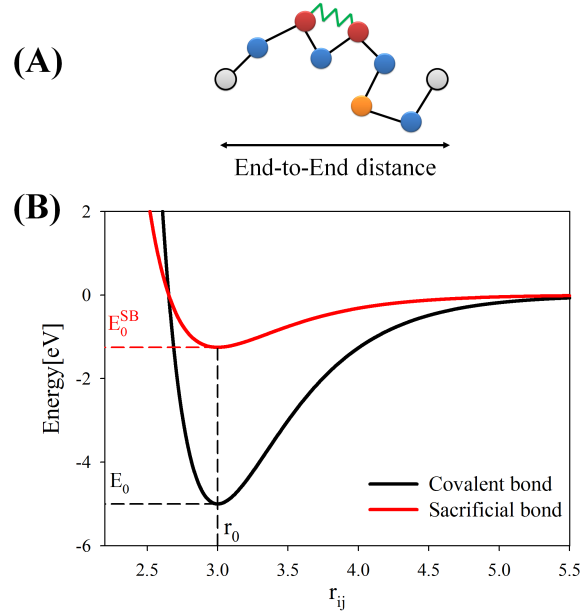
Figure 3.1.1: (A) Sketch of the used model. Gray beads denote the two fixed outer beads defining the end-to-end distance, non-sticky sites are shown in blue and sticky sites in orange, respectively. Covalent bonds are indicated by black bars, while a closed SB is shown by the green zig-zag line. (B) The Morse potential as a function of the distance between two beads. The equilibrium distance r_0 and the binding energy E_0 for covalent bonds and $E_0(SB)$ for sacrificial bonds are also shown. The Morse potential is used to describe the covalent bonds between neighboring beads and (with a reduced value of the binding energy) the energetics of sacrificial bonds.

chain is given by $L_C = (N-1)r_0$. In the framework of presented models, our model contains only covalent bonds with the excluded volume interaction.

To mimic the effect of SBs some of the monomers are defined as "sticky". It is these sticky sites that can additionally form SBs (see Figure 3.1.1(A). In the model, SBs can be only between two sticky sites and are allowed to open and close reversibly. $\rho_s = N_s/N$ is defined as the sticky site density with N_s the number of sticky sites in the chain. The energetics of the SBs are not well characterized. The experimental results available indicate that the strength of the His-rich domains as well as the dopa-Fe complex are 20 to 30 % of the strength of a covalent bond [33, 13]. To keep the model as simple as possible in the simulations, the energetics of SBs are chosen to follow an identical Morse potential as the covalent bonds with a strength reduced by a factor of 4 (i.e. $E_0^{SB} = 0.25 E_0$).

The chain-bundle system is made of nine chains each consisting of $N = 50$ beads (the total number of beads in the system is 450). At both sides the end beads of the chain are permanently grafted to a substrate, described as two hard walls impenetrable for the beads at $z = 0$ and $z = L$, respectively. The end-beads are arranged to occupy a triangular lattice with lattice constant d that essentially defines

the grafting density of the system (see Figure 3.1.2). Also in this system some of the monomers are defined as sticky. Always two of these sticky sites may form a SB that can now either link two segments of the same chain providing an *"intrachain"* cross-link or connect two segments of different chains making an *"interchain"* cross-link as is shown in Figure 3.1.2B.
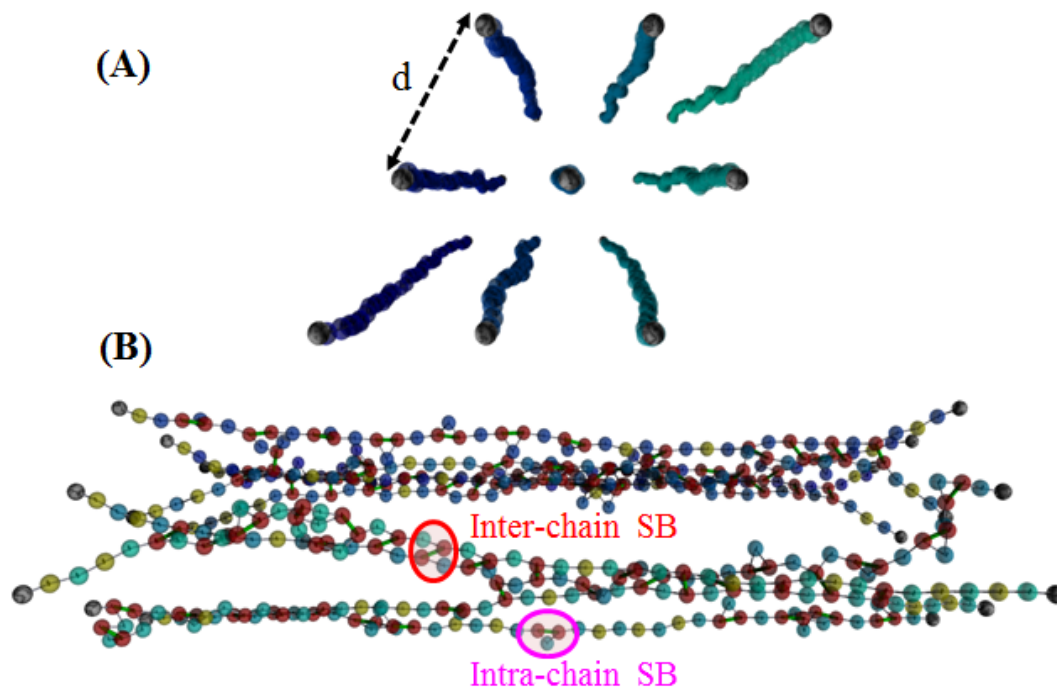
Figure 3.1.2: (A) Top view of the chain-bundle system in the stretched configuration, i.e. the end-to-end distance of the chains is equal the contour length. The end beads of the chains are permanently grafted to a hard substrate. d denotes the distance between the grafting points that are arranged as a triangular lattice. (B) Side view of the same system for a smaller end-to-end distance. Yellow beads indicate open sticky sites, red beads denote closed sticky sites. One interchain and one intrachain SB is shown.

3.2 The Monte Carlo method

Monte Carlo (MC) and molecular dynamics (MD) methods are tools from statistical mechanics to investigate systems with many degrees of freedom. They are used, when it is not possible to calculate the partition sum of a system analytically. The basic concept of MD is to calculate a time average of the investigated system by direct integration of Newton's equation of motion, while MC simulations apply special algorithms (in our case the Metropolis algorithm) to create a successive number of states of the investigated system (a so called Markov chain) where the single states

arising follow the equilibrium Boltzmann distribution (i.e. MC uses the concept of an ensemble average). Thus, in a MC simulation calculating the mean of some observable A reduces to

$$< A >= \int A e^{-E/k_B T} dr / Z = \frac{1}{N} \sum A_i \qquad (3.2.1)$$

where the A_i are the actual values of the observable A in configuration i. Since the configurations arise with their proper Boltzmann weight, no further weighting of the observables has to be performed.

Producing a Markov chain consists of two main steps: First, starting from the current state of the system o (for old state) choose a new state n by some small displacement δ [61]. Second, decide if the new state is accepted or rejected. There are several different algorithms resulting in the correct equilibrium configuration, but all of them have to fulfill the detailed balance condition ensuring that once the equilibrium distribution has been reached, further application of the algorithm has to keep this distribution. This means that in equilibrium the average number of moves out of any given state o, has to be exactly canceled by the number of moves in the state o from all other states. Detailed balance demands an even stronger condition: The number of moves from a configuration o to the new configuration n has to be exactly canceled, by moves from the configuration n to the configuration o, i.e.

$$N(o)p(o \rightarrow n) = N(n)p(n \rightarrow o)$$

with $N(o)$ $(N(n))$ the number of systems being in state o $(n$, respectively) which is given by the Boltzmann distribution and $p(o \rightarrow n)$ $(p(n \rightarrow o))$ the probability of going from state o to n $(n$ to o, respectively). The probability $p(o \rightarrow n)$ is given by

$$\alpha(o \rightarrow n) \times acc(o \rightarrow n)$$

where the α denotes the probability of choosing state n when starting from state o and $acc()$ denotes the probability of acceptance of the new state n. The Metropolis method is a special algorithm fulfilling detailed balance by choosing α symmetric, i.e. $\alpha(o \rightarrow n) = \alpha(n \rightarrow o)$, and the probability to accept the new state by

$$acc(o \rightarrow n) = min(exp \left[-(E(n) - E(o))/k_B T \right], 1) \qquad (3.2.2)$$

with $E(o)$ $(E(n))$ the energy of the old (new) configuration.

Thus, a simulation step consists of: first, choose a new position. Second, determine the energy of the current and the new configuration and calculate $acc(o \rightarrow n)$. Third, draw a random number equally distributed between zero and one. If the number is smaller than $acc(o \rightarrow n)$ then the new position is accepted, otherwise it is rejected [84, 85, 86].

3.3 Simulation procedure

There are two basic moves in the simulations: moving the beads and updating the SBs. Both steps are executed by following a Metropolis algorithm that was introduced in the preceding section. Figure 3.3.1 shows a flowchart of the program that will be explained in more detail in the following. First a random number is chosen to decide if one bead is going to be moved or the SBs updated. The numbers are chosen such that on average each time step in the simulation consists of N tries to move the beads and N_s tries to update the SBs.
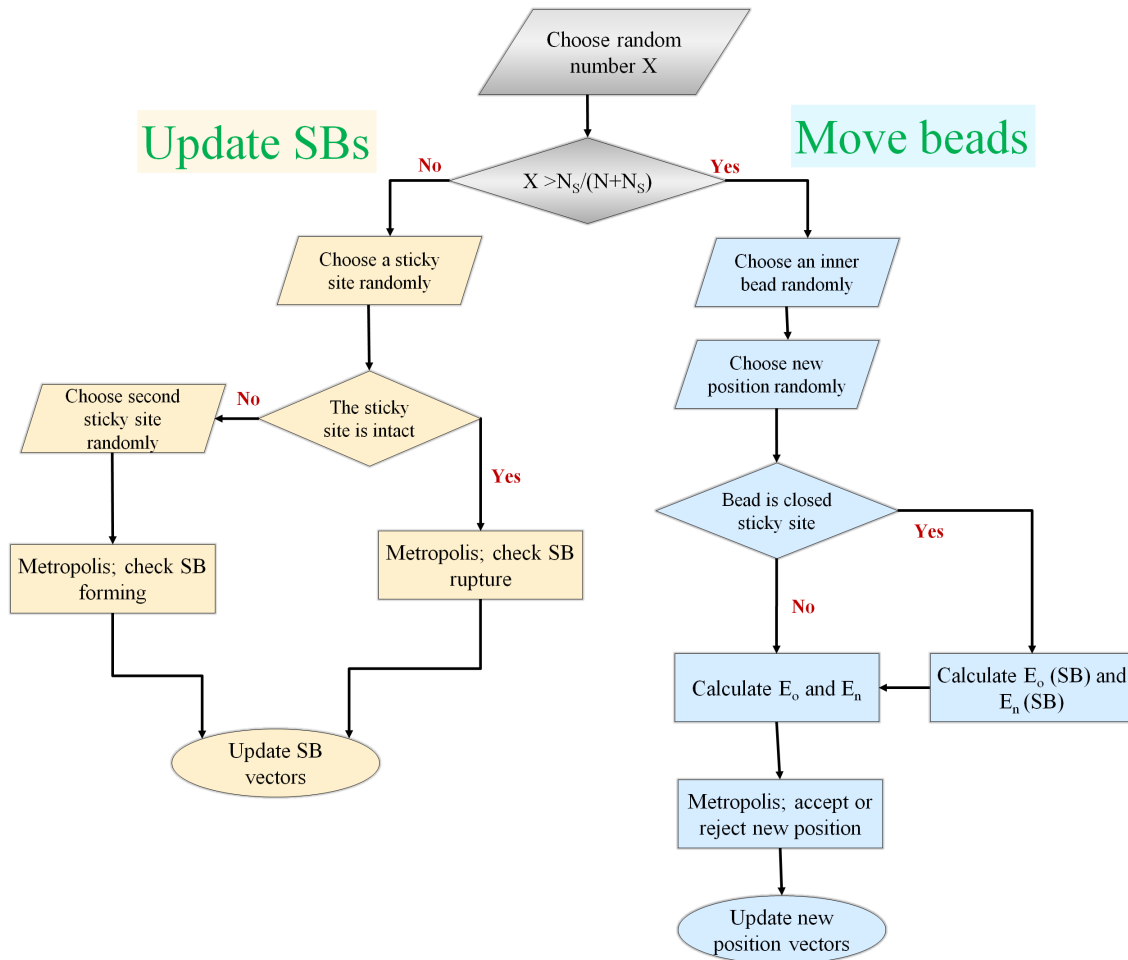
Figure 3.3.1: Flowchart of the simulation procedure used in this thesis. The two main loops consist in moving the beads and updating the bonds.

3.3.1 Move beads

The blue part in Figure 3.3.1 shows the branch corresponding to move the beads. One of the $N-2$ inner beads is chosen randomly. Then a new position is chosen

randomly in a cube around the old position.

$$R_x(new) = R_x(old) + \delta(1 - 2X)$$

$$R_y(new) = R_y(old) + \delta(1 - 2X)$$

$$R_z(new) = R_z(old) + \delta(1 - 2X)$$

where X is a random number on $(0, 1)$ and the δ is the jump length i.e. the maximum size of a trial move [86]. According to Equation 3.1.1, the energy difference of the new and of the old configuration is calculated $\Delta E = E_n - E_o$. If the bead is part of an intact SB then not only the energy due to excluded volume and the covalent bond is taken into account, but also the change in SB energy. The jump length is chosen such that the mean rate of acceptance of a new position is around $50\,\%$ [84]. Following a standard metropolis algorithm [87, 69] the new position is accepted with probability $p = \min\left\{1, \exp\left(-\frac{\triangle E}{k_B T}\right)\right\}$.

3.3.2 Update SBs

The yellow part in Figure 3.3.1 shows the branch corresponding to updating the SBs. In this process, one of the sticky sites is chosen randomly. If the chosen site is part of an intact SB, the probability of breaking this bond is calculated. Here the old energy E_o is the current energy of the sacrificial bond, while the new energy (corresponding to the broken bond) is zero. Thus, the bond opens with probability $p = \min\left\{1, \exp\left(+\frac{E_o}{k_B T}\right)\right\}$.

Otherwise, if the chosen sticky site is not part of an intact SB, a second open sticky site is chosen randomly. Then the probability for formation of a SB between these two beads is given by $p = \min\left\{1, \exp\left(-\frac{E_n}{k_B T}\right)\right\}$. Here E_n denotes the energy of the newly formed bond, while the old energy (no bond) is zero.

During the simulations, all sticky sites with every distance are allowed to form a SB. This leads to a technical detail concerning the definition of the number of closed sticky sites explained in the following. Sticky sites that are a large distance apart have a negligible energy. Thus, the energy difference of an opened and a closed bond is almost zero. Consequently, the probability of formation for such a bond is close to 1, as is the probability of rupture for this newly formed bond. This leads to the result that when the chain is completely stretched and all sticky sites are far apart on average $50\,\%$ of the bonds are closed. But of course these bonds have no influence on the mechanics or any other property of the system. In this thesis a SB is defined as "closed" whenever the bond length is smaller than 5.

3.3.3 Obtaining load-displacement curves

In the simulations up to 90 million Monte Carlo steps (MCS) were performed. One MCS defines the time scale of the simulations being defined as one jump trial per monomer. In the simulations the end-to-end distance of the chain was defined by fixing the outer beads. The force on the outer beads (as well as any other relevant parameter) was recorded and averaged

$$F = -\frac{\partial E}{\partial r} = 2\beta E_0 [e^{-\beta(r-r_0)}(1 - e^{-\beta(r-r_0)})] \tag{3.3.1}$$

Increasing (or decreasing) the end-to-end distance of the chain to perform a computational loading test is done incrementally in small steps with additional equilibration steps. Small steps and equilibration are necessary to avoid hard sphere overlap and bond rupture. A single step consists in moving each bead a small distance according to its z-coordinate

$$z_{new} = z_{old}(1 + \tfrac{\Delta L}{L_{old}})$$

with ΔL giving the displacement of the last bead with z-coordinate $z_{old} = L_{old}$

Positive ΔL stretches the chain and negative unloads the chain. During stretching changing the position of all beads does not lead to hard-sphere overlap but during unloading, the hard-sphere overlapping should be checked, If there is no hard sphere overlap the new positions of the beads are accepted (otherwise a smaller ΔL is chosen). Then equilibration of the inner beads and SBs is performed. These steps are repeated until the desired length of the chain is reached.

3.4 Load and displacement control experiments

Two different scenarios are possible to measure a load-displacement curve. These are the displacement controlled experiment (as is performed in this thesis) and the load-controlled experiment [88, 89]. In the former the displacement is set and the resulting load is measured, while in the latter it is the load that is set and the corresponding displacement measured. The displacement control led measurement represents the Helmholtz ensemble while the force control is called the Gibbs ensemble. However in the thermodynamic limit the two ensembles are equivalent [90]. In the Helmholtz ensemble the first derivative of the free energy determines the force while large fluctuations of the end-to-end distance in the Gibbs ensemble do not permit to formulate such an easy relationship for systems too small for the thermodynamic limit to be applicable [88].

3.5 Basics for mechanical analysis

This part, presents some mechanical parameters used for analyzing and describing the obtained load-displacement curves and also explains briefly, the different mechanical behavior of materials. The mechanical properties of a material are analyzed by measuring the relation between load (stress) and displacement (strain) for this material. Stress is defined as the force per area acting on the material, while strain is defined as the relative elongation of the material given by $\varepsilon = (L - L_0)/L_0$. In this thesis load-displacement curves are used throughout instead of stress-strain curves. This is because it is not possible to define a meaningful area to normalize the force in single molecule measurements. Figure 3.5.1 shows sketches of some typical responses of a material to an applied load. An elastic response is characterized by an identical loading and unloading branch. A deformation is said to be plastic, if a permanent deformation persists after release of the load. A viscoelastic behavior is characterized by a difference in the loading and unloading unbranched, but no permanent deformation persists [91].

All of these stress-strain curves are characterized by a small stress region where stress and strain are linear dependent on each other. The slope of this curve is called the stiffness or the Young's modulus E of the material and is a measure of the resistance of the material against loading. Another important characteristic of these curves is the strength, i.e. the maximum amount of load or stress that the structure can sustain before it fails. The work to fracture is the area under the loading curve and denotes the energy that is needed to break the material. This quantity is closely related to the toughness. Finally, the area between the loading and the unloading branch is a measure of the dissipated energy per loading cycle [91].
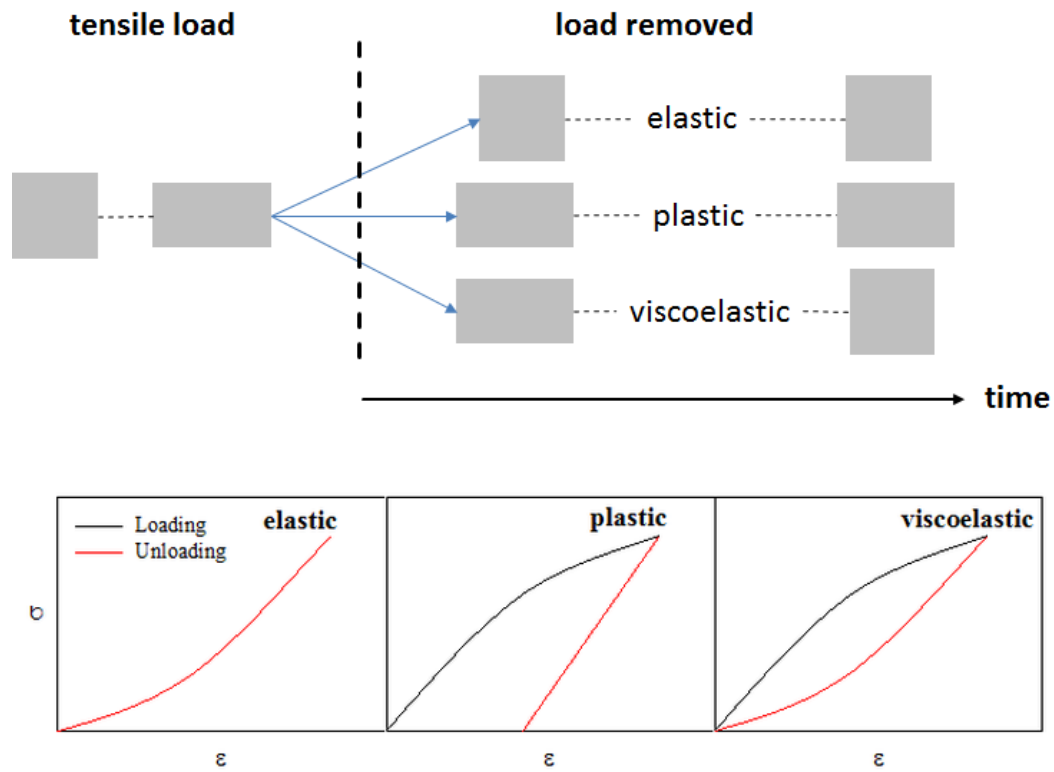
Figure 3.5.1: Different mechanical behavior of materials is shown. The top row shows the response of the material versus time when the load is released and the bottom row shows corresponding Stress-Strain curves. Elastic materials return to their original shape immediately. Materials behaving plastically do not return to their original shape and keep the deformation forever after sufficient large deformation. Viscoelastic materials return to the original shape slowly and the area of hysteresis shows the amount of dissipated energy. Note that for small deformations all of these materials show a linear dependence of stress and strain. The slope of this linear part of the curve is the stiffness of the material. Figure reproduced from [91].

4 Single Chain with Reversible Cross-links

The results from this chapter show that the SB topology determines the position of the force peaks, while the efficacy of the sacrificial bonds (the height of the peaks) is reduced due to thermal fluctuations of the backbone. Furthermore, simulations mimicking cyclic loading experiments revealed an asymmetry between loading and unloading resulting in a pronounced hysteresis. Because the mechanical properties strongly depend on the topology of the SBs, the speed of unloading determines the mechanical properties of the second loading cycle. Moreover, for chains with a similar number of SBs, the mechanical properties like the strength (maximum force) and apparent stiffness may be considerably different due to a different arrangement of the sticky sites.

This chapter presents simulation results for a single polymeric chain with reversible cross-links. The model presented in section 3.1. First, test runs on simple models are shown to validate the program and check the code for programing errors. Then the influence of SB topology on the mechanical response of single polymer chains is described. In particular, the influence of thermal backbone fluctuations on the efficacy of SBs is analyzed and discussed. Part of these results is published in [78]. In section 4.3 the influence of SB density and topology on the load-displacement curves in a computational cyclic loading experiment is presented. Furthermore, the effect of the rate of unloading on the recovery of the system is discussed. Here the focus lies on the two extreme scenarios of infinitely fast and infinitely slow (quasi-static) unloading, respectively. Finally, in section 4.4 the influence of the arrangement of sticky sites on some mechanical key parameters like the work to fracture, the apparent stiffness and the strength of the system is presented. This work has been published in [92].

4.1 Validation of the model—Test runs

To test the program, first simulations were performed with a small number of beads and no sticky sites ($\rho_S = 0$). The simulations were starting from a predefined starting configuration (see the inset of Figure 4.1.1A) and the system was slowly stretched

as explained in chapter 3. Figure 4.1.1(A) shows the resulting load-displacement curve. As expected the load is very low until $L/L_C \approx 1$. At this end-to-end distance the covalent backbone starts stretching resulting in a sharp peak in the load-displacement curve. When the chain is considerably stretched beyond its contour length, the load drops again which is characteristic for chain rupture.
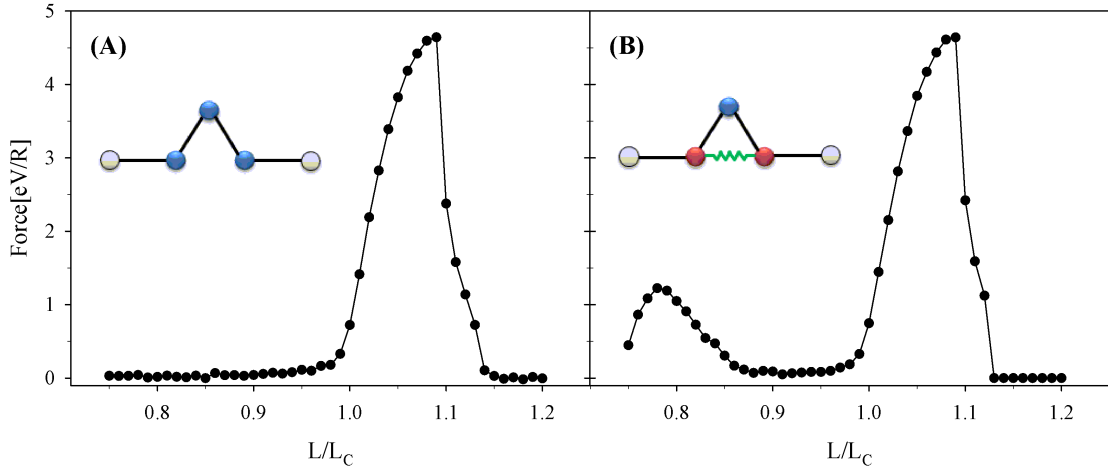
Figure 4.1.1: The Load-Displacement curve for $N = 5$ beads and no sticky sites (A) and with two sticky sites (B), respectively. The two insets shows the starting configuration. Sticky sites are shown in red, non-sticky sites in blue and the fixed end beads are shown in gray. The green zigzag line indicates the intact SB between the two sticky sites in the starting configuration for (B).

Now two sticky sites are introduced in the structure that are located at the second and fourth bead (see the inset of Figure 4.1.1B). These sticky sites (shown in red) can now reversibly form a SB (which is shown in green). The starting configuration is chosen such that the distance between the sticky sites is r_0, i.e. the equilibrium sacrificial bond length. Now this structure is stretched. Figure 4.1.1(B) shows the obtained load-displacement curve for this setting. Compared to the load-displacement curve without sticky sites the resulting curve shows an additional peak near $L/L_C = 0.8$ which is approximately four times weaker than the covalent bond contribution. This additional peak is due to stretching and breaking of the sacrificial bond that is formed between beads two and four.

Finally, structures with more than two sticky sites were tested. The length of the chains is changed according to the number of sticky sites present. In the cases investigated these are $N = 5$ and 2 sticky sites, $N = 9$ and 4 sticky sites and $N = 13$ and 6 sticky sites, respectively (see Figure 4.1.2 (A) for a sketch of the corresponding starting configurations). Figure 4.1.2 (B) shows the resulting load-displacement curves, when these structures are stretched. The figure shows the expected results that each additional SB gives an additional peak in the load-displacement curve.
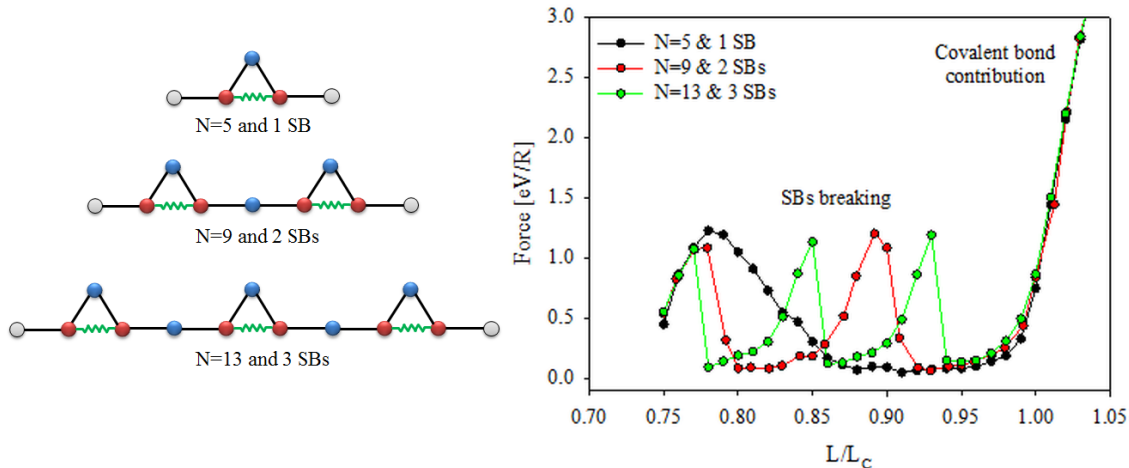
Figure 4.1.2: (A) starting configurations and (B) load-displacement curves for short chains of different length and with different number of SBs.

These first results indicate that the program is working fine and is free of programming errors.

4.2 The role of topology and thermal backbone fluctuations on sacrificial bond efficacy

In this section the influence of SB topology on the mechanical properties of a single polymeric chain is investigated. As sketched in the introduction, this model is motivated by the load-bearing metalloproteins found, e.g., in the mussel byssus threads. The strategy followed in this thesis is to start with simple models that can be completely understood and then to proceed step by step to more complicated structures. Thus, first a polymeric chain of length $N = 50$ with only four sticky sites is investigated. Load-displacement curves are obtained and analyzed. Special emphasis is put on understanding the number, spacing and height of the force peaks that are due to SB rupture during loading. It is shown that these parameters are intimately tied to the topology of SBs but also to thermal fluctuations of the polymer backbone.

Independent starting configurations were produced by slowly unloading the single chain with no sticky sites from the contour length until the desirable short end-to-end distance was reached. Then the sticky sites were introduced and the SBs allowed to form. Figure 4.2.1 shows an averaged load-displacement curve of 20 independent simulation runs for a single chain with $N = 50$ and 4 sticky sites ($\rho_S = 0.08$) at ambient temperature ($k_B T = 0.025$ meV). This curve resembles the experimentally observed "saw-tooth" pattern which has been reported for some biological materials,

e.g. nacre [4], in single molecule measurements of titin [23, 93], tenascin [26], DOPA [94] and modular proteins [95] as well as in the adhesive mucilage pads of diatoms [96, 97] and polymer brushes from rat tail tendon [98]. In particular, the curve shows four distinct peaks. The last peak (IV) that is centered around the contour length is the trivial contribution due to backbone stretching and will not be considered further. All the other peaks (I, IIA, IIB and III) stem from the breaking of SBs and will be analyzed further. Especially I will focus on the number, position and the height of the different peaks. It is the simplicity of the model of this setting that helps to understand this system completely and pave the way for understanding more complicated structures.
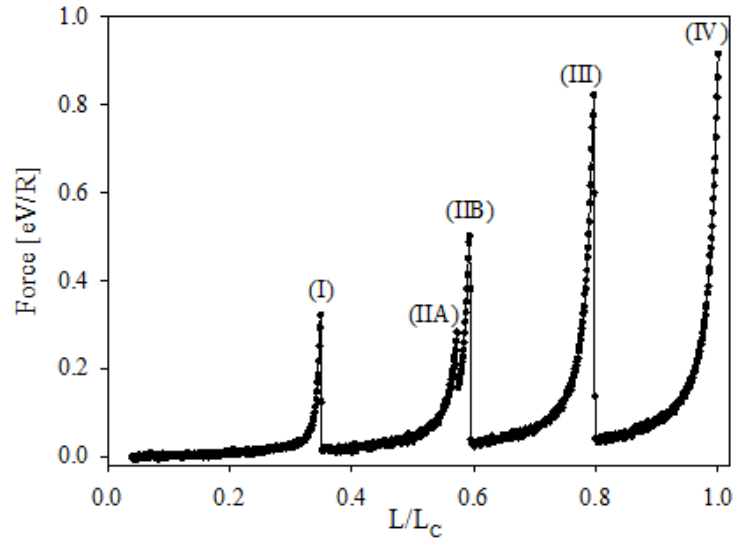
Figure 4.2.1: Averaged load-displacement curve for $N = 50$, $k_B T = 25$ meV and $\rho_s = 0.08$ of 20 independent runs.

First we focus on the positions and the number of peaks. At first sight one might expect that in a single chain with 4 sticky sites, i.e. the possibility of forming two SBs, only two peaks corresponding to SB rupture could be observed. But the result shows 4 peaks (see Figure 4.2.1). This elevated number of sacrificial force peaks comes from averaging 20 independent runs. In each single run SBs of three different topologies may form. These are the independent, pseudoknotted and nested topology as shown in Figure 4.2.2. In 20 simulation runs, 60 % showed the independent, 10 % the pseudoknotted and 30 % the nested topology. In the chain the sticky sites were introduced regularly: the sticky sites are all separated by 10 non-sticky sites. Thus, the SB separates the chain into 5 parts (see also inset of Figure 4.2.2). The two outer parts have a total length of $d_0 = 16r_0$ resulting in $L/L_C = 16r_0/L_C \approx 0.32$, which is the length below which no peak can be

observed. The inner part is divided into three segments of equal length $d = 11r_0$. Figure 4.2.2(A) shows the load displacement curve for the independent topology. Here the SBs are formed between sticky sites $(1, 2)$ and $(3, 4)$. Upon loading the SBs start being loaded around $L/L_C = (d + d_0 + 2r_0)/L_C \approx 0.59$ which is the position of peak (IIB) in Figure 4.2.1. After rupture of the first SB, the next SB starts being loaded at $L/L_C = (2d + d_0 + r_0)/L_C \approx 0.8$ (peak (III)). Figure 4.2.2(B) shows the load-displacement curve for the pseudoknotted topology. Here the SB is formed between sticky sites $(1, 3)$ and $(2, 4)$. This results in a parallel loading of the SBs at a slightly smaller extension than the first peak of the independent topology giving rise to peak (IIA) in Figure 4.2.1. This small difference in the extensions is due to the hard core repulsion of the beads that forbids the exactly parallel alignment in the direction of the load of the beads. After rupture of the pseudoknotted loop, the two intermediate sticky sites $(2, 3)$ form a new SB which fails after extending the chain to $L/L_C = 0.8$, which is exactly the same position as the second peak in the independent configuration. Finally, in the nested topology the SBs are formed between the two outer sticky sites $(1, 4)$ and the two inner SB between $(2, 3)$. Thus, upon loading the first SB first shields the inner one. The first SB starts being loaded around $L/L_C = (d_0 + r_0)/L_C \approx 0.35$. This gives rise to peak (I) in Figure 4.2.1. Finally the second SB breaks at $L/L_C = 0.8$ corresponding to peak (III).
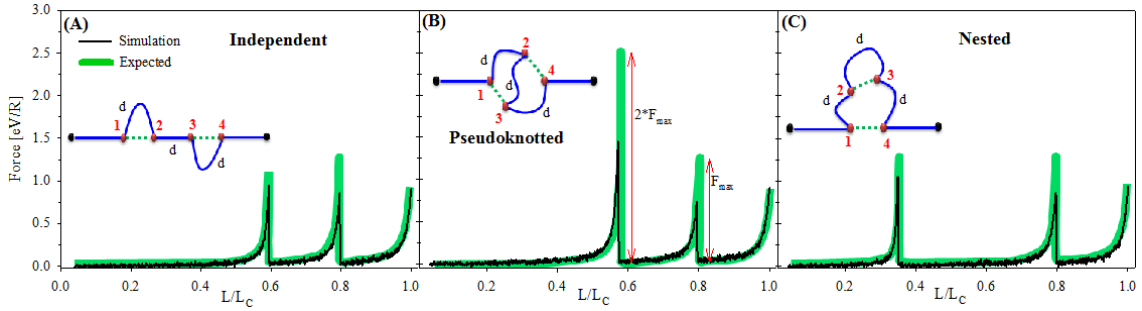
Figure 4.2.2: Load-displacement curves for $N = 50$ at $k_B T = 25$ meV with four sticky sites and different topologies of the formed SBs. The first and last bead of the chain are shown in black; sticky sites are shown in red. SBs are indicated by dotted green lines, covalent connections by blue lines. Load-displacement curves shown with thick, green lines indicate the expected curves. The thin, black line shows actual simulation results of selected single runs. (A) independent configuration: two force peaks of equal height $F_{max} = \beta E_0^{SB}/2 = 1.25$ eV/R at $L/L_C \approx 0.59$ and 0.8 are expected. (B) pseudoknotted configuration: two force peaks are expected: the first at L/L_C slightly lower than 0.59 and of height $2F_{max}$, the second of height F_{max} at $L/L_C \approx 0.8$. (C) nested configuration: two force peaks of equal height F_{max} at $L/L_C \approx 0.35$ and 0.8 are expected. Note, that not a single SB attains its theoretical strength.

Thus, the number and the positions of the peaks for loading the single chain with 4 sticky sites can be well explained with the different topologies of the involved SBs. But the height of the peaks can not be understood that easily. Partly the height

of the averaged curves shown in Figure 4.2.1 can be explained by the probability
of formation of a certain topology. Out of 20 runs, 12 showed the independent
topology, 2 the pseudoknotted and 6 the nested topology. Thus, simply due to the
improbability of the pseudoknotted configuration the peak (IIA) is much reduced in
height compared to the others. But also peak (III) that is present in all different
topologies as well as the peaks observed for the single runs shown in Figure 4.2.2
do not show their expected theoretical height, which is indicated by the green solid
lines in the figure. This theoretical height is given by the maximum force generated
by the used potential. We find the position of the maximum force by setting the
first derivative of the force (the second derivative of the energy) to zero

$$E^{SB} = E_0^{SB}[(1 - e^{-\beta(r-r_0)})^2 - 1] \implies F = -\frac{\partial E}{\partial r} = 2\beta E_0[e^{-\beta(r-r_0)}(1 - e^{-\beta(r-r_0)})]$$

$$\frac{\partial F}{\partial r} = 0 \rightarrow r_{max} = r_0 + \ln 2/\beta \approx r_0 + 0.35$$
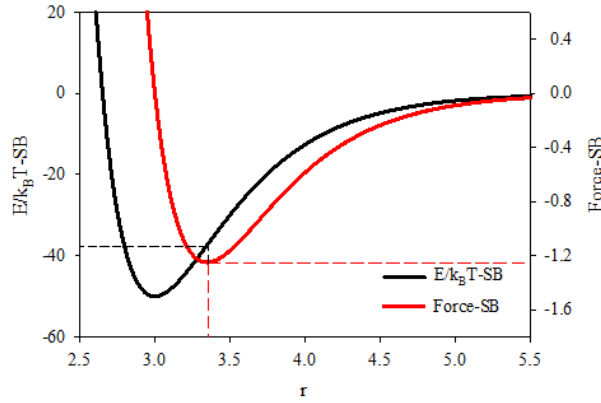
Figure 4.2.3: The black curve shows the Morse potential: E/k_BT as a function of the distance
between two sticky sites. $\exp(E/k_BT)$ gives the probability of SB breaking. The red curve
shows the force on the SB as a function of distance. The maximum force $F_{SB} = 1.25\,eV/R$
occurs when the distance between sticky site is about $r = 3.35R_0$ and the corresponding energy
is $0.933\,eV$ corresponding to $E/k_BT = -37$. Therefore breaking of SB is not expected since the
probability of SB rupture is very small $\exp(E/k_BT) = exp(-37) \approx 10^{-16}$.

Furthermore, we find the maximum force of a single SB as $F_{max} = \beta E_0^{SB}/2 = 1.25$ eV/R, the corresponding energy is given by 0.933 eV (see also Figure 4.2.3).
Because the energy at the maximum force is still large compared to k_BT, it is
expected that the SB does not fail before the bond is stretched to its maximum force.
Consequently it is also expected that the SB force peaks shown in Figure 4.2.2 attain
the theoretical maximum force. In particular, the probability of breaking one SB at

the extension of maximum force (which is corresponding to an energy of 0.933 eV) is 10^{-16} which is extremely small.

$$\implies \left\{ \begin{array}{c} F_{max} = \beta E_0^{SB}/2 = 1.25 \ eV/R \\ E^{SB} = 0.933 \ eV \end{array} \right\} \implies \exp(E^{SB}/k_B T) \approx e^{-37} \approx 10^{-16} \quad (4.2.1)$$

Although the probability of SB breaking for the maximum force is very small, the results of the simulation show that the SBs break at loads considerably lower than F_{max}. To investigate this point further, the SB bond length was monitored as a function of extension for the nested configuration (see Figure 4.2.4). The results show that for a broad range of end-to-end distances the SB length is around its equilibrium value of 3, while it considerable extends when the bonds are loaded. Nevertheless, the first SB stretches only until about $r_{max} = r_0 + 0.22$ and the second SB to $r_{max} = r_0 + 0.15$. Both values are considerable smaller than the bond length corresponding to maximum force $r_{max} = r_0 + \ln 2/\beta \approx r_0 + 0.35$.
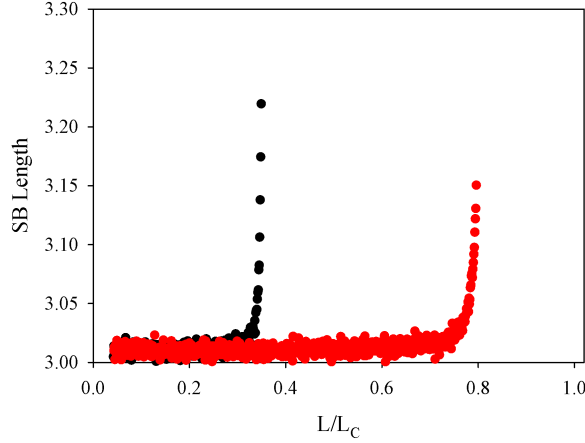
Figure 4.2.4: The sacrificial bond length upon loading for a chain with nested topology as shown in Figure 4.2.2(C) i.e. the chain with $N = 50$ at $k_B T = 25$ meV and four sticky sites.

To understand the reduced amount of force observed for SB rupture, the investigated system was even more simplified. Figure 4.2.5(A) shows the starting configuration of a linear chain with only two sticky sites in its middle. The end-to-end distance of this starting configuration is $L/L_C = (N - 2)/(N - 1) = L^*$ and denotes the length when a SB starts being loaded at zero temperature. Figure 4.2.5(B) shows the resulting load-displacement curves for two chains of different length (N=5 and N=50, respectively). The load-displacement curve of the short chain with $N = 5$ beads at $k_B T = 25$ meV shows a sacrificial force peak of approximately the expected theoretical height. This situation changes for longer chains. For $N = 50$ no peak can be observed. Thus, the SB ruptured in the very first simulation steps. As explained before at zero temperature the bond would be completely unloaded. The

reason for SB rupture can only be the elevated temperature, increasing the entropy leading to thermal backbone fluctuations. This is the more surprising, because as shown and discussed in Equation 4.2.1 the binding energies of the involved bonds are much higher than ambient temperature. Thus, at first sight one might conclude that temperature effects are of minor importance in this setting.
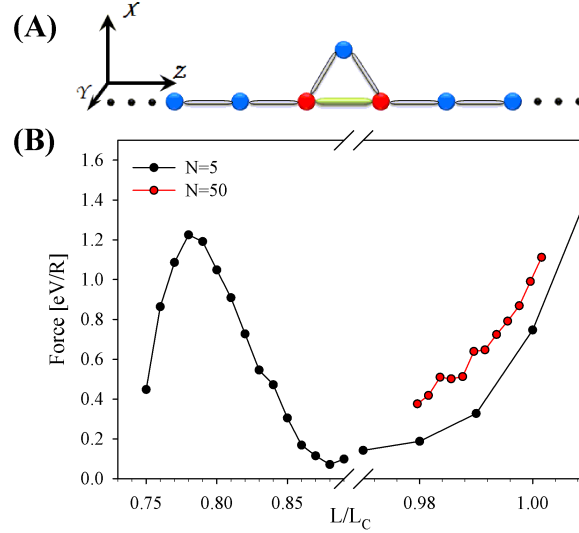
Figure 4.2.5: (A): The starting configuration of the simplified system with only two sticky sites. Only the middle beads of the chain are shown. Normal monomers are shown in blue, sticky sites in red. Longer chains are created by adding additional monomers on both sides. The simulations are started with the SB closed (green connection). Covalent bonds are shown in gray. (B): Load-displacement curves obtained by stretching the chains for $N_S = 2$, $k_BT = 25$ meV and $N = 5$ (black) and $N = 50$ (red), respectively.

To validate the hypothesis that SB rupture is due to temperature and entropy, load-displacement curves at different temperatures were obtained for the system with $N = 50$ and two sticky sites. The starting configuration was chosen such that, first, the SB was closed and, second, that the end-to-end distance was shorter than the effective length L^* (i.e. the length at which loading starts at zero temperature). The results are depicted in Figure 4.2.6. For all investigated temperatures a sacrificial force peak is observed. Its height increases with decreasing temperature approaching the theoretical expected strength of one SB for the lowest investigated temperature ($k_BT = 1$ meV). The effect of higher temperature is not only a decrease in peak height, but also a shift of the position of the peak to smaller extensions of the chain. At ambient temperature ($k_BT = 1$ meV) the SB ruptures before L^* that is indicated by the gray dashed line. This explains why no trace of the SB was seen for the simulations starting exactly at L^* at room temperature and shows that the effect of SBs at ambient temperature is completely entropic. This means that if one would lower the temperature at a length below L^* then the force would drop to

zero. Whereas for an extension larger than L^* the load is enthalpic, meaning that a load larger than zero can persist even at zero temperature. This is a very surprising result that even for relatively stable SBs with a binding energy of a quarter of a covalent bond temperature and entropy play such a major role.
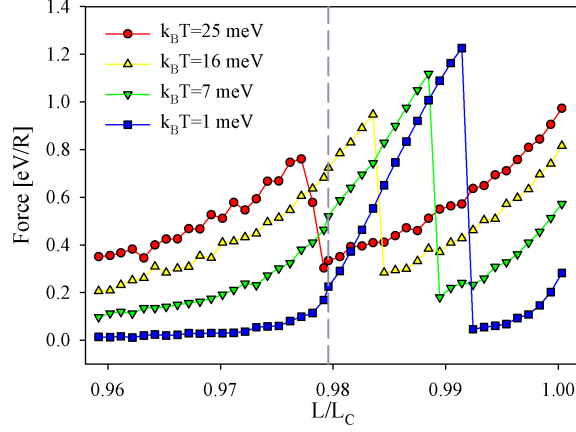

Figure 4.2.6: Load-displacement curves for chains with $N = 50$ at different temperatures. When the temperature is decreased an additional force peak due to the SB starts growing that is approaching the theoretical strength of 1.25 eV/R at temperatures below one meV. The vertical dashed line indicates L^*.

To study this effect further, the covalent force distribution for the chain with $N = 5$ and two sticky sites was recorded. Figure 4.2.7 shows the frequency of how often one bead experiences a certain amount of force. The covalent force distribution of the three beads close to the SB are shown (i.e. the two sticky sites and the one non-sticky in between). The simulation was done directly at L^*. The black line shows the covalent force distribution on the left sticky site, the green line shows the force on the right sticky site and the red line shows the force distribution on the non-sticky site located in between the two sticky sites (for a sketch of the geometry see Figure 4.2.5A). Figure 4.2.7 clearly shows that on average the two sticky sites experience a covalent force, while the non-sticky site in between is force free. This confirms the earlier results that the SB between the sticky sites is also loaded canceling out the covalent forces. Once again, it should be noted that this load is entropic because at L^* no load above zero can persist for zero temperature.

To further investigate the influence of backbone fluctuations on the efficacy of SBs, sacrificial bond length and sacrificial force distributions were recorded. These give the probability of the SB to experience a certain strain or a special amount of force at each time step. Also in these investigations the end-to-end distance of the chain was set to L^*, i.e. the onset of enthalpic loading. Chains of two different length were investigated: $N = 5$ and 33, respectively. The latter length (33) was the largest length that not a single SB rupture occurred during the simulation time.
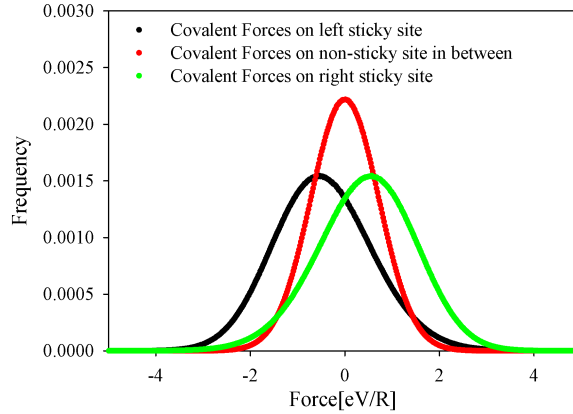
Figure 4.2.7: Covalent force histograms for the two sticky sites and one non-sticky in between for the chain shown in Figure 4.2.5A. The black and green curves show that the left and right sticky site experience a covalent force larger than zero, while the red curve shows that the non-sticky site does on average not experience any force. Thus, it is the SB in between the two sticky sites that neutralizes this covalent force.

Figure 4.2.8 shows the sacrificial bond length distribution and loading of the SB for the two investigated number of monomers, while the inset in Figure 4.2.8(B) shows the peak position (evaluated at the maximum of the curve) and width (measured as full width at half maximum) of the distributions as a function of the number of monomers. Compared to $N = 5$ the peak position of the sacrificial bond length shifts to larger lengths for $N = 33$. Simultaneously the curve also considerable broadens. Thus, increasing the number of monomers of the chain N increases the mean strain on the SB, shifting the position of the peak in the force to the higher values. It is this shift of the force peak (Figure 4.2.8(B)) to larger values that is responsible for the weakening of the SBs resulting in the rupture of premature SBs. The shift of the peaks of SB length and load as well as the simultaneous broadening of the peak are the two reasons that the SB is strained beyond r_{max} for chains with large N. Subsequently, the bond is brought close to its maximum load leading to bond rupture. Both distributions are asymmetric. The pronounced drop in the force distribution is due to the maximum load at $F = 1.25$ eV/R. This sharp drop of the force distribution at F_{max} results in a slight decrease of the width of the distribution for large N.

The small increase in the load-histogram for $N = 33$ close the maximum load is due to the following reason: The maximum load is characterized by a local extremum of the force with respect to distance (see Figure 4.2.3). Close to the extremum there are always two values of the distance corresponding to one force (one distance below and one above the maximum). Due to fluctuations the bond distance is fluctuating around the most probable value. When this most probable value is reasonably close to the maximum distance then there is also a non-negligible probability for the bond

to be strained beyond r_{max}, giving the same amount of force as for a symmetric value below r_{max}. Thus, for force values close to F_{max} there are two distances giving the same force which is effectively increasing the probability of finding this force.
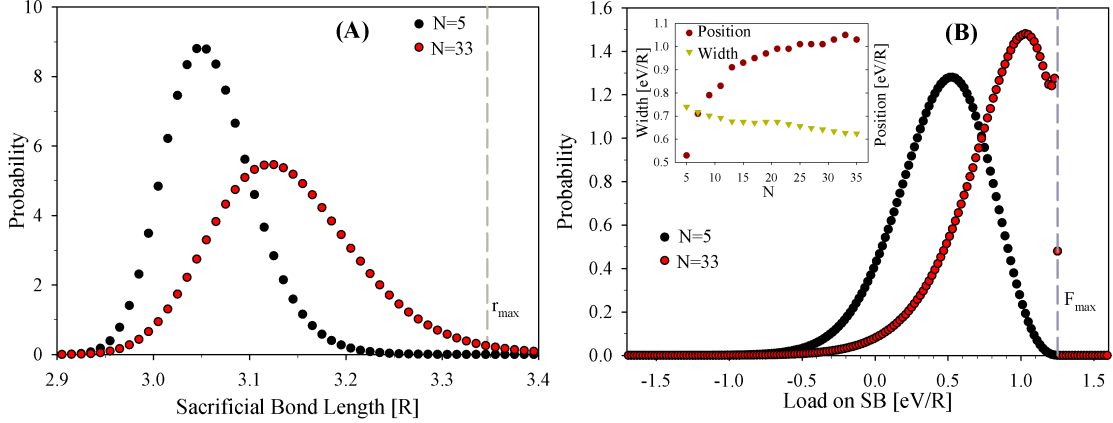
Figure 4.2.8: (A): Sacrificial bond length histograms at $k_B T = 25$ meV. The distance r_{max} corresponding to the theoretical maximum force is indicated by a gray dashed line. (B): The distribution of loads on the SBs at $k_B T = 25$ meV. The dashed gray line indicates the maximum force. The inset shows the width and position of the histograms as a function of monomer number. The data in (A), (B) were recorded at $L/L_C = L^*$.

Although the binding energy of SBs is much larger than ambient temperature, via the fluctuations of the backbone temperature and entropy have a profound effect on the behavior of SBs and can not be neglected. Figure 4.2.9(A) shows load distributions of the SB for $N = 33$ for two different temperatures, while the inset shows the width and position of the peaks as a function of temperature. Increasing the temperature makes the peak broader and leads to a shift of the position of the peaks to higher loads. While the shift of the peak maximum is similar to Figure 4.2.8(B) for increasing the number of monomers, the broadening of the peaks behaves differently. One could expect that increasing N should increase the fluctuations of the chain. But in contrast, a narrowing of the load distribution for increasing N is observed (see inset in Figure 4.2.5B). This effect comes from the change of L^* with N. While $L^* \approx 1$ for $N = 33$, for $N = 5$ $L^* = 0.75$. The smaller the effective length the easier it is for the SBs to follow the backbone fluctuations making the peak broader. For a system with larger N the number of confirmations is reduced, effectively reducing the peak width for larger N. Figure 4.2.9(B) shows the load distribution for $N = 33$ for two different end-to-end distances. This figure summarizes the the effect of end-to-end distance of the chain on the fluctuation: a smaller length leads to a shift of the peak maximum to smaller values as well as to a broadening of the peak.

Thus, it could be shown that the load on SBs is purely entropic. Such entropic loads can also be found in nature and have been reported experimentally in systems like
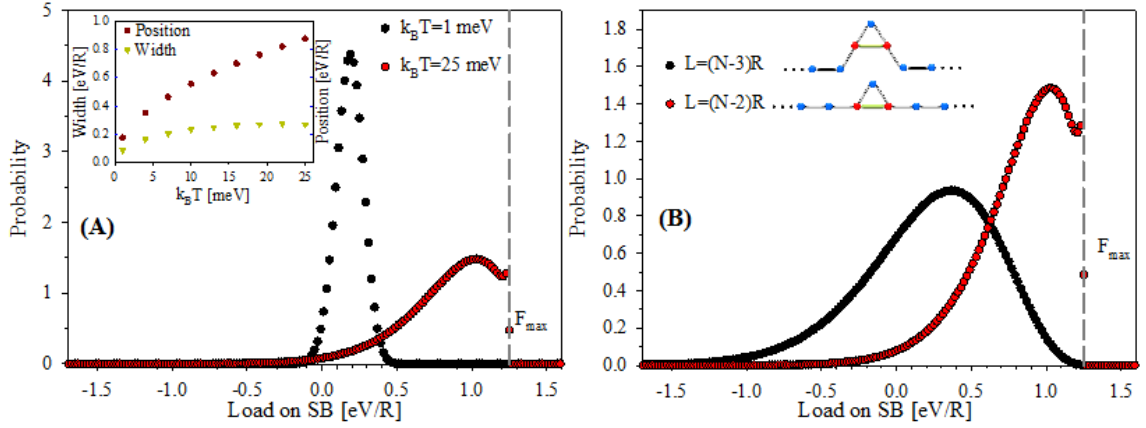
Figure 4.2.9: (A) Load distributions for $N = 33$ at two different temperatures. The inset shows the position and width of the distributions as a function of temperature. (B) Load distribution for $N = 33$ and two different end-to-end distances at $k_B T = 25$ meV. The inset shows the two starting configurations.

rat tail tendon and single chains of poly(methacrylic acid) [98, 99]. The standard theoretical model to describe such entropic loads is the Freely Jointed Chain (FJC) and the (more often used) Worm Like Chain (WLC) model. As a final confirmation of the entropic nature of the loads in the presented model, the single force peaks were fitted with the aforementioned models. The results show that the single SB rupture event can be well fitted with either the worm like chain model as well as the freely jointed chain model. The analytical form of the load as a function of end-to-end distance of the chain in the WLC model [100, 101] is given by:

$$F = \frac{k_B T}{L_P} \left[\frac{L}{L_C^{eff}} + \frac{1}{4} \frac{1}{(1 - L/L_C^{eff})^2} - \frac{1}{4} \right] \tag{4.2.2}$$

with the persistence length L_P and the effective contour length L_C^{eff} as the two fitting parameters of the model (see Figure 4.2.10A for an example of such a fit for the pseudoknotted topology). The effective contour length is smaller than the real contour length because the SBs provide some hidden length (i.e. the length of the loop that is shielded by the SB from being extended). More exact, the effective contour length is given by the real contour length minus the hidden length shielded by the SBs. The persistence length obtained by the fit for the first peak of the pseudoknotted topology is about 3.1 and it increases to 5.4 for the second peak as shown in Figure 4.2.10A. The value of the persistence length for the other two topologies is in the order of $L_P \approx 5.5$ similar to the value obtained amount for the second peak of the pseudoknotted topology. This small value of the persistence length (only one to two monomer distances) shows the high flexibility of the chain. Although it was shown that the WLC model breaks down due to excluded volume

effects for chains with a small relative length [102, 103], this does not deteriorate the fits in the model presented. In the present case close to SB rupture the chains are completely stretched and excluded volume does not play any role. This is also the deep reason why the WLC model applies well, although the chain is very flexible. Before SB rupture, when the model is applied, the available length of the polymer is stretched out, showing only minor deviations from the straight line. Thus, effectively the chain resembles a WLC characterized by a rather high bending rigidity.
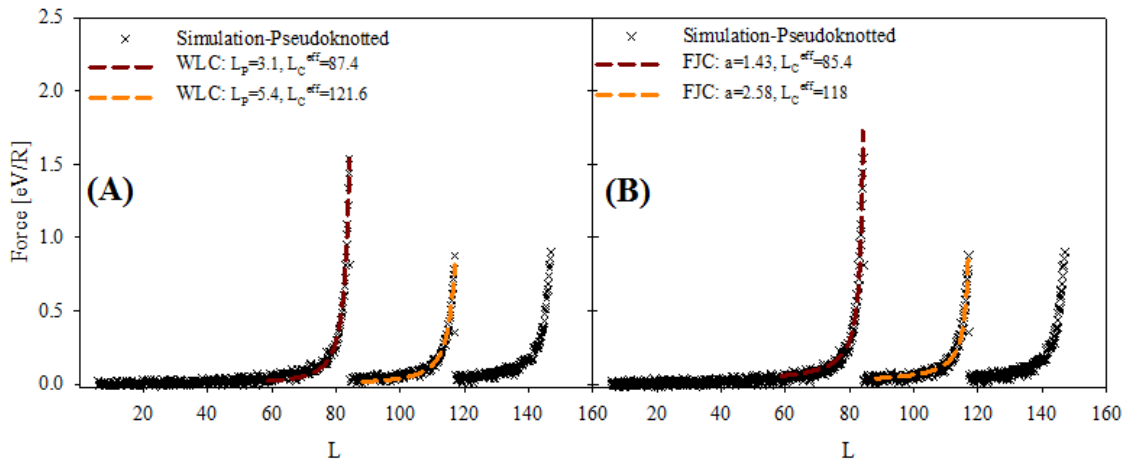
Figure 4.2.10: Two typical examples of WLC and FJC fitting curves for the pseudoknotted topology and $\rho_s = 0.08$. The crosses shows our simulation results and the dashed lines indicate the fit with the two models. Each model has two fitting parameters; for WLC model, the effective contour length L_C^{eff} and the persistence length L_P. The parameters of the FJC are the effective contour length and the Kuhn length.

The analytic form of the load-displacement curve for the freely jointed chain is given by [104, 105]:

$$F = k_B T / a (1 - L / L_C^{eff}) \tag{4.2.3}$$

here the effective contour length L_C^{eff} and the statistical segment length (Kuhn length) a are the two fitting parameters. The effective contour length for the two models is almost the same. The statistical segment length is of the order of the hard spheres diameters used in the simulations. This small value is also an indication of the flexibility of the chain. The Kuhn length for both peaks of the pseudoknotted topology are 1.43 and 2.58. The Kuhn length for the peaks of other two topologies is about $a \approx 2.5$. The effective contour length is in the order of the peak positions in the simulation. The effective contour lengths from fitting the FJC model to the

simulation results are in the order of the effective contour length obtained from a fit with the WLC model and the Kuhn length is half the value of the persistence length for all corresponding peaks.

The results presented in this chapter explain the number, spacing and especially the reduced height of the force peaks observed in Figure 4.2.1 and Figure 4.2.2 in the simple model of SBs presented. It was shown that the topology primarily influences the position and number of the peaks, while the height of the peaks is intimately tied to the fluctuations of the backbone and is, thus, an entropic effect. That the resulting force is entropic in nature could be consistently shown by changing the temperature in the simulations, by evaluating load probability distributions as well as by the fitting of the force peaks with the WLC and FJC model; two theoretical models that were especially designed for describing entropic loads. Nevertheless, that the effect of SBs is completely entropic in nature is the (surprising) main result of this chapter. It was completely unexpected that in a system where the lowest energy is a factor of 50 larger than $k_B T$ entropy and temperature play such a big role. Another important conclusion that can be drawn from the results obtained for this simple model is that the load-displacement curves do not necessarily reflect the underlying microscopic potential. The enthalpic potential of the SBs is completely smeared out due to the entropic backbone fluctuations.

4.2.1 Conclusion

Employing a simple model with reversible cross-links mimicking SBs between proteins and metal ions in the mussel byssus makes it possible to reproduce characteristic features found in experimental load–displacement curves in natural materials. Characteristic sawtooth patterns corresponding to the rupture of single bonds were observed. The distance between two peaks (the hidden length revealed) is directly linked to the topology of the bonds and corresponds to the length of the loops defined by the SBs. The height of the peak force is considerably lower than the theoretical strength of a SB. It was shown that this reduction is of entropic origin. The capability of SBs to transmit load are drastically reduced at ambient temperature due to thermal fluctuations in the backbone of the chain.

4.3 Influence of sticky site density

In the present section we investigate the influence of SB density and topology on the work to fracture and especially on the amount of dissipated energy per loading cycle. Special emphasis is put on the reforming of ruptured SBs during unloading of the system. This reforming determines the mechanical properties after one loading cycle and is, thus, strongly linked to the self healing capabilities of the structures. The mechanical properties itself depend on the topology that SBs form when closing. The

type of the topology formed is strongly influenced by the rate of return of the loaded structure into its native state. Additionally, the sacrificial bond length distribution is measured for three extreme SB topologies. As discussed in the previous section the simplicity of the model gives the advantage of understanding the system completely. It is hoped that the basic mechanisms underlying energy dissipation and recovery identified in this model and the information about the mean bond length for different topologies will help to understand the much more complex situation in real systems.

Independent starting configurations are produced by slowly unloading a completely stretched chain without sticky sites until the starting end-to-end distance was reached. Then the sticky sites were introduced in the system. Whenever not stated differently the arrangement of sticky sites is ordered, meaning that always after a certain number of non-sticky sites one sticky site is set (this number is defined by the sticky site density). The sticky site densities investigated in this thesis are $\rho_s = 0.08$, $\rho_s = 0.24$ and $\rho_s = 0.48$, respectively. Therefore for the lowest SB density each two sticky sites are separated by 10 non-sticky sites along the chain while for the other two SB densities, 4 and 1 non-sticky sites are in between each two sticky sites along the chain, respectively. The top row of Figure 4.3.1 shows the load-displacement curve for the corresponding SB densities. Black dots shows the behavior of the chain upon loading and the red dots show unloading. The bottom row shows the number of intact SBs (as explain in section 3.3 intact SB means that the sacrificial bond length is smaller than $5R$) during the cyclic loading test for each corresponding SB density.

The chain with the lowest SB density corresponds to 4 sticky sites along the chain. The corresponding loading curve shows 5 discrete peaks with special peak spacing. As explained in the last section, the position of the peaks as well as the peak spacing is determined by the different topologies of the involved SBs while the height of the peaks is intimately related to the backbone fluctuation and is significantly smaller than the theoretical strength of one SB. When the number of SBs in the chain increases the discrete peaks merge into one large plateau and the force does not drop to zero between the discrete rupture events.

When the chain reaches the contour length all SBs are open, because the distance between individual SBs is too large to form stable bonds. Now the direction of loading is reversed and the structures are unloaded until the starting contour length is reached. This completes one loading cycle. For all three SB densities, an asymmetry between the loading and unloading branch can be observed (see Figure 4.3.1(A,C and E)). This shows that more energy is needed to elongate the chain than energy is restored during unloading. The area between the loading and unloading curve is a measure of the dissipated energy per loading cycle $\Delta E = E_1 - E_2$. Here E_1 and E_2 are the area under the loading and unloading curves, respectively. While E_1 is the work to elongate the molecule, the work to fracture is given by $W = E_1 + E_C$ with $E_C = 25\,eV$ is the additional energy to break the elongated chain. Because all SBs are open for chains stretched to the contour length, E_C is a constant for all chains independent of the SB density and arrangements. Therefore, in the following E_C will be omitted and the work to fracture and the work to elongate the molecule

will be used interchangeably. Table 4.1 shows the measured work to fracture, the restored energy, the amount of dissipated energy and the relative amount of dissipated energy for each SB density. The results show that the work to fracture as well as the dissipated energy increase for chains with a larger number of sticky sites. The work to fracture changes from $E_1 = 11.4\,eV$ for $\rho_s = 0.08$ to $E_1 = 36.7\,eV$ for $\rho_s = 0.48$ and the dissipated energy changes from $\Delta E = 5.5\,eV$ to $\Delta E = 23.9\,eV$, respectively. As shown in Table 4.1 the relative amount of dissipated energy $\Delta E/E_1$ changes from $\Delta E/E_1 = 0.48$ for the lowest SB density to about 0.67 and 0.65 for the other two densities $\rho_s = 0.24$ and $\rho_s = 0.48$, respectively. Experimental results show that the relative energy dissipation for the distal part of the mussel byssus is about 0.7 [106].
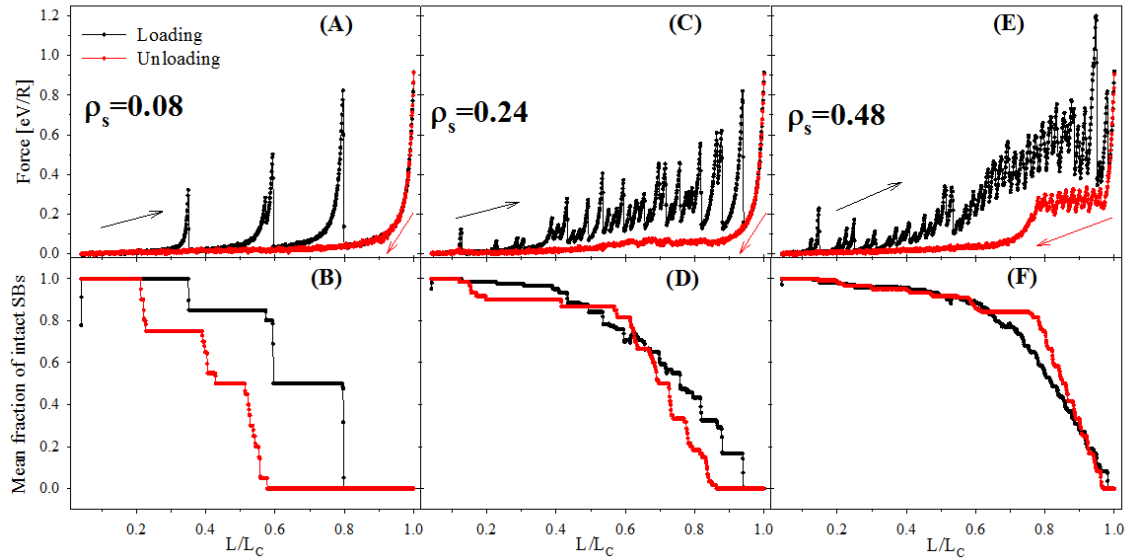
Figure 4.3.1: (A), (C) and (E): Cyclic loading curves for $N = 50$ at $k_B T = 25$ meV with three different densities of sticky sites i.e. $\rho_s = 0.08$, 0.24, and 0.48 . (B), (D), (F): The corresponding mean number of closed SBs as a function of the end-to-end distance. The presented curves are the averages of 20 runs of stretching and 10 runs of unloading. For all figures, the black symbols indicate loading and the red correspond to the unloading branch.

The bottom row of Figure 4.3.1 shows the number of intact SBs upon cyclic loading tests. The asymmetry between loading and unloading is also reflected in the different behavior of the number of closed SBs during the loading and unloading. For the lowest sticky site density, the sticky sites reform during unloading in a shorter end-to-end distance than the SBs were rupturing during loading. This is because the shorter end-to-end distance, gives the monomers of the chain enough conformational freedom that the sticky sites can fluctuate to find a partner for forming a new SB. For longer end-to-end distances it is highly improbable to find a confirmation of the fluctuating chain with the sticky sites in close spatial vicinity that is necessary

to form a stable SB. The unloading process for the chain with $\rho_s = 0.24$ is almost identical to the case of $\rho_s = 0.08$. Also here the sticky sites recombine mostly at a shorter chain length compared to the rupture during loading. Only in a small region around $L/L_C = 0.6$, the number of intact SBs during unloading is larger than during loading i.e. the sticky sites have recombined earlier than they ruptured. This effect comes from sticky sites that form between sticky sites that are closer along the chain than the sticky sites were during loading (i.e. the topology of the bonds changes). This situation is even more pronounced for the highest SB density. For the chain with $\rho_s = 0.48$ (see Figure 4.3.1(C) and (F)) the number of intact bonds shows three different stages: first, for end-to-end distances close to the contour length (from the contour length till $L/L_C \approx 0.8$), the number of intact SBs increases considerably. Here the sticky sites find their partner in close vicinity along the chain. Because of the elevated length this newly formed SBs are strained resulting in the force plateau upon unloading in the load-displacement curve. This region is absent in the low density case, because due to the low density of sticky sites the sticky sites are that much separated along the chain that it is highly improbable that a stable SB can form at large extensions of the chain. Second, for intermediate end-to-end distances from $L/L_C \approx 0.8$ to $L/L_C \approx 0.6$, the number of SBs stays constant, but the force drops sharply because the SBs relax. a Third, for small end-to-end distances the chain is relaxed enough that the remaining sticky sites that are far apart along the chain can form SBs. Because the end-to-end distance is already small the monomers have enough conformational freedom that this newly formed SBs are not strained. Thus, the number of intact SBs slowly increases again, while the force is slowly decaying to zero. For the low SB density all sticky sites are well separated along the chain and unloading of the chain is described by the third stage only (see Figure 4.3.1A).

4.3.1 Influence of the topology of the bonds

The results of the previous section showed the influence of SB density on the mechanical properties of the chain. It was shown that a higher number of SBs in the chain increases the work to fracture as well as the amount of dissipated energy. In the following section we focus on the influence of the topology of SBs on the mechanical parameters. To investigate the influence of the topology, the starting configuration of the simulations was changed. In contrast to the simulations described in the previous section that were started from a crumpled configuration where the sticky sites were allowed to find their partner randomly, the starting configurations used in this section were set up such that the SBs were forming a predefined topology: the independent, nested and pseudoknotted topology. A sketch of these different topologies can be seen in top row of Figure 4.3.2. Note, that in this set up the SB density is constant $\rho_s = 0.48$, and the only difference in the load-displacement curves stems from the different topologies of the bonds. The bottom row of Figure 4.3.2 shows the load-displacement curves for the corresponding topology. Black and red

dots denote the loading and unloading branch, respectively. Although the number of sticky sites and as a consequence, the initial number of SBs for the three topologies are the same, the loading curves show significant difference resulting a different behavior of the chains.
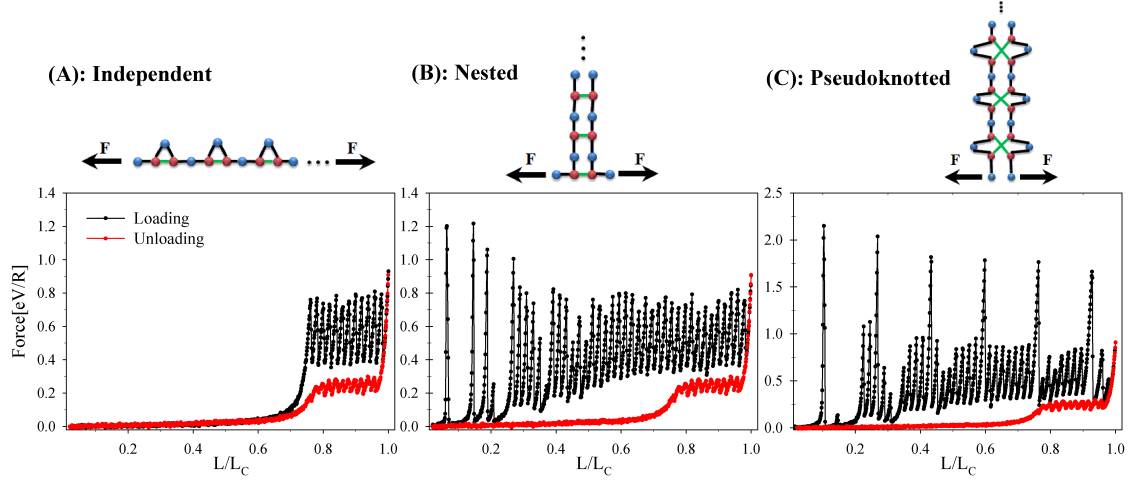
Figure 4.3.2: Starting configurations (top) and load-displacement curves (bottom) for three different topologies of SBs: independent (A), nested (B) and pseudoknotted (C). The black line shows stretching of the different starting configurations until the contour length. The red line shows the subsequent unloading curve which is identical for all structures. The length of the chains was $N = 50$ and the sticky site density $\rho_s = 0.48$. Note that the range of the force is different in (C) than in (A) and (B).

The loading curve for the independent topology starts rising at a larger end-to-end distance compared the other two topologies. In particular, for the independent topology the first SB starts to rupture at approximately $L/L_C = 1 - (\frac{N_S}{2(N-1)}) = 0.76$, while for the nested topology the first SB ruptures at an end-to-end distance of about $L/L_C = \frac{3}{N-1} = 0.06$ and the pseudoknotted topology at an extension of about $L/L_C = \frac{5}{N-1} = 0.1$ (see Figure 4.3.2). Another striking difference in the curves is the number of single peaks denoting the single rupture events upon loading. For the independent case there are exactly 12 peaks, while this number increases by a factor more than three for the other two topologies. For a sticky site density of $\rho_s = 0.48$ there are 24 sticky sites in the system, leading to a maximum number of 12 SBs that can be closed simultaneously. Thus, the number of 12 rupture events for the independent case indicates that after breaking of a SB, the sticky sites do not reform a new stable SB. The much larger number of SB ruptures found for the nested and pseudoknotted configuration shows the opposite: after bond rupture the open sticky sites reform new SBs upon loading. As a result the work under the stretching curve largely increases (see also Table 4.1). For the independent topology the lack of SB reforming during loading leads to a reduction of more than 50 % in the work to fracture compared to the other two cases. It can be concluded that the reforming of

SB has a very strong influence on the work to fracture and, thus, on the toughness of the material. Since E_2, the area under the unloading curve, is constant for all three configurations, the dissipated energy is smallest for the independent configuration $\Delta E = 11.3\ eV$ and increases considerably for the nested and pseudoknotted configuration to about $\Delta E = 41.7\ eV$ and $\Delta E = 50.1\ eV$, respectively (see also Table 4.1 for a summary of the obtained parameters for different configurations).

Starting Config.		$E_1[eV]$	$E_2[eV]$	$\Delta E[eV]$	$\frac{\Delta E}{E_1}[-]$
	$\rho_s = 0.08$	11.4	5.9	5.5	0.48
Crumpled	$\rho_s = 0.24$	22.6	7.42	15.1	0.67
	$\rho_s = 0.48$	36.7	12.84	23.9	0.65
$2nd - Stretching$	$\rho_s = 0.48$	30.0	12.84	17.0	0.57
	Independent	24.2	12.84	11.3	0.47
Regular ($\rho_s = 0.48$)	*Nested*	54.6	12.84	41.7	0.76
	Pseudoknotted	63.0	12.84	50.1	0.80

Table 4.1: The work to fracture E_1, the energy during unloading E_2, the corresponding energy dissipation $E_1 - E_2$ and the amount of dissipated energy $(E_1 - E_2)/E_1$ for the different investigated structures.

Another interesting point concerns the height of the peaks corresponding to single SB rupture events. Although the SBs in the simulation are identical, a variation of the peak height for different elongations of the chain can be observed. For instance, the peaks for the independent configuration have an almost similar height during stretching, while for the nested as well as for the pseudoknotted configuration this height changes during loading. As discussed before and explained in section 4.2 and [78] the effective SB strength is reduced by thermal backbone fluctuations and, thus, significantly depends on the effective chain length defined by the SB. Since, the effective length for the initial peaks of the nested configuration is short ($L/L_C = 0.06$), the peak height is close to the theoretical value, while for the peaks with larger end-to-end distances and, thus, larger effective length, the effective SB strength is reduced (see Figure 4.3.2B). For the independent topology the SBs start to break from $L/L_C \approx 0.75$ and the height of the peaks is almost identical for all SBs rupture events (about $0.8\ eV/R$) (see Figure 4.3.2A). In the pseudoknotted configuration 6 sharp peaks due to the rupture of 6 parallel SBs can be observed and in between these high peaks other peaks of approximately half the height are observed that are due to the rupture of reformed single SBs. Similar to the variation of the peak height for the nested topology, the height of the high peaks corresponding to the pseudoknotted topology reduces from $2.25\ eV/R$ to $1.7\ eV/R$ (see Figure 4.3.2C).

Influence of the topology on the mean bond length

As discussed before the mechanical performance of a single polymer chain crucially depends on the SBs topology. In the following part the influence of the three extreme

topologies (independent, nested and pseudoknotted) on the SB length distribution and the mean bond length is investigated. For a sketch of the topologies see the inset in Figure 4.3.3. For small end-to-end distances (not shown) all three investigated topologies show the same behavior: the SBs are unloaded and the bond-length distributions are identical and centered at the equilibrium bond length $r_0 = 3$.
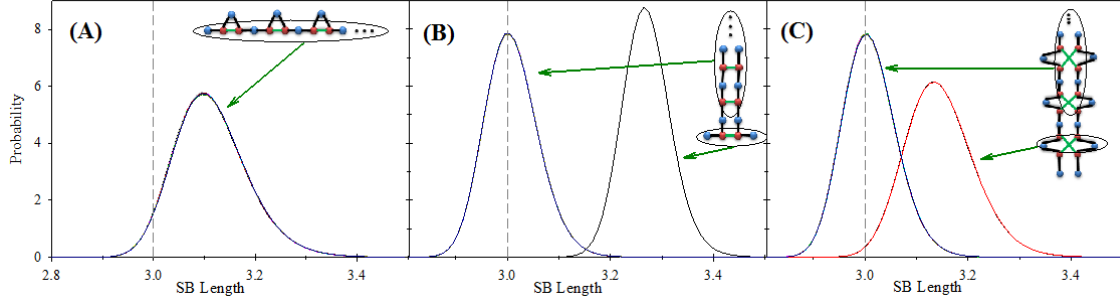
Figure 4.3.3: The sacrificial bond length distribution for different topologies. (A) Independent at an end-to-end distance $L/L_C = 0.75$. All 12 distributions are identical and centered at $d = 3.09$ ($\varepsilon = 0.03$). (B) Nested at $L/L_C = 0.06$. The SB that has been formed between the two outer sticky sites shows a shifted bond length distribution centered at $d = 3.26$ ($\varepsilon = 0.09$). The distribution of the other 11 bond lengths are identical and centered at $d = 3$. (C) Pseudoknotted at $L/L_C = 0.1$. Here we have two SBs that shield the 10 others. The two loaded SBs are centered at 3.13 ($\varepsilon = 0.04$), while the others are unloaded.

The situation changes, when the end-to-end distance is increased until the SBs start being loaded (but still in the entropic regime, i.e. with decreasing temperature the load would drop to zero). Figure 4.3.3(A) shows the bond-length distribution for the independent topology and $L/L_C = 0.75$. The histogram shows that all the 12 distributions are identical and that the mean bond length is about 3.09 (the equilibrium bond length is $r_0 = 3$, i.e. the bond strain is $\varepsilon = 0.03$). The nested and pseudoknotted topology (Figure 4.3.3B and C) break the symmetry inherent to the independent case. At the onset of loading ($L/L_C = 0.06$ for nested and $L/L_C = 0.1$ for pseudoknotted) it is only the outermost SBs that take the load, while the inner bonds are unloaded (see Figure 4.3.3B and C). As a consequence the mean sacrificial bond length decreases in the nested and pseudoknotted topology because most of the bonds are unstrained. We find for the independent topology the mean bond length is $< d >= 3.09$ ($< \varepsilon >= 0.03$), while it is $< d >= (11 * 3 + 3.26)/12 = 3.02$ ($< \varepsilon >= 0.007$) for the nested and $< d >= (10 * 3 + 2 * 3.13)/12 = 3.02$ ($< \varepsilon >= 0.007$) for the pseudoknotted topology.

As these results show at the onset of loading the mean bond length are different for different topologies. Nevertheless, the onset of loading is at significantly different end-to-end distances (compare $L/L_C = 0.75$ and 0.06 for the independent and nested topology, respectively). Consequently, it can not clearly be distinguished if the
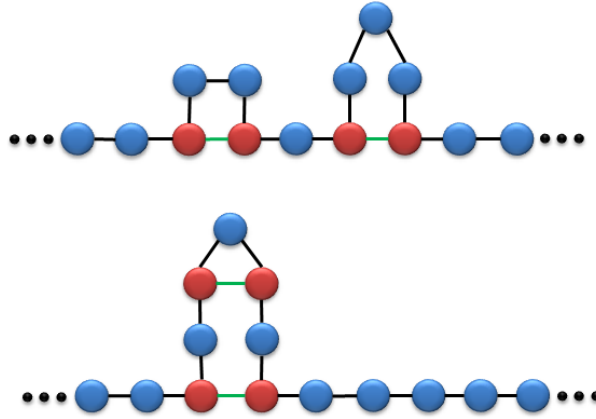
Figure 4.3.4: A simple model to measure SB length distributions for an independent (above) and nested (below) configuration. In this configuration the end-to-end distance of the chains is identical. Thus, differences in the sacrificial bond length distribution are not due to different end-to-end distances, but only stem from the different SB topology.

change in bond length is due to the different topologies or due to the different end-to-end distance. Thus, in a simplified setting with 4 sticky sites only an independent and a nested configuration was constructed that shows the onset of loading at exactly the same end-to-end distance (see Figure 4.3.4). Nevertheless it should be noted that the position of the sticky sites along the chain are not identical for the two topologies.

Figure 4.3.5 shows the load-displacement curve upon loading and the bond length distribution for the two structures shown in Figure 4.3.4 at $L/L_C = 0.897$. Both configurations experience the same amount of force at the chosen end-to-end distance. Therefore changes in the distribution can be attributed purely to the different topologies. Similar to the previous results shown in Figure 4.3.3 also here both SBs of the independent topology behave identically, while the inner nested SB is shielded by the outer. It is found that $< d >= 3.115$ and 3.06 for the independent and nested topology, respectively. Thus, also in this setting the nested topology has a reduced mean bond length compared to the independent case.

This results may have implications for experiments that measure the mean bond length in a system with SBs, like e.g. EXAFS. Measuring a change of bond length over time may indicate a change of the topology of the involved bonds. In future the results presented in this thesis may help in deciphering such processes.

Backbone rupture before L_C

Our previous results showed that the topology and arrangement of the SBs improves the mechanical response of single polymer chains. These results have been published in [78, 92]. In this section it is investigated which topology of SBs gives the highest strength. In particular, it will be shown that even if the strength of SBs (the binding energy) is weaker than the covalent bond (by factor of four in the model
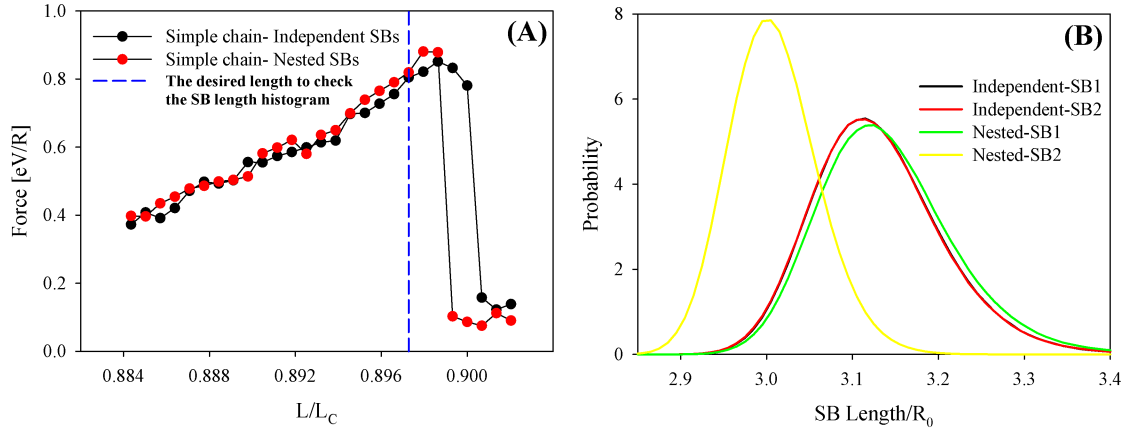
Figure 4.3.5: (A) The load-displacement curve for the two configurations shown in Figure 4.3.4. The results show that the force for the two configurations is identical. The bond length distributions were evaluated at the indicated end-to-end distance (vertical dashed line) assuring that both systems experience the same amount of mean force. (B) SB length distribution for the two configurations shown in Figure 4.3.4 at the end-to-end distance $L/L_C = 0.897$ indicated by the vertical dashed line in (A). The SB length distribution for the two SBs of independent topology are identical, while the distribution for the nested configuration is different. In the latter case the outer SB shields the inner one from an elevated load.

presented in this thesis) there exists a certain topology that the strength of the SBs exceeds the strength of the polymer backbone. In more detail, if more than four SBs are loaded in parallel and, thus, stretched simultaneously, then their combined strength exceeds that of the covalent back bone. To investigate this effect a pre-defined structure as shown in Figure 4.3.6A is investigated. In this structure the SBs are formed between pairs of $(1, 20)$, $(3, 22)$, $(5, 24)$, $(7, 26)$ and $(9, 28)$. Here the molecule forms a large loop (something like a minimal parallel β-sheet) and the five SBs present in the structure are loaded in parallel leading to an effective shear force on the backbone. The corresponding load displacement curve is the black line in Figure 4.3.6B. At $L/L_C = 0.65$ the load rises to the strength of the backbone given by 4 eV/R and then drops suddenly to zero. This behavior is characteristic for backbone rupture, because the force does not rise again. The red and green curve in the same figure shows the load-displacement curve for a similar configuration with a reduced number of 4 and 3 SBs, respectively. These two configurations are weaker than the covalent backbone. Thus, it is the SBs that rupture resulting in a sequence of peaks decaying in height. That the curve corresponding to 3 SBs shows 4 peaks is due to reforming of opened sticky sites during stretching (see Figure 4.3.6B). In summary, the configuration with 5 SBs loaded in parallel shows a higher strength than the other two other configurations with four and three SBs, respectively. Thus, the chain with five parallel SBs is considerably stiffer and stronger but on the other hand more brittle and less extensible than the other two structures. Most interest-

ingly, these mechanical properties can be tuned only by manipulating the topologies of SBs and leaving their absolute number constant.
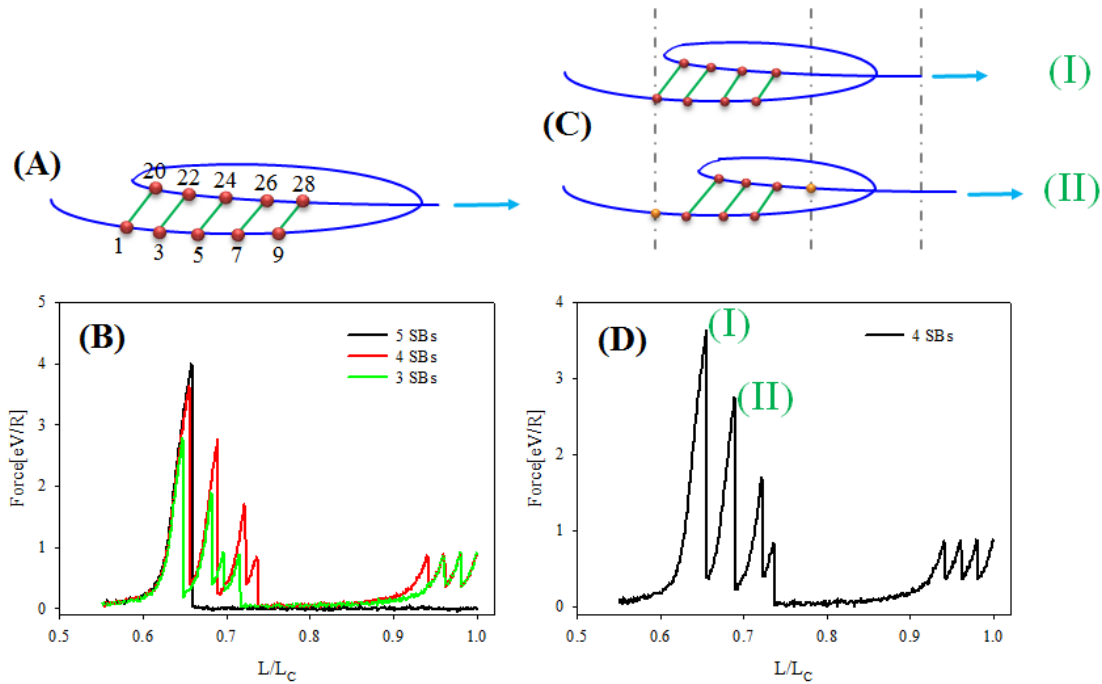
Figure 4.3.6: Stretching of a single chain with the optimal pseudoknotted SB configuration as shown in (A). (B) shows the corresponding load-displacement curve for a single chain with 5, 4 and 3 optimal SBs. Stretching of the chain causes a shear strain on the SBs loaded in parallel. (C) The configuration of the chain with 4 SBs and the mechanism of rupture during tensile loading and (D) shows the load displacement curve for the corresponding chain.

In order to understand the mechanism of SB rupture for the optimum configuration, the system with four SBs as shown in Figure 4.3.6C is investigated in more detail. Figure 4.3.6D shows the loading response of the chain. Upon loading, first, all four SBs break simultaneously and try reforming new stable SBs. Interestingly, they form another pseudoknotted loop consisting of three SBs (Figure 4.3.6D-II) instead of a random SB configuration. The reason is that when the length of the chain increases by a tensile load, the relative displacement for the upper sticky sites shown in Figure 4.3.6C is much larger than for the sticky sites in the lower part of the chain. The six inner sticky sites are still in close vicinity and form an optimal pseudoknotted loop by three SBs. A similar mechanism occurs for the chain with three SBs as is demonstrated by the green curve in Figure 4.3.6B. These results show that it is possible to tune the mechanical properties of a single polymeric chain by changing the topology of the involved SBs only and leaving the number of bonds constant. In particular, it is possible to tune the toughness, stiffness and extensibility of the involved molecules.

4.3.2 Implications on self-healing

One of the most important properties of biological materials is their ability to heal and self-repair. One way to achieve this property is to use reversible bonds in their structure. The reversibility allows the material to reorganize the structure and recover the mechanical properties such as stiffness and toughness after the load was released. Nevertheless, the repairing takes some time and the material can not heal instantaneously [107]. Furthermore, the experimental results show that the recovery depends on the temperature and that it speeds up when the temperature is increased. Thus, it was concluded that the SB formation is a random thermally activated process [11]. In the simulations, we can monitor the polymer recovery by investigating the formation of SBs in the starting configuration and during unloading of the loaded structure during a cycling loading experiment.

Although—in contrast to molecular dynamics simulations—Monte Carlo simulations do not directly give a time scale of the involved processes, it is still possible to gain insight on two extreme scenarios of unloading, i.e. infinitely fast and quasi-static unloading. For infinitely fast unloading the time for chain unloading is smaller than the time needed for SB formation. This condition is fulfilled when the sticky sites are introduced in the chain, when the small end-to-end distance of the starting configuration is reached. Here no SB is closed before the structure is completely unloaded. Thus, the unloading is much faster than SB formation. The other extreme of quasi-static unloading has been used as the standard procedure for the unloading branch of a cyclic loading experiment. Here the end-to-end distance was only gradually decreased and the system was given enough time to equilibrate during each simulation step. Thus, the SBs had enough time to form during unloading. All unloading curves shown in this thesis have been obtained for quasi static unloading (e.g. in Figure 4.3.1).

For the case of fast unloading Figure 4.3.7 shows the average number of formed SBs as a function of time in unit of Monte Carlo steps (MCS) for two different SB densities. Both densities show an initially very steep increase in the number of SBs that subsequently slows down for longer times. This behavior was also observed experimentally. For cyclic loading experiments of the mussel byssus with different waiting times between consecutive loading cycles, it was shown that during the first hour after loading almost 70 % of the mechanical properties have been recovered, while the rate of recovery then considerably slows down to a recovery of 95 % after about 168 hours [11].

Since after the chains have been stretched to their contour length all SBs are open, quasi-static unloading yields the same results for all systems with the same density and arrangement of sticky sites. The results of these unloading tests are summarized in Table 4.1. Nevertheless, the topology of SBs after quasi-static unloading differs from the topology after fast unloading that was used for preparing the starting configuration of the first loading. Therefore, the second stretching differs from the first loading as can be seen in Figure 4.3.8 for the chain with $\rho_s = 0.48$.
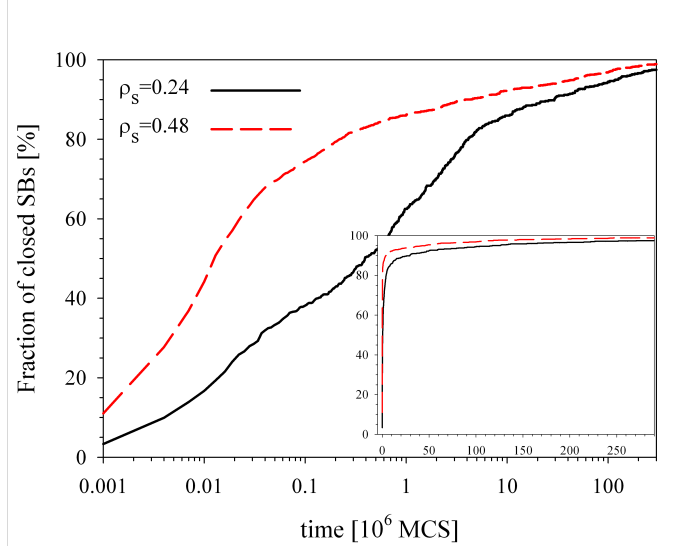
Figure 4.3.7: The number of closed SBs as a function of time for two SB densities. The data are the average of 100 independent runs for each sticky site density. Note, the logarithmic scaling of the time axis. The inset shows the same data with a linear time axis.

$\triangle F$ shown in Figure 4.3.8 is the difference between first (F_1) and second (F_2) loading e.g. $\triangle F = F_1 - F_2$. Whenever $\triangle F$ is negative (indicated by red points) this shows that the second loading had a higher load than the first, while black dots denote $\triangle F > 0$. The results clearly show that on average $\triangle F > 0$ indicating that the area under the first loading is clearly larger than the second loading. The decrease in the work to fracture is approximately 20 % from 36.7 to 30 eV (see Table 4.1) i.e. when the quasi-statically unloaded chains are stretched for the second time, the area under the curve for the second stretching is smaller than the first one. This decrease directly corresponds to the different preparation of the starting configuration that changes the SB configuration of the chain. The starting configuration for the first loading cycle has been prepared by fast unloading the system, while the starting configuration of the second stretching cycle has been prepared by quasi-static unloading. During quasi-static unloading the majority of the reformed SBs are neighbors along the chain. For the system with $\rho_s = 0.48$, $83 \pm 3\,\%$ are independent SBs and the $17 \pm 3\,\%$ are of nested configuration after quasi static unloading. The starting configuration obtained by fast unloading was made of $72 \pm 3.4\,\%$ independent, $14.5 \pm 2.4\%$ nested and $13.5 \pm 2.1\%$ pseudoknotted SBs. The decrease in the number of pseudoknotted configurations is responsible for the 20 % of the reduced area for the second stretching. Thus, the results presented indicate that one way to achieve a complete recovery is to ensure a fast unloading process. A similar mechanism might explain why there are a clear difference in the load-displacement curves of titin in consecutive cycles, where the second stretching cycle has a lower number of the characteristic saw-tooth pattern corresponding to bond rupture [4, 23].
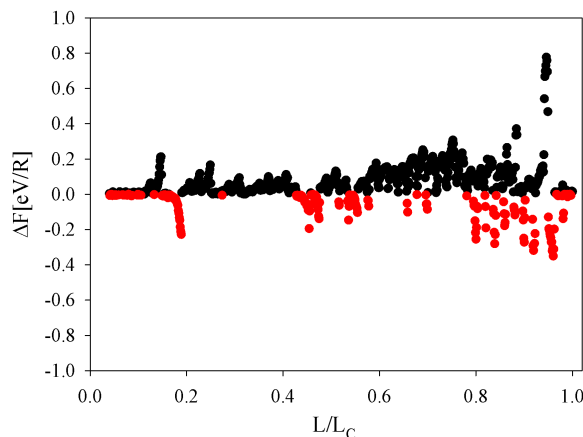
Figure 4.3.8: The difference $\Delta F = F_1 - F_2$ of the load-displacement curves for the first and second stretching. Black points denote $\Delta F > 0$ and red points $\Delta F < 0$, respectively. Clearly, on average $\Delta F > 0$ showing that the first stretching cycle shows on average a higher load than the second. This results in an approximately 20 % decrease in E_1 - see also Table 4.1.

4.3.3 Conclusion

Using a simple model, the influence of the number and topology of SBs on the mechanical behavior of polymeric chains during cyclic loading was investigated. In general both, the work to fracture E_1 and the energy dissipation ΔE, increase with increasing sticky site density. While for low sticky site densities a discrete rupture of single SBs can be observed, for high sticky site densities these single peaks merge into one large plateau. Computational cyclic loading experiments showed a pronounced asymmetry between the stretching and unloading branch for all sticky site densities. This hysteresis is due to two different reasons: first, the SBs reform at elongations smaller than they rupture and, second, the SBs reform between sticky sites with a smaller distance along the chain than they have been originally formed. Consequently upon quasi-static unloading the topology of the SBs changes. In general, the amount of SBs of the independent type increases on cost of the pseudoknotted type.

It was shown that the nested and pseudoknotted topology possess superior mechanical properties compared to the independent configuration. The work to fracture and the dissipated energy are increased a factor more than two from a purely independent to the pseudoknotted topology. This large increase is due to a pronounced reforming of the bonds ruptured during loading. After a quasi-static unloading the formation of SBs of independent type are favored on cost of the pseudoknotted behavior. Thus, the mechanical performance of the polymer is deteriorated when it is stretched a second time. It can be concluded that after release of the load a fast return to its initial state is essential for the polymer to maintain its mechanical performance.

Although simple the model presented captures several aspects of sacrificial bonding also found in experiments. These are, first, the characteristic sawtooth patterns found for low sticky site densities, second, the pronounced hysteresis in cyclic loading with an energy dissipation of 70 % for high sticky site densities, third, the characteristic time scale of reformation of SBs after unloading with an initial fast and a subsequent slow recovery, and fourth, the deterioration of mechanical properties during second loading depending on unloading speed. In addition, it has been found that the mean SB length is different for chains with a constant number of sticky sites but different SB configuration. Thus, it was shown that the SB topology may change the mean bond length of SBs, which might have important implications for the interpretation of experiments that measure the mean bond length, like e.g. EXAFS methods.

4.4 Influence of the arrangement of sticky sites

In the previous section we have discussed the influence of SB density and topology on the mechanical properties of single polymer chains. In this section we will focus on the impact of a different arrangement of SBs in the chain on their mechanics. Three different arrangements of sticky sites (ordered, patches and random, respectively) have been investigated for a chain with $\rho_s = 0.24$, and two arrangements (ordered and random) have been investigated for $\rho_s = 0.08$. For each case, 20 independent simulations were generated and tested. The starting configurations were prepared by introducing the sticky sites in the crumpled configuration with the short end-to-end distance $L/L_C = 0.04$ (corresponding to fast unloading as discussed in the previous section). The top row of Figure 4.4.2 shows a sketch of the different arrangements. For the ordered arrangement the sticky sites are introduced regularly with always the same number of non-sticky sites in between. For example, in the chain with $\rho_s = 0.08$ the sticky sites are separated by ten non-sticky sites and for $\rho_s = 0.24$ three non-sticky sites are in between two neighboring sticky sites. For the patches arrangement, the chain was divided into three segments of equal length. The sticky sites have been introduced only in the outer two patches such that each sticky site is between two non-sticky sites; the middle segment is without any sticky sites. In the third arrangement the sticky sites were distributed randomly along the chain. The only constraint was that the two ending beads were not allowed to be sticky, as well as it was forbidden that two sticky sites are direct neighbors.

Figure 4.4.1 shows load-displacement curves of a chain with $\rho_s = 0.08$ and two different sticky sites arrangements; ordered and random, respectively. The five peaks in Figure 4.4.1(A) for the ordered arrangement have been explained before section 4.3 and [78]. A parameter directly related to the toughness of the chain is the work to fracture $W = E_1 + E_C$. E_1 is the work to elongate the chain until the contour length and $E_C = 25\ eV$ is the additional contribution of backbone stretching and rupture when elongating the chain over its contour length. As discussed before in
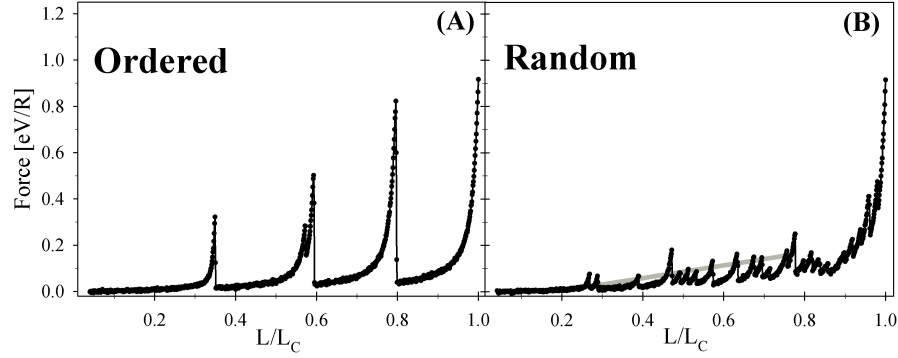
Figure 4.4.1: Load-displacement curves for an ordered and random arrangement of sticky sites with $N = 50$, $k_B T = 25$ meV and $\rho_s = 0.08$. In the random arrangement the apparent stiffness of the material (i.e. the mean slope of the initial part of the curve) is indicated.

section 4.3, the backbone contribution is identical for all systems. The work to fracture for $\rho_s = 0.08$ with the ordered and random arrangements are $E_1 = 11.38\,eV$ and $E_1 = 11.45\,eV$, respectively (E_C is omitted throughout this thesis) (see also Table 4.2).

The strength F_m of the chain is calculated as the maximum amount of force after subtracting the pure covalent contribution during the loading test. The pure covalent contribution is given by a loading test of the bare chain without any sticky sites. For the ordered arrangement it is found that $F_m = 0.77 eV/R$ for the ordered distribution (in particular also lower than the theoretical strength of $F_m^{theory} = 1.25\,eV/R$ - see section 4.2). Loading of the chain with a random distribution of sticky sites created SB rupture events in different end-to-end distances due to different distances between the sticky sites along the chain. Consequently, the load-displacement curve shown in Figure 4.4.1(B) indicates a higher number of peaks compared to the ordered arrangement, but with a lower height, because after averaging the peaks are smeared out. Thus, the strength for random arrangement is $F_m = 0.26\,eV/R$ which is almost three times smaller than the strength of the ordered arrangement.

Another parameter that can be deduced from the load-displacement curves is the apparent stiffness. In this thesis the apparent stiffness is defined as the mean slope of the first increase in the load-displacement curve. This is in contrast to the normal stiffness which is defined as the slope of the first peak in the curve and describes the elastic behavior of the material. In other words, the apparent stiffness is a measure of how much force is needed to elongate the molecule including the plastic deformation of the material, i.e. including the rupture of bonds that is characteristic for plastic deformation. For $\rho_s = 0.08$ and the random arrangement the slope of the gray line in Figure 4.4.1(B) shows the apparent stiffness which is about $Y = 1.84\,meV/R^2$ (see Table 4.2).

Three different arrangements (ordered, patches and random) have been generated

and tested for the chains with $\rho_s = 0.24$. Figure 4.4.2 shows the arrangement of sticky sites along the chain as well as the corresponding load-displacement curves. Figure 4.4.2(A) shows the load displacement curve for $\rho_s = 0.24$ and the ordered arrangement where the two neighboring sticky sites are separated by other three beads. Therefore the distance between them is much smaller than for the chain with $\rho_s = 0.08$ where ten beads are between sticky sites. Consequently, in contrast to the low SB density, the load-displacement curve does not show single peaks but after rupture of each SB the force does not drop to zero. Thus, it is possible to measure the apparent stiffness also for the ordered distribution which is given by $Y = 5.03\, meV/R^2$ and indicated by the gray line in Figure 4.4.2(A). As discussed before the work to fracture depends on the number of SBs and is larger for higher SB densities. We find $E_1 = 22.55\, eV$ for $\rho_s = 0.24$ and $E_1 = 11.38\, eV$ for $\rho_s = 0.08$, respectively. The strength of the chain with $\rho_s = 0.24$ and the ordered arrangement is $F_m = 0.7\, eV/R$ which is almost similar to the strength for $\rho_s = 0.08$ (see also Table 4.2 for a summary of the found parameters). Thus, one can conclude that the strength does not depend on the number of sticky sites for the chains with ordered arrangement.
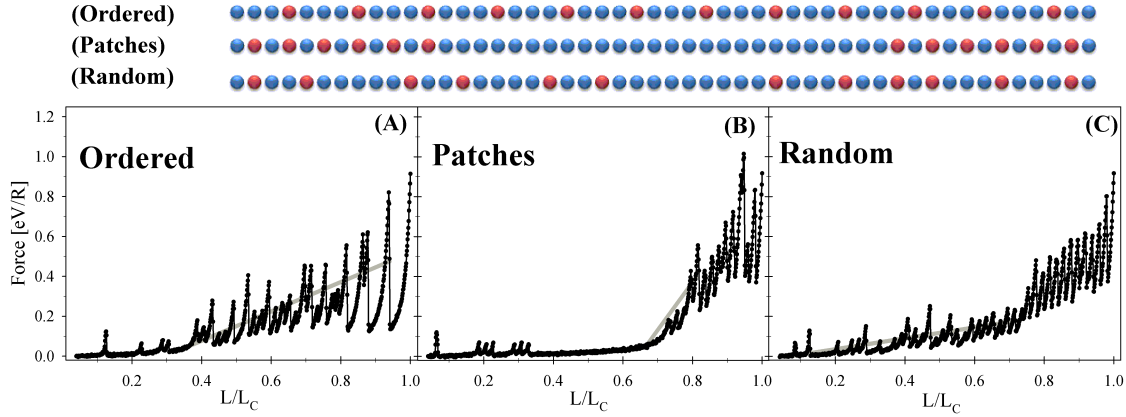
Figure 4.4.2: Load displacement curves for three different distributions of sticky sites (ordered, patches and random) and $N = 50$, $k_B T = 25$ meV and $\rho_s = 0.24$. The gray lines indicate the apparent stiffness of the materials defined as the mean slope of the first part of the load-displacement curve. In the top part of the figure a sketch of the different arrangements of sticky sites are shown (sticky sites are shown in red, non-sticky sites in blue).

When the arrangement changes from ordered to patches, the load-displacement curve shows significant changes that can be seen in Figure 4.4.2(B). For the patches arrangement, a very late onset of the force is observed ($L/L_C \approx 0.7$) and before this length, only a few small peaks can be seen which are due to breaking of a few SBs that have been formed between sticky sites between different segments. Thereafter, the intermediate non-sticky site segment stretches and no force upon loading is observed from $L/L_C \approx 0.3$ to $L/L_C \approx 0.6$. Therefore the force rises abruptly when $L/L_C \approx 0.7$ in a very short length which is the reason for the rather high apparent

stiffness ($Y = 16.26\,meV/R^2$) compared to all other SB densities and arrangements (see Table 4.2). The work to fracture ($E_1 = 19.63\,eV$) is a bit smaller than for the ordered arrangement which is due to the smaller number of reformed SBs during loading.

Finally Figure 4.4.2(C) shows the load-displacement curve for the random arrangement with two distinct regions; below $L/L_C \approx 0.8$ irregular small peaks and above this length more regular peaks with higher heights can be observed. The first region corresponds to the breaking of SBs formed by the sticky sites which are far apart along the chain. Due to the large distance between sticky sites, the SB breaks in a shorter chain length. Nevertheless, the number of intact SBs stays almost constant meaning that after breaking of each SB, the opened sticky sites which are closer together along the chain reform a new SB. When the end-to-end distance of the chain reaches $L/L_C \approx 0.8$, the chain is so much stretched that reforming of SBs stops and the number of intact SBs drops rapidly to zero during further elongation. It is the breaking of this noticeable number of SBs in a short distance that provides the number of peaks with higher amount of force. Compared to the chain with $\rho_s = 0.08$, it is clear that due to the fewer number of sticky sites, the reforming of SBs is not occurring and only a single region of rather low force is observed as shown in Figure 4.4.1(B). The chain with $\rho_s = 0.24$ and random arrangement shows the work to fracture of $E_1 = 23.51\,eV$, the apparent stiffness of $Y = 1.84\,meV/R^2$ and the strength of $F_m = 0.55\,eV/R$.

Table 4.2 summarizes the three discussed parameters to recognize the influence of SB density and arrangement on the mechanical properties of the single chain. The results demonstrate that the work to fracture strongly depends on the number of SBs in the chain and it does not change dramatically with the SB distribution. The work to fracture for the chain of $\rho_s = 0.08$ and two arrangements stays almost constant within error bars but it changes slightly for the chain with $\rho_s = 0.24$. The random and the ordered distribution have an almost similar work to fracture $E_1 = 23.51\,eV$ and $E_1 = 22.55\,eV$, respectively, that moderately decreases to $E_1 = 19.63\,eV$ for the patches arrangement which is a reduction by factor of $20\,\%$.

Thus, it is the number of broken SBs which determine the work to fracture of the material and not the arrangement. For non-reversible SBs, it is expected to have an identical amount of work to fracture for different arrangements even for chains with the two extreme configurations of SBs loaded in series or in parallel. However, the force needed to break parallel SBs is much larger than to rupture the same number of SBs loaded in parallel, but the product of elongation and strength stays constant. It is the reversibility of the SBs allowing for bond reformation after rupture that is responsible for the slight decrease in E_1. Therefore the difference of the work to fracture of the patches arrangement and the other two configurations shows that in the former case the number of reformed SBs is smaller than for the two latter cases. This is because SB rupturing starts in a large end-to-end distance comparable to the second region of the random configuration and the SB reforming is negligible.

SB density	arrangement	$Work\ to\ fracture$ $E_1[eV]$	$Apparent\ stiffness$ $Y[meV/R^2]$	$Strength$ $F_m[eV/R]$
$\rho_s = 0.08$	Random	11.45	1.84	0.26
	Ordered	11.38	–	0.77
$\rho_s = 0.24$	Random	23.51	1.84	0.55
	Ordered	22.55	5.03	0.7
	Patches	19.63	16.26	0.9

Table 4.2: The work to fracture E_1, the apparent stiffness Y and the strength F_m of the different investigated structures in this section.

This situation is reversed when the apparent stiffness is investigated. The results show that the apparent stiffness depends rather on the SB distribution and not on the number of SBs. The apparent stiffness is a measure of how much force needed to elongate the chain and therefore is a result of SB rupture. The measured apparent stiffness for chains with different SB densities (i.e. $\rho_s = 0.08$ and $\rho_s = 0.24$) and random distribution show that the apparent stiffness depends on the arrangement of sticky sites. Although the number of SBs has changed by factor of three for the two investigated densities the apparent stiffness is the same. For the chains with $\rho_s = 0.24$ and different SB distributions the apparent stiffness (shown by the gray dashed line in Figure 4.4.2) changes from $1.84\ meV/R^2$ for the random distribution to $16.26\ meV/R^2$ for the patches arrangement which is almost a factor of nine. This increase for the patches is due to very short distance between sticky sites along the chain (each two sticky sites have only one non-sticky site in between). Thus, the SBs form between sticky sites that are very close along the chain. Therefore the SBs are going to break at large extensions of the chain leading to a late but high increase in the load.

The measured results for the strength show that for the same sticky site density the random configuration has always the smallest strength due to smearing of the SB force peaks over the entire length. The two fold increase in strength for the random arrangement with $\rho_s = 0.08$ and $\rho_s = 0.24$, respectively, is due to the second region of loading for the higher SB density. The chain with $\rho_s = 0.24$ and the patches arrangement has the largest strength of all investigated structures.

This can be explained by a higher probability of formation of the pseudoknotted topology for the patches configuration. Out of 20 simulation runs only 3 showed a pseudoknotted topology for random configuration, while this number increased to 10 for the ordered and patches configuration. The higher strength of the patches configuration is because more of these 10 loops ruptured at the same elongation of the chain.

4.4.1 Conclusion

The results presented in this work suggest the following guidelines for tailoring the behavior of materials by controlling sticky site density and distribution. To maximize the work to fracture (toughness) of the systems, the number of SBs and their ability to reform should be maximized, regardless of the specific distribution of the SBs. For an equal number of SBs, the apparent stiffness of a material can be greatly enhanced when the SBs are distributed such that it is ensured that the force rises over a small change in length of the polymer. In the present study, this was achieved by arranging SBs in patches in particular regions of the polymer, effectively reducing the distance between sticky sites. Finally, any ordered arrangement of SBs yields an elevated strength (both ordered and patches) when compared with a purely random configuration.

The influence of the number and the distribution of SBs on the mechanical behavior of single polymeric chains were investigated. It was shown that the work to fracture, related to the toughness of the material, is mainly determined by the number of SBs that have to be broken when the polymer is elongated, while the apparent stiffness and, to a lesser extent, the strength of the material is strongly dependent on the distribution of SBs in the system. The results presented have important implications for the development of new materials with tailored mechanical properties that employ sacrificial bonding – a concept that is masterly applied by nature to enhance the properties of biological materials.

5 Chain Bundles

The presented results in this chapter show that there are two possibilities of backbone failure before the contour length is reached. Most surprisingly only two cross-links are sufficient to break the backbone. This failure is caused by the topology of the interchain cross-links in the chain bundle where the sticky sites are distributed in an ordered arrangement. However, the backbone failure weakens the strength of the material, but increases the amount of work to elongate the system as well as the apparent stiffness of the bundles. Three configurations prevent backbone failure, first, the small grafting density, second, the low sticky site density and third, the random distribution of sticky sites. Furthermore, the simulations showed a significant difference between consecutive loading cycles. This is due to different topologies of the cross-links.

The presented work in this chapter is based on a model of chain bundles. In our model a chain model is made of nine chains consisting of $N = 50$ beads each, i.e. a total number of 450 beads is present in the system. On each side the end beads of each chain are permanently grafted to a planer substrate. The distance of the two plates defines the end-to-end distance of the chains. The grafting points are located on the positions of triangular lattice. As in the previous chapters some of the inner beads are defined as sticky sites. Always two of these sticky sites can form one reversible cross link. If the formed cross-link is between the sticky sites located in the same chain the cross-link is called an intrachain cross-link and if the two sticky sites are in different chains, it is called an interchain cross-link. In this chapter, first we focus on the possibility of backbone failure before the contour length for a chain bundle caused by weak reversible cross-links. In the previous chapter, it was shown that by manipulating the structure and the cross-link configuration in a single chain,the backbone may rupture before the contour length is reached during elongation as is shown in Figure 4.3.6. Additionally, we also present two simple configurations of sticky sites that lead to backbone rupture before the chains reach their contour length.

The simplified models help to understand the load-displacement curves of more general models with more cross-links and chains in the system. Simulations have been performed to investigate the influence of cross-link density and the grafting density on the mechanical response of the system during loading and cyclic loading tests.

5.1 Different configurations of sticky sites leading to bundle failure

As shown in chapter 4, shearing five cross-links in one of the chains causes backbone failure. For a chain bundle there exist more configurations of cross-links that lead to backbone failure. These are depending on the interchain cross-links configuration and on the grafting density of the chains. Figure 5.1.1 presents three simple configurations containing cross-links to investigate the possibility of backbone failure in the chain-bundles system for a simple system with two chains only each of length $N = 15$. The configurations investigated differ in the grafting density. In the first model the grafting density is large. Here the ending beads of the chains have the distance equal to the equilibrium distance ($d = r_0$) as is indicated in Figure 5.1.1(a,b). The second configuration is characterized by a grafting density where the ending beads of the chains have a larger distance than the equilibrium distance ($d > r_0$) as is shown in Figure 5.1.1(c). The main difference of the two configurations is that in the case of the high grafting density, an interchain cross-link does not experience any force if the involved sticky sites have the same position on their chain. This is because in this case the equilibrium distance of cross-links is the same as the distance between the two chains.

For the case of $d = r_0$ the backbone ruptures when the system contains five interchain cross-links that experience the same force since the strength of each cross-link is the quarter of the covalent bond strength. Therefore the tensile load on the chains would be transmitted as a shear force on the five cross-link that is stronger than one covalent bond. In order to distribute the force among the five cross-link in such a way, the configuration should fulfill two conditions; first: the two connected sticky sites should not have the same positions in their chains (see Figure 5.1.1a). Otherwise the cross-links would not feel any force. E.g. the three right cross-links in Figure 5.1.1b do not experience any load. The second condition is that the distance between the sticky sites in the chains should be the same, otherwise the force does not distribute equally on the five cross-links and the cross-links start to break separately. Figure 5.1.1A shows a load-displacement curve for a configuration fulfilling these two conditions. It shows a sharp peak at $L/L_C \approx 0.8$ due to the failure of one of the two chains and the second rise of the load close to the contour length is because of contribution of the second chain.

If the cross-links have a configuration as shown in Figure 5.1.1b then the cross-links are not loaded in parallel. Here the first two cross-links are formed between beads $(1, 5)$ and $(3, 7)$ (the two number give the position of the beads in the two chains). The other three cross-links are formed between beads having the same position in the chain. In this case the load is taken by the first two cross-links leading to cross-link rupture and the other three cross-links do not contribute in loading since they have the same positions in their chains. Thus, they are not influenced by the tensile load. In Figure 5.1.1B, the first peak shows the breaking of the two cross-links $((1, 5)$
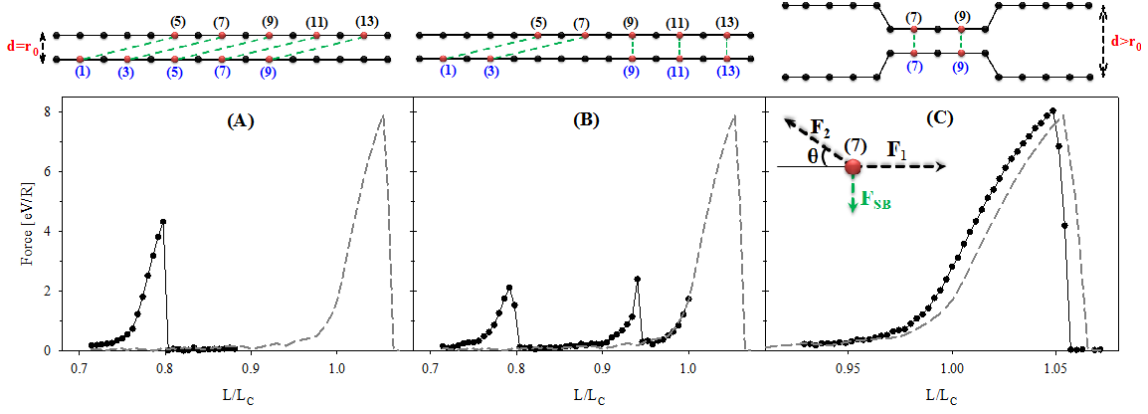
Figure 5.1.1: Different cross-link configurations that lead to backbone rupture of chain bundles. The top row shows sketches of the starting configuration of the system and the positions of the beads along the chain. The numbers shown indicate the number of the beads in the chain. In (A), the connected sticky sites do not have the same Z positions along their chain and therefore five cross-links simultaneously feel a shear load. In (B), the last three cross-links have the same Z positions in their chains and thus the three cross-links do not feel any force. Note that the distance of the chains d (defining the grafting density) is equal to the equilibrium distance of the cross-links in (A) and (B). (C) shows a system with only two cross-links where the distance between the chains is larger than the equilibrium distance of the cross-links. The bottom row shows the load-displacement curves for the corresponding configurations. The gray dashed line shows the load displacement curve for the system without sticky sites. The load-displacement curve for (A) shows a backbone rupture at $L/L_C \approx 0.8$. In (B), there is no backbone rupture and, thus, the peaks in the corresponding load-displacement curve are due to the contribution of the first two cross-links between $(1,5)$ and $(3,7)$. The Load-displacement curve for (C) shows that the backbone ruptures slightly before the system without sticky sites and the inset shows the force analysis on the bead number (7) in the corresponding configuration in the top chain.

and$(3,7)$). Then during stretching new intrachain cross-links are formed between $(1,3)$ and $(5,7)$. The rupture of these two cross-links result in the second sharp peak around $L/L_C = 0.9$. In particular in this configuration there is no failure of the backbone before $L/L_C = 1$.

Most interestingly, if the distance between the chains is larger than the equilibrium distance of the cross-links $d > r_0$, backbone failure is possible even with only two interchain cross-links. This is unexpected because the strength of one cross-link is only a quarter of a covalent bond. Thus, at first sight one would expect that a minimum of 5 sticky sites is needed for reaching a strength larger than the strength of the backbone. Figure 5.1.1C shows a sketch of the corresponding configuration and the inset shows the force analysis of the bead number 7 in the upper chain. In this configuration, the two cross-links hold the intermediate part of the chains parallel together. Thus, they are aligned in the longitudinal direction. F_1 shows the covalent force on the inner part of the loop formed by the two cross-links. F_2 shows

the outer covalent force, F_{SB} shows the force on the cross-link and θ shows the angle between the chain with the direction of tensile load. Investigating the forces show that:

$$\begin{array}{l} F_2 sin(\theta) = F_{SB} \\ F_2 cos(\theta) = F_1 \end{array} \implies F_{SB} = F_1 tan(\theta) \Rightarrow if \begin{cases} F_1 tan(\theta) > 1.25 & SB\ Rupture \\ \frac{F_{SB}}{tan(\theta)} > 5 & Backbone\ Rupture \end{cases}$$

$$(5.1.1)$$

This analysis shows that if $F_1 tan(\theta) > 1.25$ then the cross-link ruptures and if $\frac{F_{SB}}{tan(\theta)} > 5$ the backbone fails. If we insert the values of the strength of sacrificial and covalent bonds $F_{SB} = 1.25\,eV/R$ and $F_1 = 5\,eV/R$ then the backbone ruptures when $tan\,\theta < \frac{F_{SB}}{F_1} = 0.25$ (see inset of Figure 5.1.1C) and the cross-link breaks when $tan\,\theta > \frac{F_{SB}}{F_1} = 0.25$. Therefore, the backbone of the chain will fail by a rupture of one covalent bond located outside the two cross-links (the covalent bond which is not inside the loop formed by cross-links) if $\theta < 15°$, while for $\theta > 15°$, the cross-links break. In this configuration, the two cross-links hold the intermediate part of the chains parallel together. Thus, they are aligned in the longitudinal direction and the force on the backbone is a bit smaller than the net force on the outer part. Consequently, the failure of the backbone in the outer part in the structure results in a sharp peak in the load-displacement curve (see Figure 5.1.1C).

So far we have shown that for special configurations of the cross-links failure of the backbone is possible. Different to the case of a single chain, in a chain bundle even two cross-links may be sufficient to rupture the chain, although the strength of one bond is only one quarter of covalent bond. In the following parts, first we perform stretching and cyclic loading test on the bundles to investigate the influence of grafting and cross-link density on the mechanical properties of the system.

5.2 Stretching of chain bundles

The following sections discuss the mechanical properties of chain bundles containing cross-links by investigating the influence of cross-link density and grafting density on the mechanical properties of the bundles. For this experiment, the starting configuration was prepared by unloading the bundle without sticky sites from the contour length to the starting end-to-end distance $L/L_C \approx 0.18$. Then the sticky sites in the ordered arrangement were introduced and allowed to find their partner randomly to form cross-link. Then, the chain bundle is stretched from the starting end-to-end distance above the contour length i.e. from $L/L_C \approx 0.18$ to $L/L_C \approx 1.06$. The load-displacement curve, the number of intact cross-link and the mechanical parameters are calculated to understand, first, the influence of grafting density on the bundle mechanics for the system with constant cross-link density $\rho = 0.48$.

Second, the most critical grafting density has been chosen to investigate the influence of cross-link density on the mechanical responses of the system.

5.2.1 Influence of the grafting density

Chain bundles with different distances d between the chains and constant cross-link density ($\rho = 0.48$) were stretched to understand the role of grafting density on load-displacement curves. The smaller the distance between the chains, the higher the grafting density. Simulations were performed for several chain distances from $d = r_0$ to $d = 20r_0$. Figure 5.2.1 shows the results for $d = r_0, 5r_0, 6r_0$ and $20r_0$.

Figure 5.2.1 shows that for small end-to-end distances the number of intrachain cross-links is consistently larger than the number of interchain cross-links for all investigated grafting densities. Focusing on the number of interchain cross-links only it can be observed that this number decreases with decreasing grafting density. For the lowest grafting density investigated ($d = 20r_0$) the chains are that much separated that no interchain cross-links can form. Thus, this system behaves like nine independent chains loaded in parallel, i.e. the load-displacement curve is given by multiplying the load-displacement curves of the single chain by nine. During stretching mostly the intrachain cross-links rupture and the opened sticky sites form new cross-links. This reforming is dependent on the grafting density. E.g. the number of interchain cross-links rises for the system with $d = r_0$ and $d = 6r_0$ from $L/L_C \approx 0.5$ and $L/L_C \approx 0.8$, respectively while for the system with $d = 20r_0$ no interchain cross-link forms. Because the end-to-end distance increases, the crumpled starting structure straightens and the probability of forming interchain cross-link is largely increased. Most important even a small number of interchain cross-links hold the chains close together. In particular for the system with $d = 5r_0$ and $6r_0$, at first there are only few interchain cross-links but upon stretching this number suddenly increases as is shown in the insets of Figure 5.2.1.

In Figure 5.2.1 orange lines in the load-displacement curves denote the first chain rupture during stretching. For $d = r_0$ the interchain cross-link configuration as discussed shown in Figure 5.1.1a causes the backbone rupturing, while for $d = 5r_0$ both discussed models of backbone failure are possible i.e. backbone failure is possible with two or more parallel interchain cross-link (see Figure 5.1.1a and c). Because increasing the distance between the chains (i.e., decreasing the grafting density) decreases the number of interchain cross-links, grafting density is the most crucial parameter determining backbone rupture. For the systems with $r_0 \leq d \leq 5r_0$ upon stretching the number of interchain cross-links increases and the first backbone rupture occurs at smaller end-to-end distances (see also Figure 5.2.2A).

Simultaneously the work to elongate the chain to its contour length increases. This result seems to indicate that the work to elongate the molecule is directly related to the position of the first backbone rupture (see Figure 5.2.2A,C). Figure 5.2.2B shows the strength of the bundle for different grafting densities. The strength is
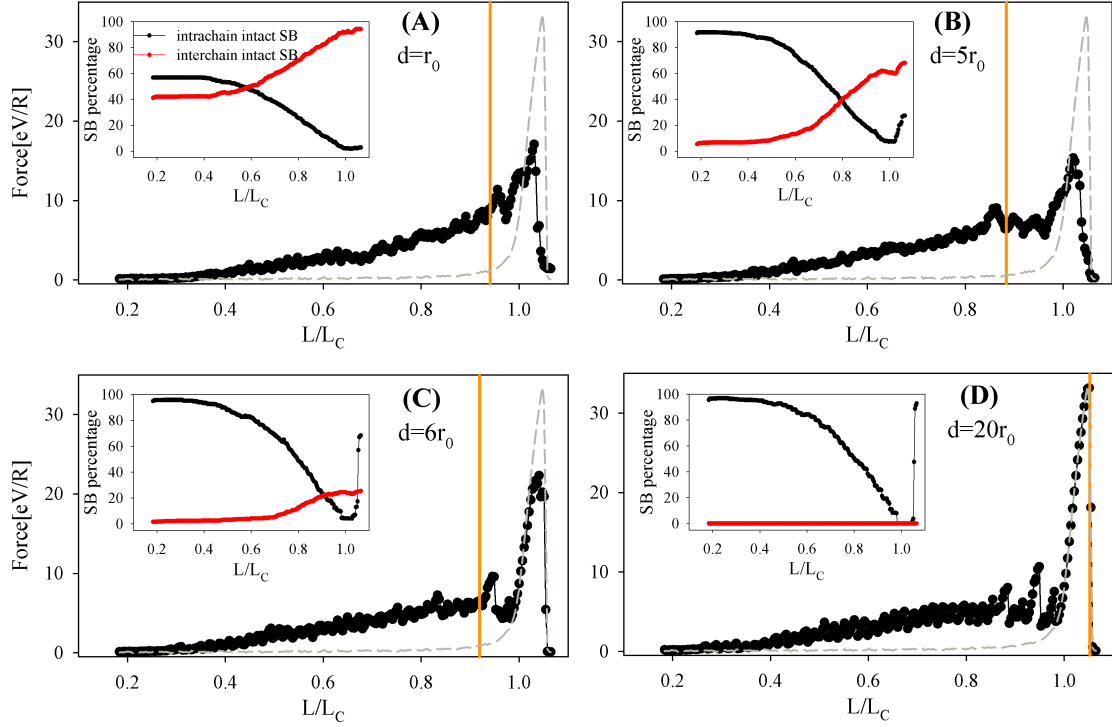
Figure 5.2.1: Load-displacement curves for systems with $\rho = 0.48$ and different grafting densities. The distance between the chains is (A)$d = r_0$, (B)$d = 5r_0$, (C)$d = 6r_0$ and (D)$d = 20r_0$. Black dots show the load-displacement of the system, while the gray dashed line shows the load-displacement curve for the bare system without cross-link. The solid orange line indicates the position of the first backbone rupture. The insets show the averaged percentage of intact cross-links. Black dots show the intrachain intact cross-links and red dots denote the interchain intact cross-links.

defined by the maximum load the system can sustain. For all investigated systems this maximum load occurs after the system was stretched to its contour length. Because at extensions larger than the contour length all covalent bonds rupture, the strength determined in our model is a measure of the number of unbroken chains when reaching the contour length. As an example, the strength for $d = r_0$ is larger than for $d = 2r_0$ showing that the number of broken chains before reaching the contour length is larger for $d = 2r_0$ than for $d = r_0$. Figure 5.2.2D shows the work to fracture that (differently from the single chain case) is significantly different from the work to elongate the system. It is the chain failure before reaching the contour length that changes the situation. The work to fracture is now related to the strength of the system. The system with larger strength need more energy to fracture the system (see Figure 5.2.2B,D).

For the configuration with $d = 6r_0$, the grafting density is a bit smaller than in the $d = 5r_0$ case, but the number of interchain cross-links upon stretching is much
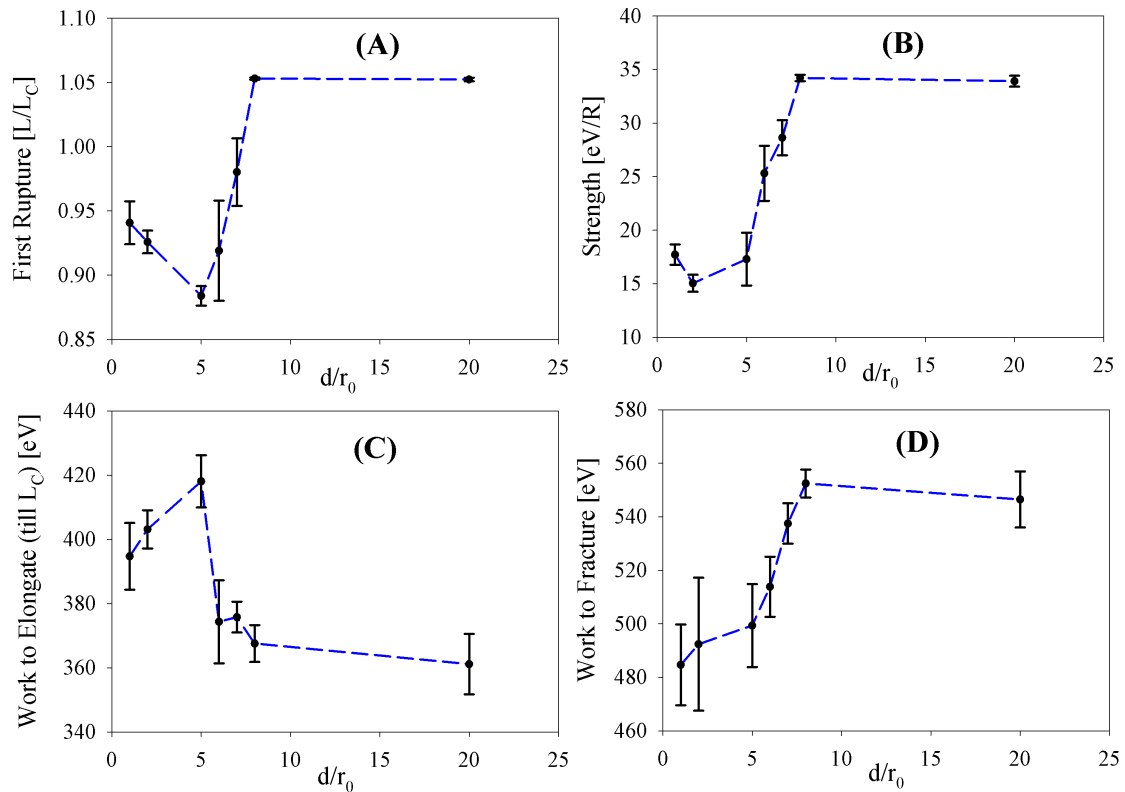
Figure 5.2.2: Mechanical parameters for systems with $\rho = 0.48$ and different grafting densities. The blue dashed line is a guide to the eye. (A) shows the position of the first backbone rupture, (B) shows the strength of the systems, (C) shows the work to elongate the chains till the contour length and (D) shows the work to fracture.

lower and thus, the probability of backbone rupture before reaching the contour length is strongly reduced (see Figure 5.2.1B,C). Comparison of the data shown in Figure 5.2.2 shows the large change in the mechanical behavior for systems with grafting densities between $d = 5r_0$ and $10r_0$. In this range of grafting densities the systems essentially evolves from a system consisting of many interacting chains to a system consisting of many non-interacting, independent chains. This is shown by the steep increase in the position of the first backbone rupture from a value well below to a value well above the contour length. Simultaneously the strength as well as the work to fracture rise considerably, while the work to elongate the molecule shows a significant drop.

5.2.2 Cross-link density

The results of the influence of the grafting density on the mechanical properties of chain bundles indicated that the first rupture happens earlier for chain bundles

with $d = 5r_0$. This system also showed the largest amount of energy to elongate the molecule till the contour length. Therefore in the following the system with $d = 5r_0$ has been chosen to investigate the role of cross-link density on the mechanical response of the systems. Three different cross-link densities $\rho = 0.08, \rho = 0.24$ and $\rho = 0.48$ were studied. For all densities the sticky sites are distributed in the ordered arrangement i.e. the distance between the sticky sites along the chains are identical.

For $\rho = 0.08$ (see Figure 5.2.3A) a few low peaks before $L/L_C = 0.8$ can be observed that are due to the rupture of mostly intrachain cross-links. The inset in the figure shows that the number of interchain cross-link increases upon loading on cost of the number of intrachain cross-links. Increasing the density of cross-links to $\rho = 0.24$ and $\rho = 0.48$ (see Figure 5.2.3B,C) causes the change of discrete cross-link rupture for $\rho = 0.08$ to the continuous rupture for cross-links in $\rho = 0.48$. During stretching, the intrachain cross-links start to break and more interchain cross-links are formed. thus the backbone rupture occurs earlier for a system with higher number of cross-links (compare the shift of the orange line indicating first backbone rupture in Figure 5.2.3 for the different densities). There is no backbone rupture before reaching the contour length for the chain with $\rho = 0.08$. Thus, the strength of the bundle with $\rho = 0.08$ is identical to the strength of the bundles without cross-link i.e. all chains are intact and are, thus, contributing to the strength when the system finally breaks at extensions larger than the contour length.
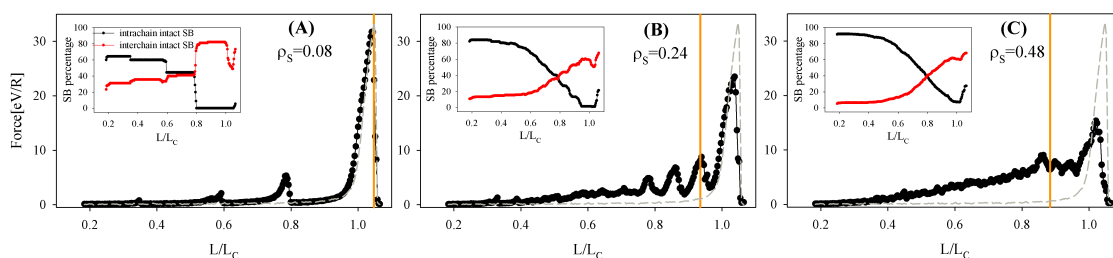
Figure 5.2.3: Load-displacement curve for the system with $d = 5r_0$ and different cross-link densities: (A) $\rho = 0.08$, (B) $\rho = 0.24$ and (C) $\rho = 0.48$. The black symbol shows the loading response of the chain bundles. The gray dash line shows the loading curve of the bundles without sticky sites and the solid orange line indicates the first backbone rupture upon loading. The inset figures denote the intact cross-link percentage whereas the black dots shows the percentage of intrachain cross-links and the red shows the interchain cross-link percentages upon loading.

The work to fracture and also the work to elongate the system till the contour length are higher for higher cross-link densities. Furthermore, Figure 5.2.3 shows that the apparent stiffness increases when the density of cross-links increases. Therefore the mechanical properties of chain bundles strongly depend on the density of cross-links in the system. In one hand increasing cross-links increases the area under the loading curves as well as the apparent stiffness, while on the other hand it may provide the

backbone failure effectively weakening the material. Additionally a broken backbone can not recover again.

5.3 Cyclic loading on chain-bundles

This section describes cyclic loading experiments on systems with a constant cross-link density of $\rho = 0.48$ and different chain distances. Then the cyclic loading test is performed on the system with $d = 5r_0$ and different cross-link densities $\rho = 0.08$, $\rho = 0.24$ and $\rho = 0.48$. The sticky sites are distributed in ordered arrangement for all densities, i.e. the distance between the sticky sites along the chains are identical. In these simulations the bundles are stretched to their contour length. Subsequently the loading is reversed to unload the system until an end-to-end distance of $L/L_C \approx 0.18$ is reached. Then the structures are stretched second time to $L/L_C = 1.06$ the extension at which all chains fail (see Figure 5.3.1, Figure 5.3.3).

5.3.1 Influence of grafting density on cyclic loading

Figure 5.3.1A shows the load-displacement curve for cyclic loading tests of bundles with $d = r_0$ and $\rho = 0.48$. The result of the first stretching is similar to the previously shown results. The only difference is that the chains are loaded till the contour length and not beyond. Thus, the behavior of intact cross-links in the system is the same as shown previously where the intrachain cross-link breaks and the interchain cross-links reform during stretching (see Figure 5.3.1A,a).

Upon unloading, the force drops fast and provides a large asymmetry between loading and unloading. Simultaneously the number of intact interchain and intrachain cross-links slightly increase. The second loading is significantly different to the first loading. During the second loading the cross-links do not contribute to the loading and the system behaves like bundles without cross-links. The significant difference between the first and second stretching cycle is caused by the different topologies of cross-links during these two tests. In the starting configuration 60 % of the cross-links were intrachain and 40 % interchain cross-links. Upon loading all intrachain and some of the interchain cross-links rupture. The only cross-links that persist are interchain cross-links that are formed between sticky sites that have the same position in their chains. This is due to the special grafting density that ensures that the distance of the chains equals the equilibrium distance of the cross-links. Furthermore, due to the ordered arrangement and the appropriate distance of the chain, most of the cross-links that reform are formed between sticky sites at the same position in different chains. As a result, during the first stretching cycle almost all the cross-links are transformed into interchain cross-links (at the end of the first stretching cycle when the contour length is reached, 96 % of the cross-links are interchain). These cross-links do not contribute to the loading. Nevertheless,

71
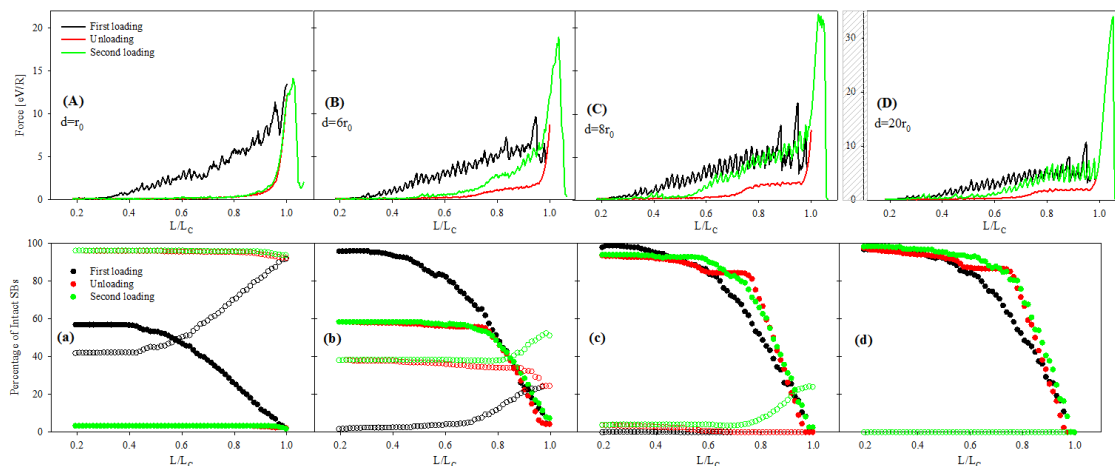
Figure 5.3.1: Cyclic loading and the number of intact cross-links for the system with $\rho = 0.48$ and different grafting densities for $d = r_0, d = 6r_0$, $d = 8r_0$ and $d = 20r_0$. The figures shows the load-displacement curve of the system (top) and the number of intact cross-links (bottom) for different grafting densities, the black curve shows the first stretching of the system until the contour length, the red curve shows the unloading and the green curve shows the second stretching failure of the system. In the bottom row the closed symbols show the number of intact intrachain cross-links and the open symbols show the number of interchain cross-links. The numbers correspond to first stretching (black), unloading (red) and second stretching (green).

the cross-links present reduce the fluctuations of the chains. This effect was also reported in the work of [74, 66] for a different rigidity of the chain. Because the topology of the starting configuration was forming randomly, there is also the possibility that some cross-links are of the topology that leads to backbone failure as discussed in the last section. On average 2.4 chains fail during the first stretching before the contour length is reached. The newly formed topology during loading and unloading of the structure does not allow for any backbone rupture before L_C is reached. Thus, during second stretching the system fails by rupture of the intact chains after the contour length was reached. Nevertheless, the ultimate force for the second loading is much smaller than for the system without cross-links because of the rupture of some chains during the first loading (see Figure 5.3.1A,a).

As discussed before the number of interchain cross-links in the starting configurations is lower for systems with smaller grafting densities. For bundles with $d \geq 6r_0$, almost no interchain cross-links are formed. During loading some interchain cross-links form but still this number is lower for systems with smaller grafting density. For example, for bundles with $d = r_0$, 40 % of the formed cross-links in the starting configuration are of interchain type and after loading to the contour length this number increases to about 91 %. For the system with $d = 6r_0$ the number of interchain cross-link changes from about 2% to 24% from the starting configuration to the fully elongated chain (see Figure 5.3.1b). During unloading this number further increases

to approximately 40%. (see Figure 5.3.1b) . Thus, the starting configuration for the second stretching cycle is characterized by 40% inter- and 60% intrachain cross-links. This difference to the initial starting configuration for the first stretching results in the difference between first and second loading as well as in the backbone rupture during the second loading cycle before the contour length (see Figure 5.3.1B). The influence of the backbone rupture can be figured out by comparing the strength (maximum force) of each system with the bundle $d = 20r_0$ where no backbone failure occurs. The strength of the system $d = 20r_0$ is about $34\ eV/R$ but this value decreases for $d = 8r_0$ and $d = 6r_0$ to ≈ 22 and $\approx 19 eV/R$, respectively (please note the different scaling of the force axis in Figure 5.3.1D compared to the others).

For a grafting density corresponding to $d = 8r_0$ (see Figure 5.3.1c) not a single interchain cross-link is formed during the first loading. Nevertheless, during unloading a small number of interchain cross-links forms at elongations of $L/L_C \approx 0.5$. These few cross-links keep the chains at a small distance such that during the second loading after rupture of some intrachain cross-links, the now open sticky sites form even more interchain cross-links starting from $L/L_C \approx 0.8$ (see the thin green dots in Figure 5.3.1c). These interchain cross-links lead to failure of the backbone before the contour length while there was no backbone rupture during first loading (see Figure 5.3.1C). This effect is effectively weakening the system. The situation for $d = 20r_0$ is completely different. The chains are completely independent from each other because their distance is so large that no interchain cross-link can form during the simulations (see Figure 5.3.1d). Nevertheless, the first and the second loading are still slightly different similar to the single chain results shown in section 4.3 (see Figure 4.3.8).

Thus, it can be concluded that increasing the distance between the chains (decreasing the grafting density) reduces the number of interchain cross-link for the first loading cycle. The number of interchain cross-link after the first loading is about 90 % for $d = r_0$ and drops to about 25 % for $d = 6r_0$ and to zero for $d = 8r_0, 20r_0$. In this elongation no intrachain cross-links is formed and thus some of the sticky sites are opened (see bottom row of Figure 5.3.1). Therefore, during unloading the open sticky sites can form intrachain cross-links specially for the systems with low grafting density $6r_0 \leq d \leq 20r_0$ resulting in a very low plateau in the corresponding force-displacement curves. The low plateau (see red curves in Figure 5.3.1B, C and D) shows that the sticky sites formed intrachain cross-link (see the increase in the number of intrachain cross-links in Figure 5.3.1b, c and d) but their distance is still larger than the equilibrium bond length providing a low plateau. The difference between the first and second loadings for $d = 6r_0$ and $8r_0$ are due to the different number of intrachain cross-links. The area under the curve is larger for the higher number of intrachain cross-links. The maximum area under the second loading curves is for the system with $d = 20r_0$ where all sticky sites formed the intrachain cross-links.

Figure 5.3.2A shows the area under the load-displacement curve for each experiment (i.e. first loading, unloading and the second loading) for different grafting densities.

As expected the unloading curve has the lowest area under the curve that is slightly increasing for lower grafting densities (red curve in Figure 5.2.2A). This increase stems from the increase in the number of intrachain cross-links for the lower grafting densities. Figure 5.3.2A shows that for the systems with large grafting densities, the first stretching needs more energy than the second one. Increasing the distance between the chains leads to a strong increase in the area under the second stretching curve finally becoming larger than the energy needed for the first stretching. This shows that the area under the stretching curve strongly depends on the number of intrachain cross-links in the system during loading.
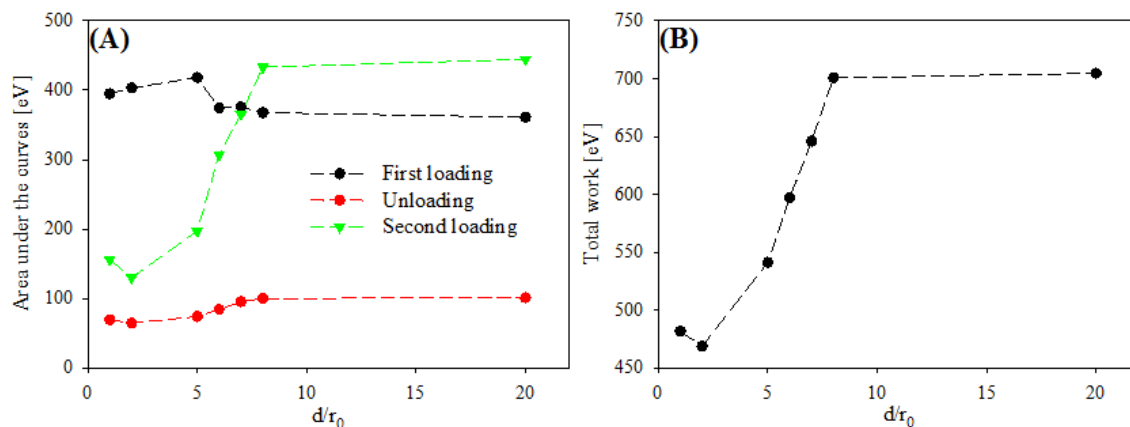
Figure 5.3.2: (A) Area under the Load-Displacement curve obtained during cyclic loading tests for the system with $\rho = 0.48$ and different grafting densities. The black dots denote the results corresponding to first stretching, red dots correspond to unloading and green dots to second stretching. (B) The dissipated energy during cyclic loading plus the work to fracture during the second stretching i.e. the total work done on the system upon the whole process of loading-unloading and second loading until failure.

In a system with a large number of interchain cross-links, the probability of backbone rupture before the contour length is reached is strongly enhanced. This increases the area under the stretching curve but decreases the work to fracture for the next loading since some of the chains have already broken and, thus, do not contribute any more to the bundle mechanics. For systems with a large number of intrachain cross-link, there are less broken chains and, thus, more chains contribute in the loading. In particular, the work done during the whole process (loading1-unloading-loading2) is highest for the lowest grafting density. Therefore the system with few interchain cross-links needs more energy in the experiments consisting of several loading tests, the area for $d = 8r_0$ is similar to the $d = 20r_0$ case. Nevertheless, if more than two loading cycles would be performed then the area would be smaller for a grafting density corresponding to $d = 8r_0$, because during the second loading a few interchain cross-links have formed and some chains ruptured before the contour length as can be inferred from the lower strength of the system with $d = 8r_0$ (see Figure 5.3.2B). For the case $d = 20r_0$ the work done during several loading

cycles stays constant because the chains are independent and the whole process is completely reversible.

5.3.2 Influence of cross-link density

In this section we discuss cyclic loading experiments on bundles with a constant grafting density corresponding to $d = 5r_0$ and different cross-link densities ($\rho = 0.08$, 0.24 and 0.48). Similar to the cyclic loading test for different grafting densities, the first and the second stretching show significant differences (see Figure 5.3.3).
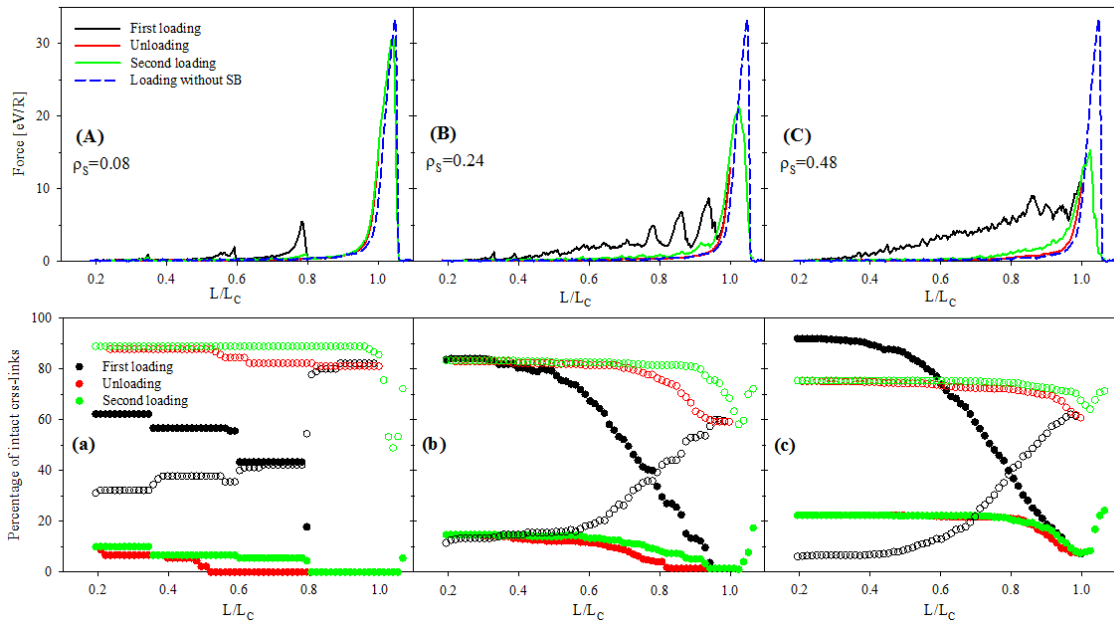
Figure 5.3.3: A,B and C shows the load-displacement curves for cyclic loading for the system with grafting density $d = 5r_0$ and different cross-link densities of $\rho = 0.08, 0.24, 0.48$. Black symbols denote the first loading till the contour length, red symbols show the unloading response of the system and the green symbols show the second loading until failure. Additionally, as a comparison the dashed blue line indicates the loading curve of the bare bundles without sticky sites. The bottom figures shows the corresponding intact cross-links for the cyclic loading test. the closed symbols show the percentage of the intrachain cross-links and the open symbols depict the percentage of interchain cross-links.

For $\rho = 0.08$, the first stretching shows few peaks due to rupture of mostly intrachain cross-links. When $L/L_C = 0.8$ is reached all intrachain cross-links have ruptured and at the same time, the number of interchain cross-links increases. During unloading, both the number of inter- and intrachain cross-links increases. The intrachain cross-links are responsible for the peaks observed before the contour length was reached for the second stretching cycle. The strength of the system is slightly reduced in comparison to the system without sticky sites. The same mechanism applies

cross-link density	E_1^L[eV]	E^U[eV]	E_2^L[eV]	E^{Total}[eV]	$F_m[eV/R]$	$Y[meV/R^2]$
0.08	114.4	70.5	268.7	312.6	30.6	-
0.24	258.6	69.4	247.6	436.8	21.4	34
0.48	418	74	197.1	541.1	15.4	71

Table 5.1: The area under the first loading E_1^L[eV], unloading E^U[eV], the second loading E_2^L[eV], the work done during the whole process loading1-unloading-loading2 i.e. E^{Total}[eV]= E_1^L-E^U+E_2^L, the strength F_m and apparent stiffness Y for different cross-link densities $\rho = 0.08, 0.24$ and $\rho = 0.48$ for the system with constant $d = 5r_0$.

to the system with higher sticky site density. Nevertheless, the form of the first loading curve changes. The discrete rupture of bonds for the low density case is transformed to a continuous breaking for the higher densities. Also the strength drops dramatically due to the breaking of some chains during the first stretching. During the second stretching, no backbone rupture before the contour length can be observed (even not for the case of $\rho = 0.48$ with many interchain cross-links).

The strength for the system with $\rho = 0.08$ is two times larger than the strength for the $\rho = 0.48$. Clearly it can be seen that, the apparent stiffness increases for large cross-link densities. The apparent stiffness increases from $34\,meV/R^2$ to $71\,meV/R^2$ for $\rho = 0.24$ and $\rho = 0.48$, respectively (see Table 5.1).

The area under the first loading curves increases significantly from $114\,eV$ to $418\,eV$ when the cross-link density changes from $\rho = 0.08$ to $\rho = 0.48$. This considerable increase is because the $\rho = 0.48$ has more intrachain cross-links providing the more peaks and also rupturing some chains which also needs energy. The area under the second loading curve decreases by increasing the density of cross-links from $270\,eV$ for$\rho = 0.08$ to $197\,eV$ for $\rho = 0.48$ since some of the chains are broken during first loading for the high cross-link density. The area under the unloading curve stays roughly constant, therefore, the total work during the process loading1-unloading-loading2 increases for higher cross-link densities. In particular, it increases from $312\,eV$ to $541\,eV$ when the density changes from $\rho = 0.08$ to $\rho = 0.48$, respectively (see Table 5.1).

5.4 Random arrangement

All results shown until now were for chain bundle systems with an ordered arrangement of sticky sites. If the sticky sites are randomly distributed along the chains, the mechanical properties of the system changes. Figure 5.4.1A,B shows the load-displacement curve for $\rho = 0.24$ and two different arrangements; ordered and random. In contrast to the ordered arrangement, the system with a random distribution shows no backbone rupture before the contour length is reached. The first loading shows a smooth increase of the force while the ordered arrangement

shows three discrete peaks. For both arrangements, in the starting configuration, the number of cross-links is about 90 % intrachain and 10 % interchain. During unloading the number of intrachain cross-links decreases and the number of interchains increases Figure 5.4.1a,b. After unloading, the total number of intact cross-links (interchain and intrachain) for the random configuration is 50 % while for the ordered configurations all sticky sites are intact.
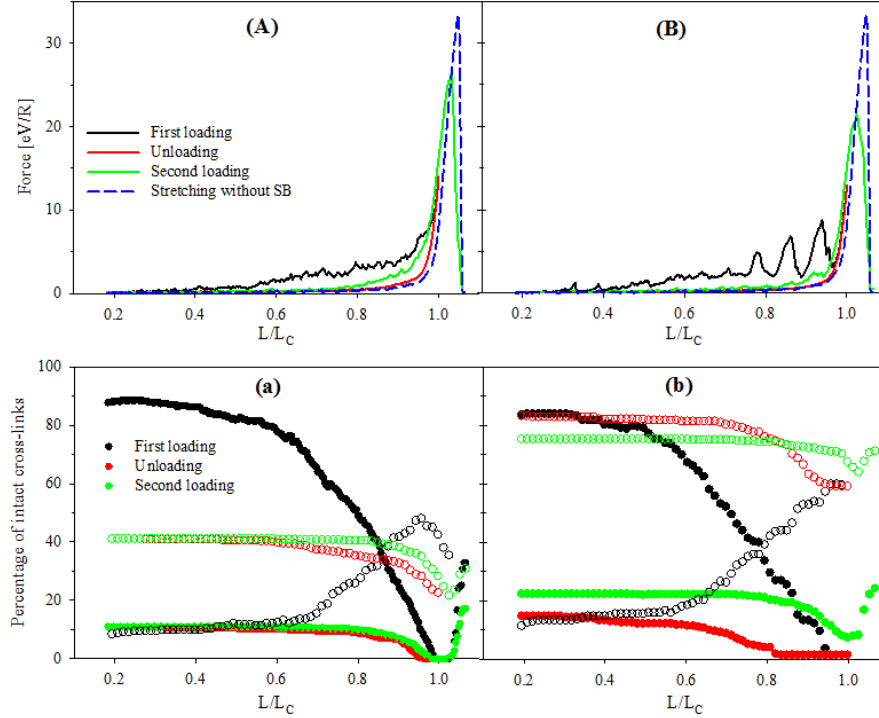
Figure 5.4.1: The load-displacement curves for cyclic loading for a system with grafting density $d = 5r_0$, sticky site density $\rho = 0.24$ and different arrangement of sticky sites along the chains: A) random and B) ordered. Black symbols denote the first loading till the contour length, red symbols show the unloading response of the system and the green symbols show the second loading until failure. Additionally, as a comparison the dashed blue line indicates the loading curve of the bare bundles without sticky sites. The bottom figures shows the corresponding intact cross-links for the cyclic loading test; a) random and b) ordered. the closed symbols show the percentage of the intrachain cross-links and the open symbols depict the percentage of interchain cross-links during cyclic loading test.

Table 5.2 shows the mechanical parameters for the two systems with similar grafting density and sticky site density but different arrangements. The work to elongate the molecule is larger for the ordered configuration, because some of the chains are broken during the first loading. The work to fracture (second loading) of the random configuration is larger because there was no backbone rupture upon first loading. In total, the work done on the system with the random configuration is slightly larger

sticky sites arrangement	E_1^L[eV]	E^U[eV]	E_2^L[eV]	E^{Total}[eV]	$F_m[\frac{eV}{R}]$	$Y[\frac{meV}{R^2}]$
Random	246.6	84	285.5	448.1	25.45	32
Ordered	258.6	69.4	247.6	436.8	21.4	34

Table 5.2: The area under the first loading E_1^L[eV], unloading E^U[eV], the second loading E_2^L[eV], the work done on the whole process loading1-unloading-loading2 i.e. E^{Total}[eV]= E_1^L-E^U+E_2^L, the strength F_m and apparent stiffness Y for different sticky site arrangements; random and ordered for the system with constant $\rho = 0.24$ and $d = 5r_0$.

than for the ordered configuration. The strength of the system with the random configuration is also higher but the apparent stiffness of the ordered configuration is larger than for the random arrangement.

5.5 Conclusion

In this chapter the mechanical properties of chain bundles including reversible cross-links were investigated to understand the influence of the grafting density and the cross-link density on the mechanical response of the system. The results show that there are two possibilities of backbone rupture upon loading before the contour length is reached. This failure of the backbone is caused by the topology of the cross-links in the system. Two simple cases of such topologies were analyzed in this thesis (see Figure 5.1.1). If the distance between the chains is equal to the equilibrium distance of cross-links, then the backbone ruptures if the bundle contains 5 parallel interchain cross-links. Most surprisingly for larger distances between the chains (i.e. smaller grafting densities), backbone failure is possible with only two parallel cross-links. On first sight this is completely unexpected because one cross-link has only a quarter of the strength of a covalent bond. The results from loading chain bundles with constant density of cross-link ($\rho = 0.48$) and different grafting densities showed that the backbone rupture occurs earlier for bundles with $d = 5R_0$ resulting in a lower strength of the system but increasing the work to elongate the chain till the contour length. The mechanical behavior of the bundles also depends on the density of cross-link in the system in such a way that more cross-links lead to an earlier backbone rupture upon loading reducing the strength of the material but increases the energy to elongate the bundles as well as the work to fracture.

Furthermore, the results showed a considerable difference between the first and second loading cycle. This difference is mostly due to the formation of interchain cross-links. The number of interchain cross-links depends more on the grafting density (i.e. the distance between the chains) and the end-to-end distance of the chain. For the system with a large number of interchain cross-links, no backbone rupture was observed during the second loading and the system behaved like a bundle without cross-links and of course with some broken chains. Thus, the interchain cross-links do not experience any force during second loading providing a significant

difference with the first loading test. As a consequence, the interchain cross-links increases the work to elongate for the first loading but also some chains failure. In order to have a material with a recoverable mechanical performance, it is better to have a chain bundle (ordered arrangement of sticky sites) with no interchain cross-links. This can be achieved by increasing the distance between the chains to prevent the formation of interchain cross-links or decreasing the number of sticky sites in the system. Another way to make the system recoverable is using a random arrangement for the sticky sites along the chains.

To summarize, for the system with ordered arrangement of sticky sites along the chains, the grafting density determines the number of interchain cross-link. The interchain cross-links provide the backbone failure before the contour length is reached and thus the system needs more energy to elongate (large work to elongate). On the other hand, the backbone failure decreases the strength of the system significantly. Also increasing the cross-link density increases the apparent stiffness but reduces the strength of the system and the mechanical properties of the bundle is not recoverable. In order to prevent the failure there are three possible configurations of the system; first: decreasing the grafting density, second: decreasing the density of cross-links and third: the random arrangement of the sticky sites along the chains.

6 Final Remarks

The findings of the presented thesis give new insight into the role of reversible crosslinks on the mechanical properties of single polymer chains as well as of chain-bundle systems. Cross-linking of polymeric materials is a strategy widely used to develop new biomedical instruments and drugs as well as to improve the mechanical properties of materials e.g. by creating super tough hydrogels with the capability of mechanical recovery.

Computational approaches are an indispensable tool in analyzing experimental results and in testing simple models making the enormous complexity of polymeric systems theoretically tractable. In this thesis a simple generic model was investigated to study the role of reversible crosslinks (sometimes called sacrificial bonds) on the mechanical behavior of single polymeric chains and chain bundles. The model consisted of a standard bead-spring model. Additionally some of the beads were defined as "sticky". These sticky sites were allowed to form additional cross links in the systems. For different number and arrangement of sticky sites cyclic load-displacement curves were obtained using Monte Carlo simulations.

For single chains it could be shown that the efficacy of sacrificial bonds is strongly reduced due to backbone fluctuations of the polymer chain. Furthermore, it was shown that mechanical response of the system is strongly dependent on the topology of sacrificial bonds. This is the reason why the speed of unloading has a large influence on the mechanical response, because it is the rate of unloading that determines which topology may form. It was also shown that a different distribution of sticky sites has a large impact on the mechanical properties of the chain. The work to fracture is dependent on the number of sacrificial bonds that have to be broken and, thus, crucially depends on the capability of re-forming of ruptured bonds. The strength is higher for any ordered arrangement compared to a random arrangement of sticky sites. The apparent stiffness can be enhanced by ensuring that the forces rises over a small distance. This can be achieved by confining the sticky sites to certain regions of the polymer (the patches configuration). Finally, the energy dissipation of these structures was investigated by performing computational cyclic loading experiments.

The effect of grafting density and sticky site density was investigated also for the system made of chain bundles. The most surprising result for this system is that only two sacrificial bonds are sufficient to break the backbone of the system. In general it was shown that the possibility of forming inter-chain crosslinks leads to material that is quite stiff on one hand, but also more brittle on the other. Comparison of

the random and ordered arrangement of sticky sites showed significant differences between the two systems. It was shown that the stiffness of the ordered arrangement was higher than of the random arrangement, while the strength showed the opposite trend. The mechanical properties of a chain bundle can be dramatically altered by controlling the ratio of inter- to intra-chain SBs.

Comparing the mechanical parameters of the chain bundle and single chains shows that the apparent stiffness of the chain bundles are much larger than of the single chains. The apparent stiffness of a single chain was varying from 1.8 to 5 meV/R^2 for the random and ordered configuration, respectively, while it was increasing to more than 30 meV/R^2 for both configurations of the chain bundle.

In this study no additional backbone rigidity other than stretching was included. In particular bending contributions were neglected. It is likely that additional interactions resulting in spatial folding pattern may effectively reduce the fluctuation which stabilizes the SBs. The interplay of backbone rigidity, thermal fluctuations and the ratio of covalent and sacrificial bond strength dictate the mechanical properties of this single polymer chain. Two open questions in this context that still need to be answered are, first, is there an optimum value of the ratio of the strength of sacrificial to covalent bonds? Second, what is the influence of the width and the equilibrium distance of the SB potential on the mechanical properties. In the thesis presented these two values were set equal to the corresponding properties of the covalent bonds.

While the crosslinks in this thesis were modeled as bonds between two monomers, in reality often more than two monomers take part in one cross-link. E.g. it is known that depending on the concentration of Fe-ions and the pH-value the dopa-Fe complex may exist in the mono-, bis- or tris-state [37, 36]. One possible route to continue the present work would be to effectively model such crosslinks consisting of more than two monomers. It is expected that this new geometry gives rise to a variety of new topologies strongly influencing the mechanics. In particular the force flow through such a cross-link will be dramatically changed compared to a bis-complex. Furthermore, also the dynamic behavior of such crosslinks is expected to be different, because rupture of a cross-link is now always a two stage process. After detachment of the first monomer additionally to the possibility of complete rupture there is also the possibility of reforming the cross-link by attachment of a new sticky site.

Another route that can be taken to extend this work is to investigate the energetics of the crosslinks from a more fundamental point of view. Almost no work exists so far where the formation of metal coordination bonds and their mechanics are addressed by ab-initio methods. [20] is one of the few examples of such a work. Hybrid molecular dynamics simulations [108], where the cross-link itself is described by quantum mechanical DFT methods and the rest of the protein is described classically might close this gap.

Bibliography

[1] R. H. Landau, M. J. Páez, and C. C. Bordeianu, *A Survey of Computational Physics: Introductory Computational Science.* Princeton Universty Press, 2008.

[2] T. H. Creighton, *Proteins: structures and molecular properties.* W. H. Freeman and Company, 1993.

[3] P. Fratzl and R. Weinkamer, "Nature's hierarchical materials" *Prog. Mater Sci.*, vol. 52, pp. 1263–1334, 2007.

[4] B. L. Smith, T. E. Schäffer, M. Viani, J. B. Thompson, N. A. Frederick, J. Kindt, A. Belcher, G. D. Stucky, D. E. Morse, and P. K. Hansma, "Molecular mechanistic origin of the toughness of natural adhesives, fibres and composites" *Nature*, vol. 399, pp. 761–763, 1999.

[5] J. Keckes, I. Burgert, K. Frühmann, M. Müller, K. Kölln, M. Hamilton, M. Burghammer, S. V. Roth, S. Stanzl-Tschegg, and P. Fratzl, "Cell-wall recovery after irreversible deformation of wood" *Nat. Mater.*, vol. 2, pp. 810–814, 2003.

[6] G. E. Fantner, T. Hassenkam, J. H. Kindt, J. C. Weaver, H. Birkedal, L. Pechenik, J. A. Cutroni, G. A. G. Cidade, G. D. Stucky, D. E. Morse, and P. K. Hansma, "Sacrificial bonds and hidden length dissipate energy as mineralized fibrils separate during bone fracture" *Nat. Mater.*, vol. 4, pp. 612–616, 2005.

[7] H. S. Gupta, P. Fratzl, M. Kerschnitzki, G. Benecke, W. Wagermaier, and H. O. K. Kirchner, "Evidence for an elementary process in bone plasticity with an activation enthalpy of 1 eV" *J. R. Soc. Interface*, vol. 4, p. 277, 2007.

[8] E. Oroudjev, J. Soares, S. Arcidiacono, J. B. Thompson, S. A. Fossey, and H. G. Hansma, "Segmented nanofibers of spider dragline silk: Atomic force microscopy and single-molecule force spectroscopy" *Proc. Natl. Acad. Sci. USA*, vol. 99, p. 6460, 2002.

[9] N. Becker, E. Oroudjev, S. Mutz, J. P. Cleveland, P. K. Hansma, C. Y. Hayashi, D. E. Makarov, and H. G. Hansma, "Molecular nanosprings in spider capture-silk threads" *Nat Mater*, vol. 2, no. 4, pp. 278–283, Apr. 2003.

[10] S. Keten, Z. Xu, B. Ihle, and M. J. Buehler, "Nanoconfinement controls stiffness, strength and mechanical toughness of β-sheet crystals in silk" *Nat. Mater.*, vol. 9, pp. 359–367, 2010.

[11] M. J. Harrington, H. S. Gupta, P. Fratzl, and J. H. Waite, "Collagen insulated from tensile damage by domains that unfold reversibly: In situ X-ray investigation of mechanical yield and damage repair in the mussel byssus" *J. Struct. Biol.*, vol. 167, pp. 47–54, 2009.

[12] M. J. Harrington, A. Masic, N. Holten-Andersen, J. H. Waite, and P. Fratzl, "Iron-Clad Fibers: A Metal-Based Biological Strategy for Hard Flexible Coatings" *Science*, vol. 328, pp. 216–220, 2010.

[13] D. S. Hwang, H. Zeng, A. Masic, M. J. Harrington, J. N. Israelachvili, and J. H. Waite, "Protein- and Metal-dependent Interactions of a Prominent Protein in Mussel Adhesive Plaques" *J. Biol. Chem.*, vol. 285, pp. 25 850–25 858, 2010.

[14] B. P. Lee, P. Messersmith, J. Israelachvili, and J.H.Waite, "Mussel-Inspired Adhesives and Coatings" *Annu. Rev. Mater. Res.*, vol. 41, pp. 99–132, 2011.

[15] A. Miserez, S. S. Wasko, C. F. Carpenter, and J. H. Waite, "Non-entropic and reversible long-range deformation of an encapsulating bioelastomer" *Nat. Mater.*, vol. 8, p. 910, 2009.

[16] M. J. Harrington, S. S. Wasko, A. Masic, F. D. Fischer, H. S. Gupta, and P. Fratzl, "Pseudoelastic behaviour of a natural material is achieved via reversible changes in protein backbone conformation" *J. R. Soc. Interface*, vol. 9, pp. 2911–2922, 2012.

[17] S. Krauss, T. H. Metzger, P. Fratzl, and M. J. Harrington, "Self-repair of a biological fiber guided by an ordered elastic framework" *Biomacromolecules*, vol. 14, pp. 1520–1528, 2013.

[18] W. C. Yount, D. M. Loveless, and S. L. Craig, "Strong Means Slow: Dynamic Contributions to the Bulk Mechanical Properties of Supramolecular Networks" *Angew. Chem. Int. Ed.*, vol. 44, p. 2746, 2005.

[19] L. Schmitt, M. Ludwig, H. E. Gaub, and R. Tampe, "A Metal-Chelating Microscopy Tip as a New Toolbox for Single-Molecule Experiments by Atomic Force Microscopy" *Biophys. J.*, vol. 78, p. 3275, 2000.

[20] Z. Xu, "Mechanics of metal-catecholate complexes: The roles of coordination state and metal types" *Sci. Rep.*, vol. 3, p. 2914, 2013.

[21] M. A. Hartmann and P. Fratzl, "Sacrificial Ionic Bonds Need To Be Randomly Distributed To Provide Shear Deformability" *Nano Lett.*, vol. 9, pp. 3603–3607, 2009.

[22] K. S. Suh, S. J. Hwang, and C. R. Lee, "Charge behavior in polyethylene-ionomer blends" *IEEE Trans. Dielectr. Electr. Insul.*, vol. 4, no. 1, pp. 58–63, Feb 1997.

[23] M. Rief, M. Gautel, F. Oesterhelt, J. M. Fernandez, and H. E. Gaub, "Reversible Unfolding of Individual Titin Immunoglobulin Domains by AFM" *Science*, vol. 276, p. 1109, 1997.

[24] M. Rief, J. M. Fernandez, and H. E. Gaub, "Elastically Coupled Two-Level Systems as a Model for Biopolymer Extensibility" *Phys. Rev. Lett.*, vol. 81, pp. 4764–4767, Nov 1998.

[25] M. Rief, M. Gautel, A. Schemmel, and H. E. Gaub, "The Mechanical Stability of Immunoglobulin and Fibronectin III Domains in the Muscle Protein Titin Measured by Atomic Force Microscopy" *Biophys. J.*, vol. 75, p. 3008, 4998.

[26] A. F. Oberhauser, P. E. Marszalek, H. P. Erickson, and J. M. Fernandez, "Themolecular elasticity of the extracellular matrix protein tenascin" *Nature*, vol. 393, p. 181, 1998.

[27] A. F. Oberhauser, P. E. Marszalek, M. Carrion-Vazquez, and J. M. Fernandez, "Single protein misfolding events captured by atomic force microscopy" *Nat. Struct. Mol. Biol.*, vol. 6, no. 11, pp. 1025–1028, Nov. 1999.

[28] M. A. Lantz, S. P. Jarvis, H. Tokumoto, T. Martynski, T. Kusumi, C. Nakamura, and J. Miyake, "Stretching the alpha-helix: a direct measure of the hydrogen-bond energy of a single-peptide molecule" *Chem. Phys. Lett.*, vol. 315, pp. 61 – 68, 1999.

[29] H. Janovjak, J. Struckmeier, M. Hubain, A. Kedrov, M. Kessler, and D. J. Müller, "Probing the Energy Landscape of the Membrane Protein Bacteriorhodopsin" *Structure*, vol. 12, no. 5, pp. 871 – 879, 2004.

[30] D. A. Cisneros, D. Oesterhelt, and D. J. Müller, "Probing Origins of Molecular Interactions Stabilizing the Membrane Proteins Halorhodopsin and Bacteriorhodopsin" *Structure*, vol. 13, no. 2, pp. 235 – 242, 2005.

[31] M. A. Haque, T. Kurokawa, and J. P. Gong, "Super tough double network hydrogels and their application as biomaterials" *Polymer*, vol. 53, pp. 1805–1822, 2012.

[32] H. Gao and H. Yao, "Shape insensitive optimal adhesion of nanoscale fibrillar structures" *Proc. Natl. Acad. Sci. USA*, vol. 101, no. 21, pp. 7851–7856, 2004.

[33] G. E. Fantner, E. Oroudjev, G. Schitter, L. S. Golde, P. Thurner, M. M. Finch, P. Turner, T. Gutsmann, D. E. Morse, H. Hansma, and P. K. Hansma, "Sacrificial Bonds and Hidden Length: Unraveling Molecular Mesostructures in Tough Materials" *Biophys. J.*, vol. 90, pp. 1411–1418, 2006.

[34] D. S. Barnes and L. D. Pettit, "Stereoselectivity in enthalpy changes accompanying the formation of metal complexes of histidine and other amino-acids" *J. Inorg. Nucl. Chem.*, vol. 33, pp. 2177–2184, 1971.

[35] M. J. Harrington and J. H. Waite, "Holdfast heroics: comparing the molecular and mechanical properties of Mytilus californianus byssal threads" *J. Exp. Biol.*, vol. 210, pp. 4307–4318, 2007.

[36] N. Holten-Andersen, M. J. Harrington, H. Birkedal, B. P. Lee, P. B. Messersmith, K. Y. C. Lee, and J. H. Waite, "pH-induced metal-ligand

cross-links inspired by mussel yield self-healing polymer networks with near-covalent elastic moduli" *Proc. Natl. Acad. Sci. USA*, vol. 108, pp. 2651–2655, 2011.

[37] M. Krogsgaard, M. A. Behrens, J. S. Pedersen, and H. Birkedal, "Self-Healing Mussel-Inspired Multi-pH-Responsive Hydrogels" *Biomacromolecules*, vol. 14, p. 297, 2013.

[38] M. J. Harrington and J. H. Waite, "pH-Dependent Locking of Giant Mesogens in Fibers Drawn from Mussel Byssal Collagens" *Biomacromolecules*, vol. 9, no. 5, pp. 1480–1486, 2008.

[39] D. G. Barrett, D. E. Fullenkamp, L. He, N. Holten-Andersen, K. Y. C. Lee, and P. B. Messersmith, "pH-Based Regulation of Hydrogel Mechanical Properties Through Mussel-Inspired Chemistry and Processing" *Adv. Funct. Mater.*, vol. 23, pp. 1111–1119, 2013.

[40] F. Oesterhelt, M. Rief, and H. E. Gaub, "Single molecule force spectroscopy by AFM indicates helical structure of poly(ethylene-glycol) in water" *New J. Phys.*, vol. 1, no. 1, p. 6, 1999.

[41] C.-L. Chyan, F.-C. Lin, H. Peng, J.-M. Yuan, C.-H. Chang, S.-H. Lin, and G. Yang, "Reversible Mechanical Unfolding of Single Ubiquitin Molecules" *Biophys. J.*, vol. 87, p. 3995, 2004.

[42] J. B. Thompson, J. H. Kindt, B. Drake, H. G. Hansma, D. E. Morse, and P. K. Hansma, "Bone indentation recovery time correlateswith bond reforming time" *Nature*, vol. 414, pp. 773–776, 2001.

[43] P. Hansma, G. Fantner, J. Kindt, P. Thurner, G. Schitter, P. Turner, S. Udwin, and M. Finch, "Sacrificial bonds in the interfibrillar matrix of bone" *J Musculoskelet. Neuronal. Interact.*, vol. 5, p. 313, 2005.

[44] Q. Lin, D. Gourdon, C. Sun, N. Holten-Andersen, T. H. Anderson, J. H. Waite, and J. N. Israelachvili, "Adhesion mechanisms of the mussel foot proteins mfp-1 and mfp-3" *Proc. Natl. Acad. Sci. USA*, vol. 104, p. 3782, 2007.

[45] Z. Qin and M. J. Buehler, "Impact tolerance in mussel thread networks by heterogeneous material distribution" *Nat. Commun.*, vol. 4, p. 2187, 2013.

[46] E. Bell and J. Gosline, "Mechanical design of mussel byssus: material yield enhances attachment strength" *J. Exp. Biol.*, vol. 199, p. 1005, 1996.

[47] S. L. Brazee and E. Carrington, "Interspecific Comparison of the Mechanical Properties of Mussel Byssus" *Biol. Bull.*, vol. 211, p. 263, 2006.

[48] T. Hassenkam, T. Gutsmann, P. Hansma, J. Sagert, and J. Waite, "Giant bentcore mesogens in the thread forming process of marine mussels" *Biomacromolecules*, vol. 5, p. 1351, 2004.

[49] K. Bertoldi and M. C. Boyce, "Mechanics of the hysteretic large strain behavior of mussel byssus threads" *J. Mater. Sci.*, vol. 42, p. 8943, 2007.

[50] N. Holten-Andersen, G. E. Fantner, S. Hohlbauch, J. H. Waite, and F. W. Zok, "Protective coatings on extensible biofibres" *Nat. Mater.*, vol. 6, pp. 669–672, 2007.

[51] N. Holten-Andersen, T. E. Mates, M. S. Toprak, G. D. Stucky, F. W. Zok, and J. H. Waite, "Metals and the Integrity of a Biological Coating: The Cuticle of Mussel Byssus" *Langmuir*, vol. 25, p. 3323, 2009.

[52] N. Holten-Andersen, H. Zhao, and J. H. Waite, "Stiff Coatings on Compliant Biofibers: The Cuticle of Mytilus californianus Byssal Threads" *Biochemistry*, vol. 48, pp. 2752–2759, 2009.

[53] M. Myhre and D. A. MacKillop, "Rubber Recycling" *Rubber Chem. Technol.*, vol. 75, no. 3, pp. 429–474, Jul. 2002.

[54] J. P. Gong, "Why are double network hydrogels so tough?" *Soft Matter*, vol. 6, p. 2583, 2010.

[55] J. Hu, T. Kurokawa, T. Nakajima, Z. L. Wu, S. M. Liang, and J. P. Gong, "Fracture Process of Microgel-Reinforced Hydrogels under Uniaxial Tension" *Macromolecules*, vol. 47, no. 11, pp. 3587–3594, 2014.

[56] M. A. Haque, G. Kamita, T. Kurokawa, K. Tsujii, and J. P. Gong, "Unidirectional Alignment of Lamellar Bilayer in Hydrogel: One-Dimensional Swelling, Anisotropic Modulus, and Stress/Strain Tunable Structural Color" *Adv. Mater.*, vol. 22, no. 45, pp. 5110–5114, 2010.

[57] M. A. Haque, T. Kurokawa, G. Kamita, and J. P. Gong, "Lamellar Bilayers as Reversible Sacrificial Bonds To Toughen Hydrogel: Hysteresis, Self-Recovery, Fatigue Resistance, and Crack Blunting" *Macromolecules*, vol. 44, p. 8916, 2011.

[58] J. Hu, K. Hiwatashi, T. Kurokawa, S. M. Liang, Z. L. Wu, and J. P. Gong, "Microgel-Reinforced Hydrogel Films with High Mechanical Strength and Their Visible Mesoscale Fracture Structure" *Macromolecules*, vol. 44, p. 7775, 2011.

[59] J. Hu, T. Kurokawa, T. Nakajima, T. L. Sun, T. Suekama, Z. L. Wu, S. M. Liang, and J. P. Gong, "High Fracture Efficiency and Stress Concentration Phenomenon for Microgel-Reinforced Hydrogels Based on Double-Network Principle" *Macromolecules*, vol. 45, p. 9445, 2012.

[60] M. Rubinstein and R. H. Colby, *Polymer Physics.* Oxford University Press, 2003.

[61] D. P. Landau and K. Binder, *A Guide to Monte Carlo Simulations in Statistical Physics.* Cambridge University Press, 2009.

[62] K. Binder, Ed., *Monte Carlo and Molecular Dynamics Simulations in Polymer Science.* Oxford University Press, 1995.

[63] L. H. Sperling, *Introduction to Physical Polymer Science.* John Wiley & Sons, Inc., 2006.

[64] N. Saitô, K. Takahashi, and Y. Yunoki, "The Statistical Mechanical Theory of Stiff Chains" *J. Phys. Soc. Japan*, vol. 22, p. 219, 1967.

[65] C. Bouchiat, M. D. Wang, J.-F. Allemand, T. Strick, S. M. Block, and V. Croquette, "Estimating the Persistence Length of a Worm-Like Chain Molecule from Force-Extension Measurements" *Biophys. J.*, vol. 76, p. 409, 1999.

[66] P. Benetatos, S. Ulrich, and A. Zippelius, "Force-extension relation of cross-linked anisotropic polymer networks" *New J. Phys.*, vol. 14, p. 115011, 2012.

[67] J. F. Marko and E. D. Siggia, "Stretching DNA" *Macromolecules*, vol. 28, pp. 8759–8770, 1995.

[68] A. D. MacKerell, D. Bashford, Bellott, R. L. Dunbrack, J. D. Evanseck, M. J. Field, S. Fischer, J. Gao, H. Guo, S. Ha, D. Joseph-McCarthy, L. Kuchnir, K. Kuczera, F. T. K. Lau, C. Mattos, S. Michnick, T. Ngo, D. T. Nguyen, B. Prodhom, W. E. Reiher, B. Roux, M. Schlenkrich, J. C. Smith, R. Stote, J. Straub, M. Watanabe, J. Wirkiewicz-Kuczera, D. Yin, and M. Karplus, "All-Atom Empirical Potential for Molecular Modeling and Dynamics Studies of Proteins" *J. Phys. Chem. B*, vol. 102, no. 18, pp. 3586–3616, 1998, pMID: 24889800.

[69] D. Landau and K. Binder, *A Guide to Monte Carlo Simulations in Statistical Physics.* Cambridge University Press, 2009.

[70] S. K. Kumar and A. Z. Panagiotopoulos, "Thermodynamics of Reversibly Associating Polymer Solutions" *Phys. Rev. Lett.*, vol. 82, pp. 5060–5063, Jun 1999.

[71] R. A. Jones, *Soft Condensed Matter.* Oxford University Press, 2002.

[72] P. Benetatos and A. Zippelius, "Anisotropic Random Networks of Semiflexible Polymers" *Phys. Rev. Lett.*, vol. 99, p. 198301, Nov 2007.

[73] S. Ulrich, A. Zippelius, and P. Benetatos, "Random networks of cross-linked directed polymers" *Phys. Rev. E*, vol. 81, p. 021802, 2010.

[74] A. von der Heydt, D. Wilkin, P. Benetatos, and A. Zippelius, "Elasticity of cross-linked semiflexible biopolymers under tension" *Phys. Rev. E*, vol. 88, p. 032701, 2013.

[75] P. Benetatos, "Crosslink-induced shrinkage of grafted Gaussian chains" *Phys. Rev. E*, vol. 89, p. 042602, Apr 2014.

[76] K. W. Plaxco, K. T. Simons, and D. Baker, "Contact order, transition state placement and the refolding rates of single domain proteins" *J. Mol. Biol.*, vol. 277, no. 4, pp. 985 – 994, 1998.

[77] D. E. Makarov and G. J. Rodin, "Configurational entropy and mechanical properties of cross-linked polymer chains: Implications for protein and RNA folding" *Phys. Rev. E*, vol. 66, p. 011908, 2002.

[78] S. S. Nabavi, M. J. Harrington, O. Paris, P. Fratzl, and M. A. Hartmann, "The role of topology and thermal backbone fluctuations on sacrificial bond efficacy in mechanical metalloproteins" *New J. Phys.*, vol. 16, p. 013003, 2014.

[79] A. E. Elbanna and J. M. Carlson, "Dynamics of Polymer Molecules with Sacrificial Bond and Hidden Length Systems: Towards a Physically-Based Mesoscopic Constitutive Law" *PLOS one*, vol. 8, p. e56118, 2013.

[80] C. K. C. Lieou, A. E. Elbanna, and J. M. Carlson, "Sacrificial bonds and hidden length in biomaterials: A kinetic constitutive description of strength and toughness in bone" *Phys. Rev. E*, vol. 88, p. 012703, Jul 2013.

[81] K. Eom, P.-C. Li, D. E. Makarov, and G. J. Rodin, "Relationship between the Mechanical Properties and Topology of Cross-Linked Polymer Molecules: Parallel Strands Maximize the Strength of Model Polymers and Protein Domains" *J. Phys. Chem. B*, vol. 107, p. 8730, 2003.

[82] K. Eom, D. E. Makarov, and G. J. Rodin, "Theoretical studies of the kinetics of mechanical unfolding of cross-linked polymer chains and their implications for single-molecule pulling experiments" *Phys. Rev. E*, vol. 71, p. 021904, 2005.

[83] H. P. Erickson, "Stretching Single Protein Molecules: Titin Is a Weird Spring" *Science*, vol. 276, no. 5315, pp. 1090–1092, 1997.

[84] D. Frenkel and B. Smit, *Understanding Molecular Simulation: From algorithms to applications.* Academic Press, 2002.

[85] J. M. Thijssen, *Computational Physics.* Cambridge University Press, 1999.

[86] M. P. Allen and D. J. Tildesley, *Computer Simulation of Liquids*, reprint ed., ser. Oxford science publications. Oxford University Press, USA, Jun. 1989.

[87] N. Metropolis, A. W. Rosenbluth, M. N. Rosenbluth, A. Teller, and E. Teller, "Equation of State Calculations by Fast Computing Machines" *J. Chem. Phys*, vol. 21, p. 1087, 1953.

[88] D. E. Makarov, Z. Wang, J. B. Thompson, and H. G. Hansma, "On the interpretation of force extension curves of single protein molecules" *J. Chem. Phys*, vol. 116, p. 7760, 2002.

[89] F. Manca, S. Giordano, P. L. Palla, R. Zucca, F. Cleri, and L. Colombo, "Elasticity of flexible and semiflexible polymers with extensible bonds in the Gibbs and Helmholtz ensembles" *J. Chem. Phys.*, vol. 136, p. 154906, 2012.

[90] F. Manca, S. Giordano, P. L. Palla, and F. Cleri, "On the equivalence of thermodynamics ensembles for flexible polymer chains" *Physica A*, vol. 395, no. 0, pp. 154 – 170, 2014.

[91] P. Fratzl, *Collagen: Structure and Mechanics.* Springer, 2008, ch. Collagen: Structure and Mechanics, an Introduction, p. 1.

[92] S. S. Nabavi, M. J. Harrington, P. Fratzl, and M. A. Hartmann, "Influence of sacrificial bonds on the mechanical behaviour of polymer chains" *Bioinspired, Biomimetic and Nanobiomaterials*, vol. 3, pp. 139–145, 2014.

[93] P. E. Marszalek, H. Lu, H. Li, M. Carrion-Vazquez, A. F. Oberhauser, K. Schulten, and J. M. Fernandez, "Mechanical unfolding intermediates in titin modules" *Nature*, vol. 402, p. 100, 1999.

[94] H. Lee, N. F. Scherer, and P. B. Messersmith, "Single-molecule mechanics of mussel adhesion" *Proc. Natl. Acad. Sci. USA*, vol. 103, pp. 12 999–13 003, 2006.

[95] T. E. Fisher, P. E. Marszalek, and J. M. Fernandez, "Stretching single molecules into novel conformations using the atomic force microscope" *Nat. Struct. Biol.*, vol. 7, p. 719, 2000.

[96] T. M. Dugdale, R. Dagastine, A. Chiovitti, P. Mulvaney, and R. Wetherbee, "Single Adhesive Nanofibers from a Live Diatom Have the Signature Fingerprint of Modular Proteins" *Biophys. J.*, vol. 89, p. 4252, 2005.

[97] T. M. Dugdale, R. Dagastine, A. Chiovitti, and R. Wetherbee, "Diatom Adhesive Mucilage Contains Distinct Supramolecular Assemblies of a Single Modular Protein" *Biophys. J.*, vol. 90, p. 2987, 2006.

[98] T. Gutsmann, T. Hassenkam, J. A. Cutroni, and P. K. Hansma, "Sacrificial Bonds in Polymer Brushes from Rat Tail Tendon Functioning as Nanoscale Velcro" *Biophys. J.*, vol. 89, pp. 536–542, 2005.

[99] C. Ortiz and G. Hadziioannou, "Entropic Elasticity of Single Polymer Chains of Poly(methacrylic acid) Measured by Atomic Force Microscopy" *Macromolecules*, vol. 32, pp. 780–787, 1999.

[100] O. Kratky and G. Porod, "Röntgenuntersuchung gelöster Fadenmoleküle" *Rec. Trav. Chim. Pays-Bas.*, vol. 68, p. 1106, 1949.

[101] M. Fixman and J. Kovac, "Polymer conformational statistics. III. Modified Gaussian models of stiff chains" *J. Chem. Phys.*, vol. 58, p. 1564, 1973.

[102] H.-P. Hsu, W. Paul, and K. Binder, "Breakdown of the Kratky-Porod wormlike chain model for semiflexible polymers in two dimensions" *Europhys. Lett.*, vol. 95, p. 68004, 2011.

[103] H.-P. Hsu and K. Binder, "Stretching semiflexible polymer chains: Evidence for the importance of excluded volume effects from Monte Carlo simulation" *J. Chem. Phys.*, vol. 136, p. 024901, 2012.

[104] W. Kuhn, "Über die Gestalt fadenförmiger Moleküle in Lösungen" *Kolloid Z.*, vol. 68, p. 2, 1934.

[105] E. Guth and H. Mark, "Zur innermolekularen Statistik, insbesondere bei Kettenmolekülen I." *Monatsh. Chem.*, vol. 65, p. 93, 1934.

[106] M. J. Harrington and J. H. Waite, *Fibrous Proteins.* Landes Bioscience, 2008, ch. Short-Order Tendons: Liquid Crystal Mesophases, Metal-Complexation and Protein Gradients in the Externalized Collagens of Mussel Byssal Threads, p. 30.

[107] E. Carrington and J. M. Gosline, "Mechanical design of mussel byssus: load cycle and strain rate dependence" *Am. Malacol. Bull.*, vol. 18, p. 135, 2004.

[108] M. Sparta, D. Shirvanyants, F. Ding, N. Dokholyan, and A. Alexandrova, "Hybrid Dynamics Simulation Engine for Metalloproteins" *Biophys. J.*, vol. 103, no. 4, pp. 767 – 776, 2012.

7 Publications

S. Soran Nabavi, Mathew J. Harrington, Oskar Paris, Peter Fratzl, Markus A. Hartmann
The role of topology and thermal backbone fluctuations on sacrificial bond efficacy in mechanical metalloproteins
*New Journal of Physics **16** (2014), 013003.*

S. Soran Nabavi, Mathew J. Harrington, Peter Fratzl and Markus A. Hartmann
Influence of sacrificial bonds on the mechanical behaviour of polymer chains
*Bioinspired, Biomimetic and Nanobiomaterials **3** (2014), 139-145.*

S. Soran Nabavi, Peter Fratzl and Markus A. Hartmann
Energy dissipation and recovery in a simple model with reversible cross-links
Submitted

8 Appendix *I*

The role of topology and thermal backbone fluctuations on sacrificial bond efficacy in mechanical metalloproteins

S Soran Nabavi[1]**, Matthew J Harrington**[2]**, Oskar Paris**[1]**, Peter Fratzl**[2] **and Markus A Hartmann**[1,3]

[1] Institute of Physics, Montanuniversitaet Leoben, Franz-Josef Strasse 18, A-8700 Leoben, Austria
[2] Max-Planck-Institute of Colloids and Interfaces, Department of Biomaterials, Research Campus Golm, D-14476 Potsdam, Germany
E-mail: markus.hartmann@unileoben.ac.at

Abstract

Sacrificia bonding is a ubiquitous cross-linking strategy for increasing toughness that is found throughout nature in various biological materials such as bone, wood, silk and mussel byssal threads. However, the molecular mechanism of sacrificia bonding remains only poorly understood. Molecular modeling possesses a strong potential to provide insights into the behavior of these cross-links. Here we use Monte Carlo simulations to investigate the effect of reversible sacrificia binding sites on the mechanical properties of single linear polymer chains based on load-bearing metalloproteins found in the mussel byssus. It is shown that the topology of the bonds determines the position and spacing of sacrificia force peaks, while the height of these peaks is intimately tied to the magnitude of thermal fluctuation in the chain that are dependent on effective chain length. These results bear important implications for understanding natural systems and for the generation of strong and ductile biomimetic polymers.

[3] Author to whom any correspondence should be addressed.

1. Introduction

Evolution via natural selection has provided an effective means for achieving practical and economic solutions to various physical challenges encountered by load-bearing structures in nature. Natural materials, therefore, are a potentially valuable source of inspiration for the design of novel man-made materials. However, this firs requires a thorough understanding of the underlying structure-function relationships that determine the material behavior. For example, in many natural materials increased toughness is achieved via careful tuning of molecular interactions at numerous levels of hierarchy [1]. One particularly effective strategy for increasing toughness found in bone [2, 3], wood [4] and some softer biological fibers such as silk [5–7], mussel byssus [8–10] and whelk egg capsule [11], is the use of sacrificia bonds (SBs). SBs are load-bearing cross-links which are weaker than covalent bonds making up the backbone structure of the materials that rupture 'sacrificially in order that the overall material integrity survives [2]. In doing so, these bonds dissipate mechanical energy by unraveling of 'hidden' folded protein length. These bonds can often be reformed after rupture leading to a kind of molecular repair and possibly self-healing behavior in the material. This combination of hidden length unraveling and self-repair capability makes SBs a very effective energy dissipation mechanism and increases the toughness of a material dramatically [2, 12].

Hydrogen bonding, electrostatic interactions and most recently, protein–metal coordination bonds have been identifie as SBs in natural materials. In metal coordination complexes, several ligands (amino acid side chains such as 3,4-dihydroxyphenylalanine (DOPA) and histidine in protein based systems) contribute lone pairs of electrons to the outer orbitals of transition metal ions. These bonds are ideal as reversible SBs because they require large energy inputs to rupture, but, unlike typical covalent cross-links, will reform rapidly afterwards [13, 14]. For example, in mussel byssal threads that are produced by marine mussels to adhere to rocky substrates, load-bearing protein–metal complexes based on histidine–Zn^{2+} and DOPA–Fe^{3+} interactions have been implicated in increased toughness, hardness and self-healing behavior in various structures of the threads [8–10].

While SBs have been correlated with increased toughness in biological materials, as well as in some recently developed supramolecular polymers [15] and bio-inspired metallopolymers [16, 17], there is not a solid understanding of how the molecular environment of the SBs influence mechanics. Cao *et al* [18] demonstrated at the molecular level that recombinantly engineered metal bonds can increase the force to unfold a protein and the total energy dissipated via unfolding. However, the magnitude of this increase was found to be highly dependent upon the location of the cross-link in the folded structure. In other words, the mechanical behavior of the system is influence by how the SBs are situated within the rest of the chain. Along these lines, it was suggested from molecular simulation that there is an ideal size of β-sheet nanocrystals for maximizing toughness in spider silk, which reflect the most effective use of sacrificia hydrogen bonds [7]. Clearly, there is more to be understood regarding the molecular mechanism of toughening inherent to SBs. Here, we take a step toward unraveling this phenomenon by using Monte Carlo (MC) simulations to examine the influenc of topology, chain length and thermal fluctuation on the mechanical behavior of SB reinforced fibrou systems. As a starting point for our model, we consider the histidine- and DOPA-containing proteins from the mussel byssus; however, the extracted concepts can be abstracted and applied more broadly, such as in the design of mechanical metallopolymers. The results of

the simulations show that the effica y of these SBs is closely related to the magnitude of thermal fluctuation in the backbone of the chain, which depends upon chain length and temperature.

2. The model

The biological system inspiring this work are the SB-forming histidine-rich regions of the load-bearing proteins in the tough fibrou core of mussel byssal threads [8] and DOPA-rich proteins found in the plaque [10] and the protective cuticle [9]. The his-rich sequences from the core proteins are relatively short segments that consist typically of 30–80 amino acids [19] and are clamped between collagen and flankin domains [8]. This clamping define an effective length of the polymer over which it is free to fluctuate The DOPA-rich proteins from the thread plaque and cuticle consist of short tandemly repeated amino acid sequences containing between 5 and 25 mol% DOPA [20]. In the present paper this situation was modeled by a linear chain of N hard spheres with radius R (which we set as the unit of length). The covalent interaction between neighboring beads was described by a Morse potential

$$E(r_{ij}) = E_0 \left\{ [1 - \exp(-\beta(r_{ij} - r_0))]^2 - 1 \right\} \tag{1}$$

with the depth $E_0 = 5$ eV, the width $\beta^{-1} = 0.5$ R, the equilibrium bond length $r_0 = 3$ R and the actual distance between two neighboring beads i and j, r_{ij}. The contour length of the chain is given by $L_0 = (N - 1)r_0$. To model the presence of SBs, N_s of the beads were define as sticky, two of which could form a SB ($\rho_s = N_s/N$ is the sticky site density). The sticky sites were introduced regularly: the same number of non-sticky sites separating them. The protein backbone is a linear polymer consisting of C–C and C–N bonds which possess average bond energies of several eV. The energetics of the SBs in proteins have not been well characterized; however, several studies on DOPA and histidine-based metal complexes suggest they possess binding energies that range between 20–30% of a C–N bond [21, 22]. Thus a value of $E_0^{\text{SB}} = 1.25$ eV was chosen for the SB in this study, corresponding to 25% of the bond energy of the covalent backbone bond in our simulated polymer. Additionally, the SBs were allowed to open and close reversibly. Simulations mimicking loading experiments were performed by starting from a small end-to-end distance L that was define by pinning the two outer beads. The positions of the inner beads were updated according to a standard MC procedure using the Metropolis algorithm [23]. For SB updating, one sticky site was chosen randomly and the probability for bond breaking or bond formation was calculated using the Metropolis algorithm, depending on whether the bond was intact or already broken, respectively. During the simulation the forces on the outer beads were recorded and averaged. Subsequently, L was increased and the simulation re-run until the contour length L_0 was reached. Up to 90 million MC step (i.e. jump trials per bead) were performed for the single step. For each simulation an independent starting configuratio was produced by relaxing a fully stretched chain $L/L_0 = 1$ without sticky sites. When the initial end-to-end distance was reached the sticky sites were added and allowed to form SBs. Subsequently this structure was stretched. The model presented bears some resemblance to the dynamic loop model used to describe mitotic chromosomes [24]. The main differences are, firstl , in our model SBs can't form between all monomers but only between sticky sites. Secondly, SB formation and rupture are determined by a distance dependent potential, rather than by rate constants and lifetimes drawn from a Poisson distribution. Thirdly, the monomers can move freely in space, because no lattice model is used.
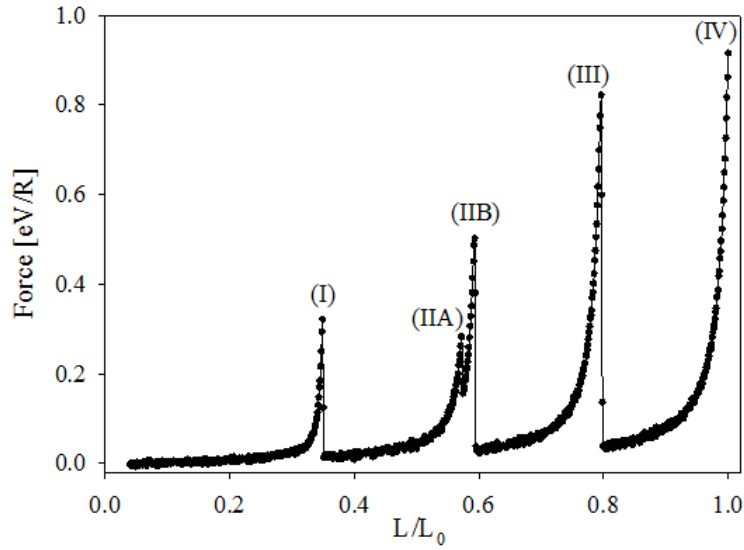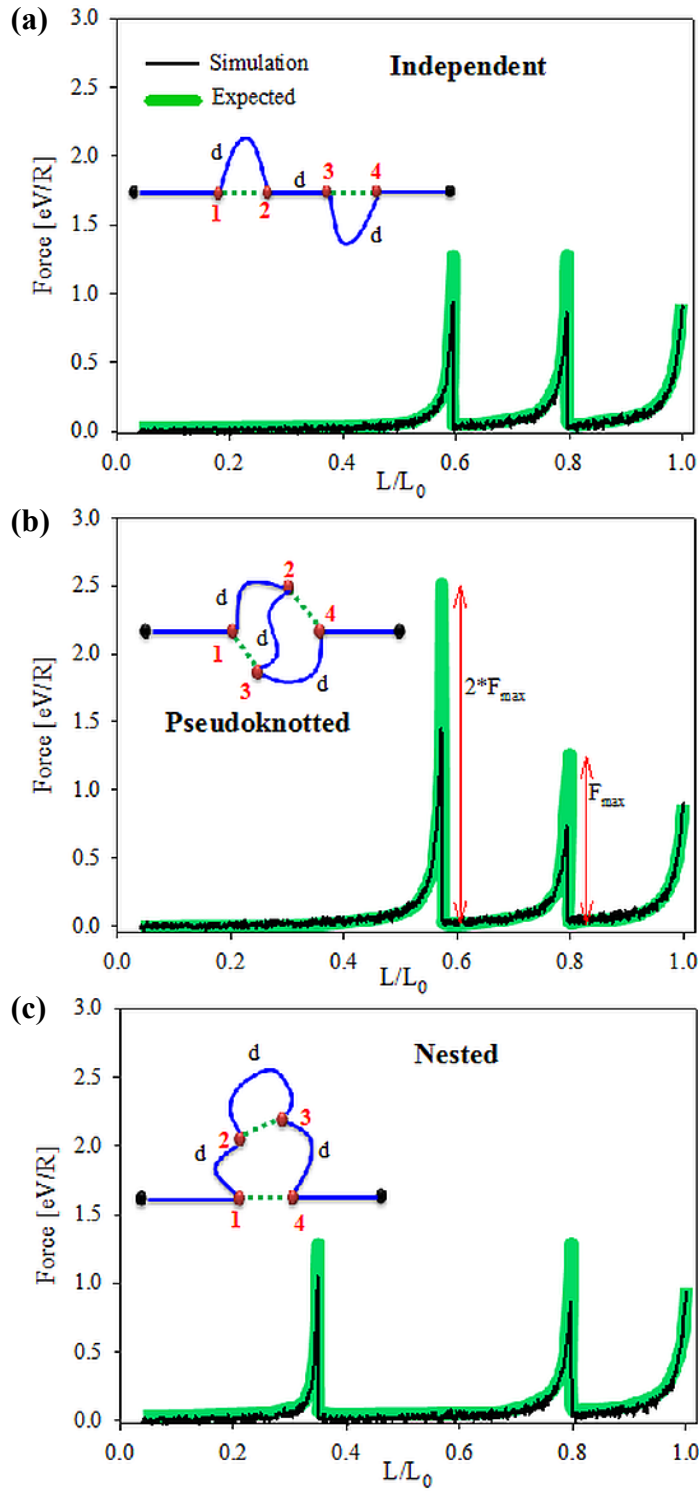
Figure 1. Mean load–displacement curve for $N = 50$, $k_B T = 25$ meV and $\rho_s = 0.08$. The presented curve is the average of 20 independent runs.

3. Results and discussion

Figure 1 shows an averaged load–displacement curve for a chain with $N_s = 4$ sticky sites separated by ten monomers (sticky site density $\rho_s = 0.08$) at ambient temperature of $k_B T = 25$ meV. The curve shows four distinct peaks (the second being a double peak II*A* and II*B*) approximately equally spaced but with significantl different heights. This behavior closely resembles the experimentally found sawtooth patterns, which were reported in a variety of biological systems, e.g. in nacre [25], in single molecule measurements of titin [26, 27], tenascin [28], DOPA [22] and modular proteins [29] as well as in the adhesive mucilage pads of diatoms [30, 31] and polymer brushes from rat tail tendon [32]. In the following we will focus at explaining the number, position and especially the height of the observed peaks. Peak IV is the trivial contribution corresponding to the onset of backbone stretching and will not be considered here.

First, we focus on the number and position of the peaks. In the crumpled starting configuratio the four sticky sites form two SBs out of three possible topologies: the independent, pseudoknotted and nested configuratio [33]. Figure 2 shows a sketch of the different topologies together with the expected load–displacement curve and a simulated one. For the case of the independent configuratio the SBs form between sticky sites (1,2) and (3,4), respectively (see figur 2(a)). Due to symmetry the inner part of the chain is now divided into three parts of equal length $d = 11r_0$, the outer part of the chain having a total length of $d_0 = 16r_0$. The firs bond starts stretching when $L/L_0 = (d_0 + d + 2r_0)/L_0 \approx 0.59$ (the additional term $2r_0$ taking into account the two SBs). The opening of this loop reveals an additional length of d giving rise to another force peak at $L/L_0 \approx 0.8$. When this second SB has broken backbone stretching sets in at $L/L_0 \approx 1$. These two bond stretching events correspond to peak (II*B*) and (III) in the averaged load–displacement curves shown in figur 1. In the pseudoknotted configuratio (figur 2(b)) sticky sites (1,3) and (2,4) form SBs. Ideally the force peak corresponding to the stretching of this structure should be found at the same value of the

Figure 2. Load–displacement curves for $N = 50$ at $k_B T = 25\,\text{meV}$ with four sticky sites and different topologies of the formed SBs. The firs and last bead of the chain are shown in black; sticky sites are shown in red. SBs are indicated by dotted green lines, covalent connections by blue lines. Load–displacement

Figure 2. (Continued) curves shown with thick, green lines indicate the expected curves. The thin, black line shows actual simulation results of selected single runs. (a) independent configuration two force peaks of equal height $F_{max} = \beta E_0^{SB}/2 = 1.25$ eV R^{-1} at $L/L_0 \approx 0.59$ and 0.8 are expected. (b) pseudoknotted configuration two force peaks are expected: the firs at L/L_0 slightly lower than 0.59 and of height $2F_{max}$, the second of height F_{max} at $L/L_0 \approx 0.8$. (c) nested configuratio : two force peaks of equal height F_{max} at $L/L_0 \approx 0.35$ and 0.8 are expected. Note, that not a single SB attains its theoretical strength.

chain extension as the firs peak in the independent configuratio $L/L_0 = (d_0 + d + 2r_0)/L_0$. Nevertheless, it is found at a slightly lower chain extension giving rise to the peak (IIA) in figur 1. This decrease can be attributed to the hard core repulsion of beads that forbid that the chain can exactly align in the direction of the load, which is possible for the independent topology. Whenever the pseudoknotted configuratio ruptures the reversibility of SBs assures that another SB is formed between sticky sites (2,3). Like in the independent configuratio this SB starts stretching at $L/L_0 \approx 0.8$ corresponding to peak (III). Finally, in the nested configuratio (see figur 2(c)) the SBs form between sticky sites (1,4) and (2,3), respectively. Thus, the firs SB stretching occurs already at extensions $L/L_0 = (16r_0 + r_0)/L_0 \approx 0.35$ corresponding to peak (I) in figur 1. As in the preceding case the second stretching takes place whenever the chain is elongated to $L/L_0 \approx 0.8$ once again contributing to peak (III).

While the position of the peaks occurring in figure 1 and 2 can well be explained with the different topologies of the involved SBs, their height can not be understood that easily. Partly the height of the peaks in the averaged load–displacement curve shown in figur 1 can be attributed to the different occurrences of the different topologies. Out of 20 simulation runs there were 12 independent, 2 pseudoknotted and 6 nested configurations It is due to this different frequency that peak (I) and (IIA) belonging to the less probable pseudoknotted and nested configuratio are reduced in height compared to peak (IIB) and (III). Nevertheless, the different probability of topologies can explain only partly the different heights. Also in the single runs shown in figur 2 not a single SB in any topology attains its expected strength (which we defin as the maximum force that can be generated by the used potential) shown by the solid lines. For all bond rupture events except for peak (IIA) this expected peak height coincides with the theoretical strength of one SB $F_{max} = \beta E_0^{SB}/2 = 1.25$ eV R^{-1}. In the case of the pseudoknotted configuratio the rupture force should be twice the strength of one SB, because the force can be simultaneously distributed between the two SBs. Nevertheless, the simulation results show that all forces are considerably reduced compared to the expected value of F_{max}. This is surprising because the energy of SBs at the distance of maximum force $r_{max} = \ln 2/\beta + r_0$ compared to temperature is $E(r_{max})/k_B T = 37.5$. Thus, the probability of bond failure at this point is extremely small. Therefore it is not expected that the SBs fail, before they are stretched beyond r_{max} corresponding to a peak with height F_{max} in the load–displacement curve.

To understand the reduced height of the forces, a very simple distribution of sticky sites in the chain was investigated. The number of sticky sites was set to $N_s = 2$ (i.e. the formation of only one SB was possible). The position of the sticky sites was in the middle of the chain, one non-sticky site separating them. The starting configuratio was chosen such that the system was in its energetic ground state with $L/L_0 = (N-2)/(N-1) \equiv L^*$ (see also figur 3(a)). Figure 3(b) shows the resulting load–displacement curve in stretching for a chain with $N = 5$ at $k_B T = 25$ meV. When the chain is stretched from its equilibrium configuration the SB starts
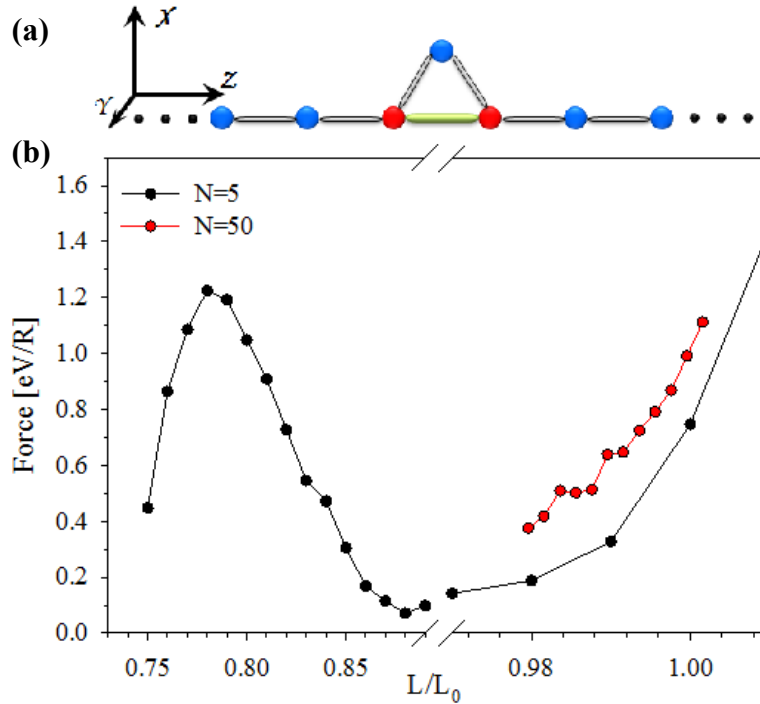
Figure 3. (a) The starting configuratio of the simplifie system with only two sticky sites. The middle beads of the chain are shown. Normal monomers are shown in blue, sticky sites in red. Longer chains are created by adding additional monomers on both sides. The simulations are started with the SB closed (green connection). Covalent bonds are shown in gray. (b) Load–displacement curves in stretching for $N_s = 2$, $k_B T = 25$ meV and $N = 5$ (black) and $N = 50$ (red), respectively.

stretching, resulting in an elevated force that reaches its maximum around $F = 1.25$ eV R^{-1}, in good agreement with the theoretical strength of a SB. Eventually, the SB fails and the chain is further stretched until backbone elasticity sets in around $L/L_0 \approx 1$. The situation changes, however, when the same simulation is repeated on the longer chain with $N = 50$ (see figur 3(b)). In the corresponding length region no additional load on SB can be observed. Only elevated backbone stretching takes place, being due to a higher entropic contribution from the higher number of monomers. The reason for this unexpected absence of the sacrificia force peak is due to SB opening during the very firs simulation steps of the unstretched chain. As discussed before, due to the high ratio of binding energy to thermal energy from a purely energetic point of view the SBs should be thermally stable producing an additional peak in the load–displacement curve as observed for the short chain. The only reasonable physical explanation for SB bond breaking at these low temperatures is that for longer chains, fluctuation of the covalent backbone bonds lead to such large loads on the SB that it fails already before the external load sets in. In other words, it is backbone entropy that leads to SB failure. To validate this explanation the temperature in the simulation was changed. Figure 4 shows load–displacement curves for chains with $N = 50$ for different temperatures and for a larger range of L/L_0. A sacrificia force peak is observed for all temperatures and comes close to the theoretical strength of SBs for low temperatures. When the temperature is increased this peak shifts to smaller values of L/L_0 and decreases in height. Simultaneously the entropic
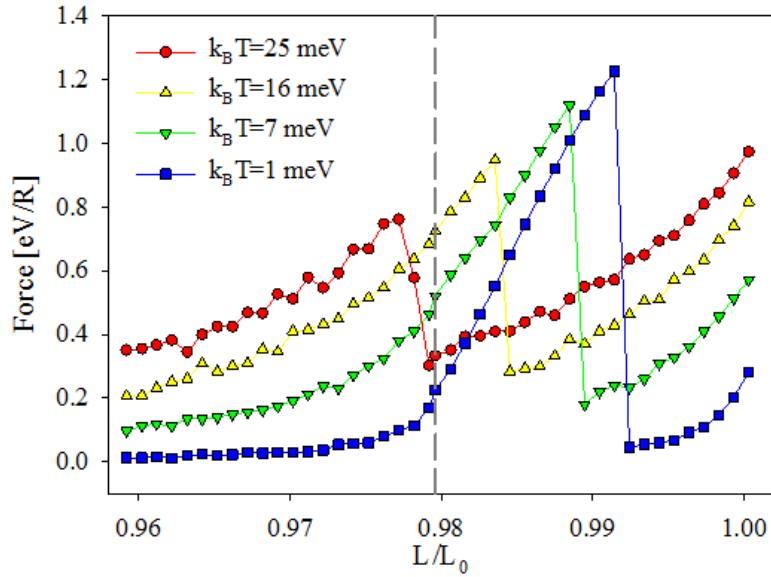
Figure 4. Load–displacement curves for chains with $N = 50$ at different temperatures. When the temperature is reduced an additional force peak due to the SB starts growing that is approaching the theoretical strength of $1.25 \, \text{eV} \, \text{R}^{-1}$ at temperatures below one meV. The vertical dashed line indicates L^*.

background (the baseline of the curves) is rising. Finally, for $k_\text{B}T = 25 \, \text{meV}$ the sacrificia force peak is shifted below L^*. This means that for this temperature, the elevated loading is a purely entropic effect stemming from internal thermal fluctuation and not from external loading. For $L/L_0 < L^*$ no load larger than zero can prevail when the temperature is reduced to zero.

To investigate the effect of chain fluctuation on SBs further, the force experienced by SBs during the simulation was recorded. Figure 5 shows the distribution of bond lengths (a) and the loading of SBs (b) for two different chain lengths: $N = 5$ and $N = 33$, the latter one corresponding to the longest chain where no SB rupture was observed below L^*. For all chains longer than 33 monomers backbone fluctuation are sufficientl large to rupture SBs without external loading. An increase in monomer number leads to an increase of the mean bond length and a corresponding shift toward higher forces. These effects correspond to an effective weakening of the SB and are the reason for premature SB rupture. For increasing chain length, the most probable bond length is shifted to higher values and the distribution is broadened significantl . These two effects lead to a non-zero probability that the SB is strained beyond r_max. Subsequently, the bond is brought close to its maximum load, leading to bond rupture. Both distributions show a pronounced asymmetric shape, but—in contrast to the bond length distribution—the force distribution shows a pronounced drop at its right flank This drop takes place at the maximum load, since above a value of $F = 1.25 \, \text{eV} \, \text{R}^{-1}$ the distribution is exactly zero by definition This is also the reason for the slight narrowing of the force histogram for larger N. Therefore, whenever the number of monomers is high enough that the SB length fluctuation considerably exceed r_max or—equivalently—the position of the force histograms coincides with the theoretical maximum force, the SB spontaneously fails. The inset in figur 5(b) shows the width and position of the distributions as a function of N. The position was evaluated at the maximum of the curve, while the width was define to be the full width at half maximum.
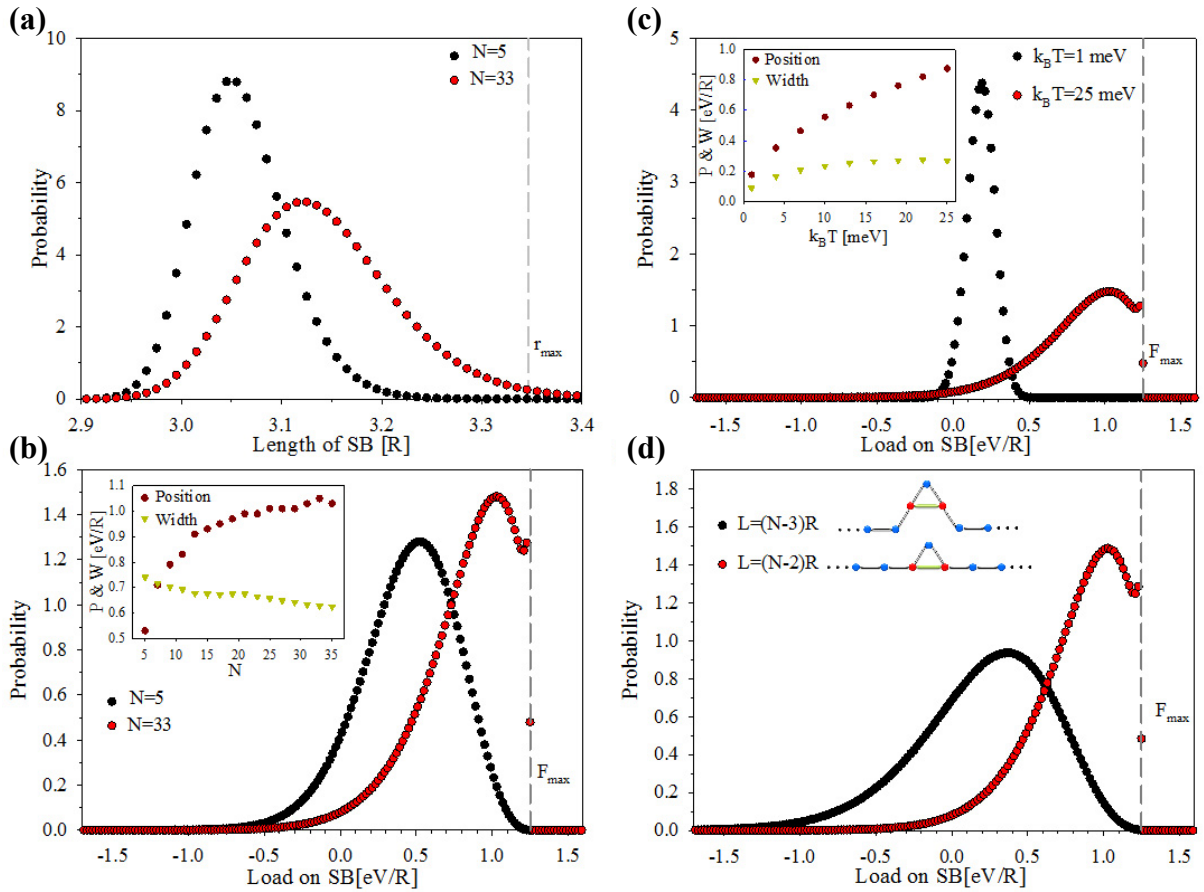
Figure 5. (a) SB lengths histograms at $k_B T = 25$ meV. The distance r_{max} corresponding to the theoretical maximum force is indicated by a gray dashed line. (b) The distribution of loads on the SBs at $k_B T = 25$ meV. The inset shows the width and position of the histograms as a function of monomer number. (c) Load distributions for $N = 33$ at two different temperatures. The inset shows the position and width of the distributions as a function of temperature. (d) Load distribution for $N = 33$ at $k_B T = 25$ meV. The inset shows the two starting configurations The data in (a)–(c) were recorded at $L/L_0 = L^*$.

The temperature, although small compared to the involved binding energies, is a crucial parameter in determining SB rupture. Figure 5(c) shows sacrific al force probability distributions for $N = 33$ at two different temperatures. An increased temperature leads to a broadening of the distribution and to a shift of the maximum to higher loads. While the shift of the maximum with increasing temperature is similar to the behavior of the probability distributions for increasing N (figur 5(b)), the width of the distributions behaves differently. On firs sight, the observed narrowing of the curve with increasing N is counter-intuitive since one would expect stronger fluctuation with larger N. However, it is the difference in relative length that explains this effect. For large N, the relative length of the chain in the starting configuratio reaches $L^* \approx 1$, while it is $L^* = 0.75$ for $N = 5$. A short relative length gives the SB enough freedom to follow the covalent bond fluctuation and transmit additional load through the system (see figur 3(b)). On the other hand, a relative length close to 1 reduces the number of possible configuration of the system (in the limit of $T = 0$ there is only one single state), thus effectively reducing its fluctuations

Figure 5(d) summarizes this effect. Force histograms for $N = 33$ at two different starting lengths are shown. Clearly, the distribution shifts to larger loads and narrows upon increasing L. For chains longer than $N = 33$ the SB already fails, when the relative length of the chain is below L^*. Thus, only a reduced sacrificia load of $\approx 0.8\,\mathrm{eV\,R^{-1}}$ that is purely entropic in nature can be transmitted (see figur 4). Such entropic loads have been found experimentally [32, 34] and are often described using the freely jointed or —its variant for small bond angles—the worm like chain (WLC) model [35]. Also the shape of the single rupture events in figur 2 can be well fitte with the analytical load–displacement expression obtained for the WLC model [36]

$$F = \frac{k_\mathrm{B}T}{L_\mathrm{p}} \left[\frac{L}{L_0^\mathrm{eff}} + \frac{1}{4} \frac{1}{(1 - L/L_0^\mathrm{eff})^2} - \frac{1}{4} \right] \tag{2}$$

with the persistence length L_p and an effective contour length L_0^eff as the two fittin parameters. The fittin results yielded a similar persistence length of approximately $L_\mathrm{p} = 5.63$ for all peaks except the firs rupture of the pseudoknotted configuratio that gives $L_\mathrm{p} = 3.1$. The effective contour lengths obtained are smaller than the actual contour lengths L_0. This effective contour length is given by L_0 minus the hidden length shielded by the SBs. The rather small persistence length of the chain reflect its rotational freedom resulting in the high entropic forces. Thus, close to bond rupture the chain behaves as a WLC that is effectively stretched close to its contour length and whose elasticity is described as an entropic spring. Although the WLC equation can well reproduce the found curves, it should be noted that care has to be taken when analyzing polymer stretching using this simple model. Recently it has been shown that the WLC model breaks down for chains too short due to excluded volume effects [37, 38]. Nevertheless, because in the present case the chain is rather extended close to bond rupture it can be expected that these effects can be neglected.

These results explain the reduced peak forces observed in figure 1 and 2. Furthermore, the results also explain why SBs that rupture at lower chain extensions are effectively stronger than those that rupture at larger chain lengths (compare e.g. the firs and second peak in figur 2(c)). This is because at lower chain extensions the effective length of the chain is reduced which effectively stabilizes SBs. This shows that a reduction in effective bond strength upon loading can also be found for identical SBs, which is an alternative interpretation to the view that such a reduction can only be explained by a successive decrease in SB strength or by multiple molecules loaded in parallel [39]. These results bear the important conclusion that load–displacement curves measured in single-molecule experiments need not necessarily directly reflec the underlying microscopic potential. Rather, the effective potential may be smeared out and significantl reduced in its strength due to entropic contributions. Single-molecule measurements with different chain length might clarify this question. Furthermore, our results indicate that the effective breaking forces of ligand-metal bonds could be considerable lower than the previously measured breaking forces of single bonds (e.g. His–metal complexes [40, 41]), if they were embedded in a chain that is free to vibrate. This has important consequences for our understanding of the biological materials and for the design of biomimetic metallopolymers.

The idealized model presented in this paper is a simplifie representation of the real situation. Firstly, one isolated polymeric chain is investigated here while in biological systems many protein chains are assembled into larger structures into which the SBs are embedded. This confine the chain into a reptation tube hindering its transverse fluctuation [35, 42]. We

studied the magnitude of the root mean-square transversal fluctuation in our model and found them to be less than a monomer-monomer distance. This is a very short length compared to the reptation tube diameters of several nanometers found for polymer melts, for instance [43]. This short length indicates that the hinderance of transversal fluctuation due to local reptation is not sufficien to prevent SB rupture. Secondly, the polymer model chosen in this letter corresponds to a freely jointed chain without considering any bending or torsional contributions to the energy. It is likely that additional interactions resulting in special folding patterns may effectively reduce monomer fluctuations thus stabilizing SBs. Third, in the presented model a SB is always formed between two monomers, while real metal coordination bonds involve three or more partners that are cross linked. Thus, even when one partner detaches, there remain ligands that hold the structure together. However, since the effect of bond weakening is significan for SBs with a rather high but realistic binding energy compared to ambient temperature, it can be concluded that despite the obvious simplification of the model, protein backbone fluctuation will definitel reduce SB strength in real biological materials. These fluctuation may even prove beneficia for the self-healing process. Thus, the interplay of thermal fluctuations backbone rigidity, covalent bond strength and SB strength dictate the overall mechanical behavior of these structures. An important question to answer in this context is, whether there is an optimum value of the strength of SBs compared to covalent bonds and if there is an optimum length of the protein chains? Our results indicate that the relatively short segment length of the SB rich domains of only 30–80 amino acids is not incidental, but rather due to SB weakening for longer segments. For hydrogen bonded beta sheet configuration it has already been shown that thermodynamic stability determines the optimum length of the involved beta-strands [44]. Our results in addition indicate that there is a strong temperature dependence of the mechanical properties of materials relying on SBs. Thus, mechanical tests on e.g. byssus fiber at different temperatures seem promising to further decipher the secrets of their mechanical performance. First experiments confirmin the importance of temperature have shown that self-healing proceeds faster at higher temperatures [8].

4. Conclusion

Employing a simple model with reversible crosslinks mimicking SBs between proteins and metal ions in the mussel byssus makes it possible to reproduce characteristic features found in experimental load–displacement curves in natural materials. Characteristic sawtooth patterns corresponding to the rupture of single bonds were observed. The distance between two peaks (the hidden length revealed) is directly linked to the topology of the bonds and corresponds to the length of the loops define by the SBs. The height of the peak force is considerably lower than the theoretical strength of a SB. It was shown that this reduction is of entropic origin. The capability of SBs to transmit load are drastically reduced at ambient temperature due to thermal fluctuation in the backbone of the chain.

Acknowledgments

References

[1] Fratzl P and Weinkamer R 2007 Nature's hierarchical materials *Prog. Mater. Sci.* **52** 1263

[2] Fantner G E *et al* 2005 Sacrificia bonds and hidden length dissipate energy as mineralized fibril separate during bone fracture *Nature Mater.* **4** 612

[3] Gupta H S, Fratzl P, Kerschnitzki M, Benecke G, Wagermaier W and Kirchner H O K 2007 Evidence for an elementary process in bone plasticity with an activation enthalpy of 1 eV *J. R. Soc. Interface* **4** 277

[4] Keckes J, Burgert I, Frühmann K, Müller M, Kölln K, Hamilton M, Burghammer M, Roth S V, Stanzl-Tschegg S and Fratzl P 2003 Cell-wall recovery after irreversible deformation of wood *Nature Mater.* **2** 810

[5] Oroudjev E, Soares J, Arcidiacono S, Thompson J B, Fossey S A and Hansma H G 2002 Segmented nanofiber of spider dragline silk: atomic force microscopy and single-molecule force spectroscopy *Proc. Natl Acad. Sci. USA* **99** 6460

[6] Becker N, Oroudjev E, Mutz S, Cleveland J P, Hansma P K, Hayashi C Y, Makarov D E and Hansma H G 2003 Molecular nanosprings in spider capture-silk threads *Nature Mater.* **2** 278

[7] Keten S, Xu Z, Ihle B and Buehler M J 2010 Nanoconfineme t controls stiffness, strength and mechanical toughness of β-sheet crystals in silk *Nature Mater.* **9** 359

[8] Harrington M J, Gupta H S, Fratzl P and Herbert Waite J 2009 Collagen insulated from tensile damage by domains that unfold reversibly: *in situ* x-ray investigation of mechanical yield and damage repair in the mussel byssus *J. Struct. Biol.* **167** 47

[9] Harrington M J, Masic A, Holten-Andersen N, Herbert Waite J and Fratzl P 2010 Iron-clad fibers a metal-based biological strategy for hard fl xible coatings *Science* **328** 216

[10] Hwang D S, Zeng H, Masic A, Harrington M J, Israelachvili J N and Herbert Waite J 2010 Protein- and metal-dependent interactions of a prominent protein in mussel adhesive plaques *J. Biol. Chem.* **285** 25850

[11] Harrington M J, Scott Wasko S, Masic A, Dieter Fischer F, Gupta H S and Fratzl P 2012 Pseudoelastic behaviour of a natural material is achieved via reversible changes in protein backbone conformation *J. R. Soc. Interface* **9** 2911

[12] Hartmann M A and Fratzl P 2009 Sacrificia ionic bonds need to be randomly distributed to provide shear deformability *Nano Lett.* **9** 3603

[13] Yount W C, Loveless D M and Craig S L 2005 strong means slow: dynamic contributions to the bulk mechanical properties of supramolecular networks *Angew. Chem. Int. Edn Engl.* **44** 2746

[14] Schmitt L, Ludwig M, Gaub H E and Tampe R 2000 A metal-chelating microscopy tip as a new toolbox for single-molecule experiments by atomic force microscopy *Biophys. J.* **78** 3275

[15] Cordier P, Tournilhac F, Soulié-Ziakovic C and Leibler L 2008 Self-healing and thermoreversible rubber from supramolecular assembly *Nature* **451** 977

[16] Holten-Andersen N, Harrington M J, Birkedal H, Lee B P, Messersmith P B, Lee K Y C and Herbert Waite J 2011 pH-induced metal-ligand cross-links inspired by mussel yield self-healing polymer networks with near-covalent elastic moduli *Proc. Natl Acad. Sci. USA* **108** 2651

[17] Barrett D G, Fullenkamp D E, He L, Holten-Andersen N, Lee K Y C and Messersmith P B 2013 pH-based regulation of hydrogel mechanical properties through mussel-inspired chemistry and processing *Adv. Funct. Mater.* **23** 1111

[18] Cao Y, Yoo T and Li H 2008 Single molecule force spectroscopy reveals engineered metal chelation is a general approach to enhance mechanical stability of proteins *Proc. Natl Acad. Sci. USA* **105** 32

[19] Harrington M J and Herbert Waite J 2007 Holdfast heroics: comparing the molecular and mechanical properties of *Mytilus californianus* byssal threads *J. Exp. Biol.* **210** 4307

[20] Lee B P, Messersmith P B, Israelachvili J N and Waite J H 2011 Mussel-inspired adhesives and coatings *Annu. Rev. Mater. Res.* **41** 99

[21] Barnes D S and Pettit L D 1971 Stereoselectivity in enthalpy changes accompanying the formation of metal complexes of histidine and other amino-acids *J. Inorg. Nucl. Chem.* **33** 2177

[22] Lee H, Scherer N F and Messersmith P B 2006 Single-molecule mechanics of mussel adhesion *Proc. Natl Acad. Sci. USA* **103** 12999

[23] Landau D and Binder K 2009 *A Guide to Monte Carlo Simulations in Statistical Physics* (Cambridge: Cambridge University Press)

[24] Zhang Y and Heermann D W 2011 Loops determine the mechanical properties of mitotic chromosomes *PLOS ONE* **6** e29225

[25] Smith B L, Schäffer T E, Viani M, Thompson J B, Frederick N A, Kindt J, Belcher A, Stucky G D, Morse D E and Hansma P K 1999 Molecular mechanistic origin of the toughness of natural adhesives, fibre and composites *Nature* **399** 761

[26] Rief M, Gautel M, Oesterhelt F, Fernandez J M and Gaub H E 1997 Reversible unfolding of individual titin immunoglobulin domains by AFM *Science* **276** 1109

[27] Marszalek P E, Lu H, Li H, Carrion-Vazquez M, Oberhauser A F, Schulten K and Fernandez J M 1999 Mechanical unfolding intermediates in titin modules *Nature* **402** 100

[28] Oberhauser A F, Marszalek P E, Erickson H P and Fernandez J M 1998 The molecular elasticity of the extracellular matrix protein tenascin *Nature* **393** 181

[29] Fisher T E, Marszalek P E and Fernandez J M 2000 Stretching single molecules into novel conformations using the atomic force microscope *Nature Struct. Biol.* **7** 719

[30] Dugdale T M, Dagastine R, Chiovitti A, Mulvaney P and Wetherbee R 2005 Single adhesive nanofiber from a live diatom have the signature fingerprin of modular proteins *Biophys. J.* **89** 4252

[31] Dugdale T M, Dagastine R, Chiovitti A and Wetherbee R 2006 Diatom adhesive mucilage contains distinct supramolecular assemblies of a single modular protein *Biophys. J.* **90** 2987

[32] Gutsmann T, Hassenkam T, Cutroni J A and Hansma P K 2005 Sacrificia bonds in polymer brushes from rat tail tendon functioning as nanoscale velcro *Biophys. J.* **89** 536

[33] Makarov D E and Rodin G J 2002 Configurationa entropy and mechanical properties of cross-linked polymer chains: implications for protein and RNA folding *Phys. Rev.* E **66** 011908

[34] Ortiz C and Hadziioannou G 1999 Entropic elasticity of single polymer chains of poly(methacrylic acid) measured by atomic force microscopy *Macromolecules* **32** 780

[35] Rubinstein M and Colby R H 2003 *Polymer Physics* (Oxford: Oxford University Press)

[36] Marko J F and Siggia E D 1995 Stretching DNA *Macromolecules* **28** 8759

[37] Hsu H-P, Paul W and Binder K 2011 Breakdown of the Kratky–Porod wormlike chain model for semifl xible polymers in two dimensions *Europhys. Lett.* **95** 68004

[38] Hsu H-P and Binder K 2012 Stretching semifl xible polymer chains: evidence for the importance of excluded volume effects from Monte Carlo simulation *J. Chem. Phys.* **136** 024901

[39] Fantner G E *et al* 2006 Sacrificia bonds and hidden length: unraveling molecular mesostructures in tough materials *Biophys. J.* **90** 1411

[40] Kienberger F, Kada G, Gruber H J, Pastushenko V Ph, Riener C, Trieb M, Knaus H-G, Schindler H and Hinterdorfer P 2000 Recognition force spectroscopy studies of the NTA–His6 Bond *Single Mol.* **1** 59

[41] Verbelen C, Gruber H J and Dufrêne Y F 2007 The NTA–His6 bond is strong enough for AFM single-molecular recognition studies *J. Mol. Recognit.* **20** 490

[42] de Gennes P G 1971 Reptation of a polymer chain in the presence of fi ed obstacles *J. Chem. Phys.* **55** 572

[43] Wischnewski A, Monkenbusch M, Willner L, Richter D and Kali G 2003 Direct observation of the transition from free to constrained single-segment motion in entangled polymer melts *Phys. Rev. Lett.* **90** 058302

[44] Keten S and Buehler M J 2008 Geometric confinemen governs the rupture strength of H-bond assemblies at a critical length scale *Nano Lett.* **8** 743

9 Appendix *II*

Reprinted with permission from:

S. Soran Nabavi, Mathew J. Harrington, Peter Fratzl and Markus A. Hartmann

Influence of sacrificial bonds on the mechanical behaviour of polymer chains

ice | **science**

Influence of sacrificial bonds on the mechanical behaviour of polymer chains

1 **S. Soran Nabavi**
Institute of Physics, Montanuniversitaet Leoben, Leoben, Austria
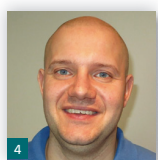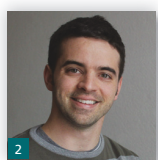
2 **Matthew J. Harrington**
Department of Biomaterials, Max-Planck-Institute of Colloids and
Interfaces, Potsdam, Germany

3 **Peter Fratzl**
Department of Biomaterials, Max-Planck-Institute of Colloids and
Interfaces, Potsdam, Germany

4 **Markus A. Hartmann***
Institute of Physics, Montanuniversitaet Leoben, Leoben, Austria

A growing focus in modern materials science is the attempt to transfer principles found in nature into new technological concepts with the goal of producing novel materials with tailored mechanical properties. One of these principles used in nature is the concept of sacrificial bonding (i.e. non-covalent cross-links that rupture prior to the protein backbone), which is associated with increased toughness in many biological materials. In the present work, the influence of the number and distribution of sacrificial bonds (SBs) on three main mechanical parameters—strength, work to fracture and apparent stiffness—is investigated in a simple model system using computer simulations. The results show that the work to fracture is mainly determined by the number of SBs present in the system, while the apparent stiffness and, to a lesser extent, the strength is altered when the distribution of SBs is changed.

1. Introduction

In contrast to engineered materials, biological organisms utilize a relatively limited selection of building blocks to synthesize materials (e.g. proteins, sugars, environmentally abundant ions). In spite of this, however, natural materials span an extremely wide range of mechanical properties, which is achieved by hierarchical structuring of the material over multiple length scales and by a combination of materials with opposing mechanical properties.[1] One common and successful strategy to increase the toughness of protein-based biological materials is to use so-called sacrificial bonds (SBs).[2] These non-covalent cross-links are weaker than the covalent bonds that comprise the protein backbone, and consequently, upon loading, they rupture before the covalent bonds fail. By doing so, SBs reveal hidden length (i.e. the length increase associated with unfolding of folded proteins) providing an efficient energy dissipation mechanism, while the overall material integrity survives.[3] Furthermore, these bonds are reversible and may reform when the load is released, allowing for molecular repair. SBs have been found in a large variety of biologial materials like wood,[4] bone[5–7] and in some softer biological fibres such as silk,[8] whelk egg capsule[9] and mussel byssus threads.[10–13]

In materials such as silk, SBs are often weak hydrogen bonds combined in large numbers in regular protein conformations in order to collectively produce high stiffness[14]; however, in the case of the mussel byssus, much stronger interactions between metal ions and proteins are employed. In this regard, the mussel byssus is an especially fascinating material. The mussel secretes the collageneous byssal threads as a means of creating a secure attachment in wave-swept rocky seashore habitats. Among the impressive properties of the mussel byssus are its high extensibility of over 100%, high stiffness and toughness,[10] its hard and wear-resistant outer coating[15–18] and, last but not least, its ability to create strong and long-lasting underwater adhesion to a variety of surfaces.[17] A fundamental aspect shaping each of these properties is the interaction of proteins with metal ions. In particular, histidine–zinc and 3,4-dihydroxyphenylalanine (DOPA)–iron coordination complexes in the protein building blocks of the material serve as reversible SBs with a relatively high binding energy of 20–30% of a covalent bond.[19,20]

Recently, a number of technological materials have emerged that attempt to draw inspiration from the aforementioned notable

*Corresponding author e-mail address: markus.hartmann@unileoben.ac.at

Bioinspired, Biomimetic and Nanobiomaterials
Volume 3 Issue BBN3

Influence of sacrificial bonds on the
mechanical behaviour of polymer chains
Nabavi, Harrington, Fratzl and Hartmann

properties of the mussel byssus, for example, strong biocompatible surgical adhesives,[21] implantable drug-eluting devices in human blood vessels capable of withstanding blood flow[22] and super tough hydrogel materials that may serve as artificial cartilage.[23] Additionally, a new generation of biomimetic self-repairing metallopolymers has arisen, which directly draw inspiration from the byssal threads.[24–27] In spite of these advances, many challenges still persist. Thus, a thorough experimental and theoretical understanding of the molecular processes underlying the SB mechanism is crucial.

In particular, the specific details of the topology and nature of the metal-binding domains have been found to be increasingly important in determining material properties. It was shown, for example, that the type of coordination bond (i.e. the metal and ligand utilized) affects the stiffness and strength of a polymer[25,27,28] and that the fracture toughness as well as the extensibility of materials based on SBs is strongly dependent on the pulling speed.[29,30] Furthermore, it was shown that the topology of SBs and thermal backbone fluctuations strongly affect the efficacy of SBs[31] and that the spatial distribution of SBs can have a strong effect on mechanics[32]—a random distribution of SBs is necessary to provide the system with shear deformability. Along these lines, the histidine-rich domains in the load-bearing proteins comprising the self-healing mussel thread core contain numerous variations in sequence depending on the protein variant and species.[33] Sequence variations result in differences in distribution and number of metal-binding histidine residues and are believed to be associated with differences in the mechanics between threads from different species.[33] It has been demonstrated that the binding energy of histidine–metal complexes can be greatly affected by the number and spacing of histidine residues in short peptides[34] and that the position of the metal-coordination bond in the folded protein chain influences the mechanical stability of the proteins.[35] In the current study, the influence of the distribution of SBs on the mechanical properties in fibrous systems inspired by the mussel byssus is further investigated utilizing computer simulations. Monte Carlo simulations mimicking tensile experiments were carried out on a simple model system, and the main mechanical properties (strength, work to fracture and apparent stiffness) as a function of the number and distribution of SBs was assessed. It was shown that the work to fracture is mainly determined by the number of SBs, while their distribution has a significant impact on the strength and apparent stiffness.

2. The model

The histidine-rich regions of the load-bearing proteins in the tough fibrous core of mussel byssal threads[10,33] and the DOPA-rich proteins found in the plaque[12] and the protective cuticle[18] form protein–metal SBs that provide the inspiration for the presented model, already introduced in Ref. 31. The histidine-rich sequences from the byssal core, for example, are relatively short segments that

consist typically of 30–80 amino acids.[33] This motif is described by a linear chain of $N = 50$ covalently bonded beads. To prevent self-interaction of the chain, the beads were assigned a hard-sphere radius R that essentially forbids the overlap of two beads and that we set as the unit of length in the simulations. The covalent bonds were described via a Morse potential

1.
$$E(r_{ij}) = E_0 \left[\left\{ 1 - \exp\left[-\beta(r_{ij} - r_0) \right] \right\}^2 - 1 \right]$$

$E_0 = 5\,\text{eV}$ is the depth of the potential, $\beta^{-1} = 0.5R$ is the width of the potential, $r_0 = 3R$ is the equilibrium distance and r_{ij} is the distance between two neighbouring beads (Figure 1b). Consequently, the contour length of the chain is given by $L_c = (N-1)r_0$. SBs were described by defining N_s of the beads as sticky, setting the sticky site density as $\rho_s = N_s / N$. SBs in this model always formed from only two sticky sites and were allowed to open and close reversibly (see Figure 1a for a schematic sketch of the model). Not much is known
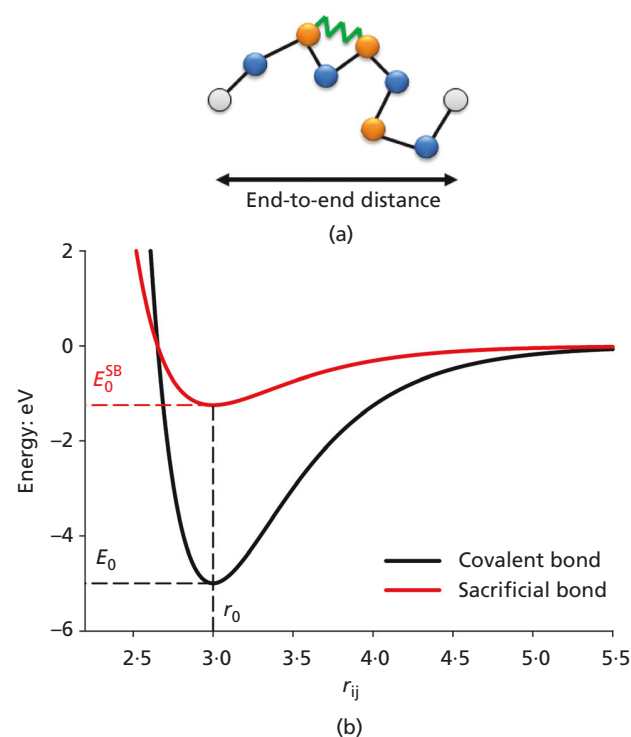
Figure 1. (a) Sketch of the used model. Gray beads denote the two fixed outer beads defining the end-to-end distance, non-sticky sites are shown in blue and sticky sites in orange, respectively. Covalent bonds are indicated by black bars, while a closed sacrificial bond is shown by the green zigzag line. (b) The Morse potential used to describe the energetics of covalent (black) and sacrificial (red) bonds. The vertical dotted line indicates the equilibrium distance r_0, while the two horizontal lines indicate the used binding energies E_0 and E_0^{SB}, respectively.

Bioinspired, Biomimetic and Nanobiomaterials
Volume 3 Issue BBN3

**Influence of sacrificial bonds on the
mechanical behaviour of polymer chains**
Nabavi, Harrington, Fratzl and Hartmann

about the energetics of SBs. Nevertheless, there are experimental indications that the binding energy of a histidine–metal complex lies between 20 and 30% of a covalent bond.[19,20] For the sake of simplicity, in this study, the SBs are also described with a Morse potential as are the covalent bonds. The binding energy of the SBs is set to 25% of the value of a covalent bond, $E_0^{SB} = 1 \cdot 25$ eV.

In the simulations, we investigated two different sticky site densities ($\rho_s = 0 \cdot 08$ and $0 \cdot 24$, respectively) and three different arrangements of sticky sites: (a) ordered, (b) patches and (c) random (see top row of Figure 3). In the ordered case, the sticky sites were introduced regularly with always the same number of non-sticky sites in between. In the second arrangement, the chain is divided into three segments of equal length (the patches). The sticky sites are distributed regularly on the outer two patches, while the middle patch is sticky site free. In the third arrangement, the sticky sites are distributed randomly under the additional constraint that two sticky sites are not allowed to be directly neighbouring.

In the simulations, load-displacement curves were obtained using the Helmholtz ensemble.[36] The end-to-end distance L of the polymer was defined by pinning its two outer beads. The position of the inner beads and the SBs were updated using a standard Metropolis algorithm[37] and the force on the outer beads was recorded and averaged. Starting from a small end-to-end distance L was slowly increased until $L/L_C = 1$. Up to 20 independent simulation runs have been done for each density and arrangement. Up to 3 million Monte Carlo steps (i.e. jump trials per bead) were performed for each single point. The temperature was set to the ambient value of $k_B T = 25$ meV.
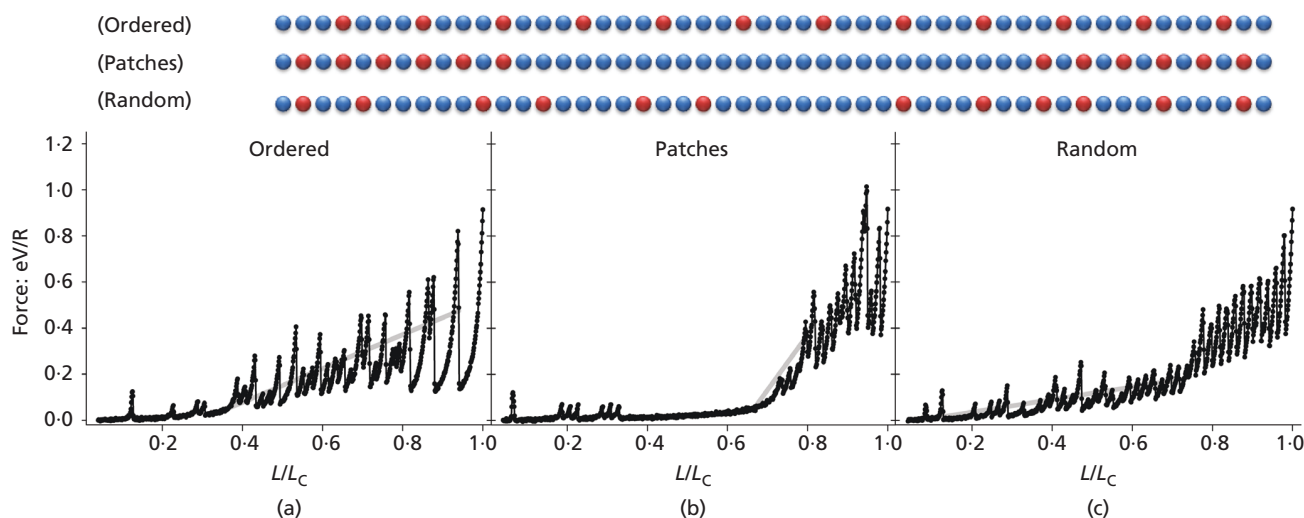
3.   Results and discussion

Figure 2 shows the averaged load-displacement curves of a single polymer chain with $\rho_s = 0 \cdot 08$ for an ordered and random arrangement of sticky sites. In the ordered arrangement, five peaks can be observed. The first four peaks correspond to the rupture of SBs with different topologies, the last peak is due to backbone stretching (Figure 2a).[31] Each of these single peaks can be well fitted with the worm-like chain model[38] that was shown to describe entropic forces due to the tendency of elongated polymers to recoil.[39,40] A parameter that is connected to the toughness of the material is the work to fracture $W_0 = W + \Delta W$ that is given by the area under the curve. $W = 11 \cdot 38$ eV is the work to straighten the molecule, that is, to elongate the molecule to its contour length, and $\Delta W = 25$ eV is the additional contribution due to the rupture of the covalent backbone. Because all SBs are open when the chain is fully elongated, ΔW is the same for all configurations and is omitted in the following. The strength of the material F_m due to SBs is calculated as the maximum load of the curve after subtracting the pure, covalent interaction. For the ordered distribution of sticky sites, the rather high value of $F_m = 0 \cdot 77$ eV/R is found. Nevertheless, due to thermal fluctuations of the backbone, this
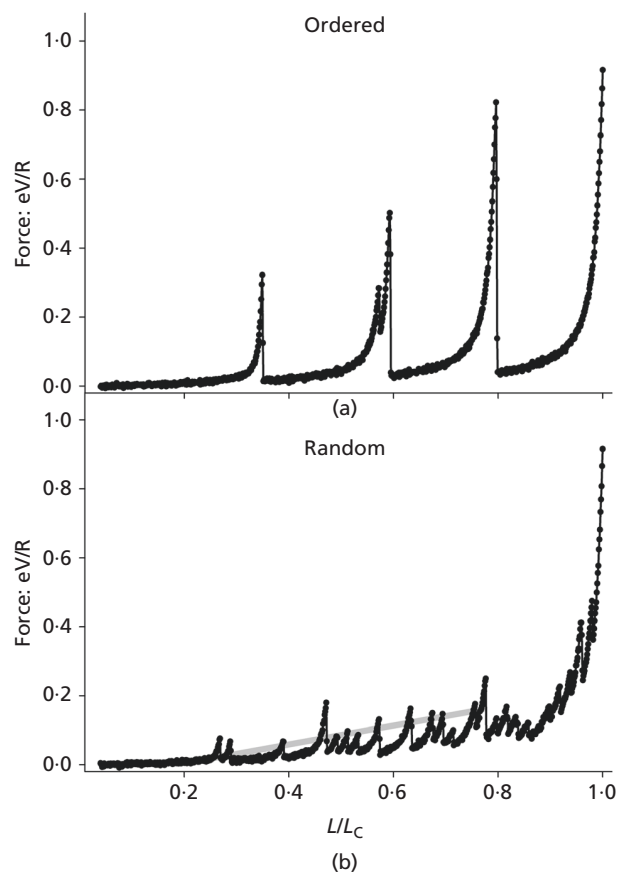
Figure 2. Load-displacement curves for an (a) ordered and (b) random arrangement of sticky sites with $N = 50$, $k_B T = 25$ meV and $\rho_s = 0 \cdot 08$. In the random arrangement, the apparent stiffness of the material (i.e. the mean slope of the initial part of the curve) is indicated.

value is considerably lower than the theoretical strength of one SB $F_m^{th} = E_0 \beta / 2 = 1 \cdot 25$ eV/R.[31]

In the random distribution of sticky sites, 20 independent configurations were generated and tested. The single force peaks of the loading curve are smeared out compared to the ordered distribution, an effect that considerably reduces the strength to $F_m = 0 \cdot 26$ eV/R. Because of the randomness of the sticky site distribution, their positions along the chain and thus the corresponding positions of the force peaks are not fixed. Consequently, the load is distributed over the entire range of the load-displacement curve leading to a lowering of the peak height compared to the ordered case. Nevertheless, within error, the work to fracture $W = 11 \cdot 45$ eV is identical with the result for the ordered arrangement. Furthermore, the random arrangement allows one to define an apparent stiffness E of the material that is defined as the mean slope of the first increase in the load-displacement curve. It is found that $E = 1 \cdot 84$ meV/R^2. Analogous to an ordinary stiffness, the apparent stiffness is a measure of how much force is needed

Bioinspired, Biomimetic and Nanobiomaterials
Volume 3 Issue BBN3

**Influence of sacrificial bonds on the
mechanical behaviour of polymer chains**
Nabavi, Harrington, Fratzl and Hartmann

Figure 3. Load-displacement curves for three different distributions of sticky sites ((a) ordered, (b) patches and (c) random) and N =50, k_BT =25 meV and ρ_s = 0·24. The gray lines indicate the apparent stiffness of the materials defined as the mean slope of the first part of the load-displacement curve. In the top part of the figure, a sketch of the different arrangements of sticky sites are shown (sticky sites are shown in red, non-sticky sites in blue).

to elongate the structure to a certain length. While the ordinary stiffness describes the elastic behaviour of a material, the apparent stiffness is determined by the rupture of bonds that is characteristic for plastic deformation. Nevertheless, due to the reversibility of the SBs, they are able to reform over time following unloading, and the initial apparent stiffness is recovered.

Figure 3 shows the load-displacement curves for a high sticky site density ρ_s = 0·24 and three different arrangements of sticky sites. In the ordered arrangement, two successive sticky sites are separated by three non-sticky sites. In contrast to the low-density ordered arrangement, the stretching part of the load-displacement curve does not show single peaks corresponding to SB rupture, but rather a continuous shape (Figure 3a). This shows that after a single SB rupture, the force does not drop to zero but is taken up by some other SBs. Similar to the low-density arrangement (Figure 2), this allows the definition of an apparent stiffness E = 5·03 meV/R² that is also indicated by the gray line in the figure. The strength of this material is found to be F_m = 0·7 eV/R and the work to fracture W = 22·55 eV.

The load-displacement curve changes significantly when the arrangement of sticky sites is changed to the patches configuration (Figure 3b). When stretched, the intermediate patch that contains non-sticky sites only fully elongates before the SBs starts to rupture. Thus, the force starts rising only when the chain is stretched to L/L_C = 0·7 (the few rupture events at small end-to-end distances correspond to SBs that have been formed between sticky sites in different patches). Compared to the ordered distribution, this late onset of the force slightly reduces the area under the curve to W =

19·63 eV, but largely enhances the apparent stiffness of the material to E = 16·26 meV/R². The reason for this large value of the apparent stiffness is that due to the late onset of the force, the force has to rise over a smaller distance, yielding a large slope. The strength of the material is given by F_m = 0·9 eV/R.

Finally, Figure 3c shows the load-displacement curve for the random arrangement and ρ_s = 0·24. The curve shows two distinct regions: below L/L_C = 0·8, an irregular region of low force and above this value, a more regular region of higher forces. The first of these two regions corresponds to the rupture of SBs that connect sticky sites that are far apart along the chain. Due to their long distance along the chain, these SBs rupture at smaller end-to-end distances than SBs between neighbouring sticky sites. Nevertheless, in this regime, the number of intact SBs stays roughly constant showing that new SBs are reformed, but now, between sticky sites in closer distances along the chain. When the elongation L/L_C = 0·8 is reached, the chain is stretched to the extent that SB reformation ceases, and on further elongation, the number of intact SBs rapidly decreases to zero. It is the large number of SB rupture events distributed over a short length that is responsible for the higher value of the force in the region above L/L_C = 0·8. Due to the small number of sticky sites for the random arrangement and ρ_s = 0·08, SB reforming is not possible, and the load-displacement curve shows a single region of low force only (Figure 2b). The random arrangement with ρ_s = 0·24 shows an apparent stiffness of E = 1·84 meV/R², a work to fracture W = 23·51 eV and a strength of F_m = 0·55 eV/R.

Table 1 summarizes the different mechanical parameters obtained for the different structures characterized by the number

Bioinspired, Biomimetic and Nanobiomaterials
Volume 3 Issue BBN3

Influence of sacrificial bonds on the
mechanical behaviour of polymer chains
Nabavi, Harrington, Fratzl and Hartmann

		Work to fracture (W): eV	Apparent stiffness (E): meV/R^2	Strength (Fm): eV/R
$\rho_s = 0\cdot08$	Random	11·45	1·84	0·26
	Ordered	11·38	—	0·77
$\rho_s = 0\cdot24$	Random	23·51	1·84	0·55
	Ordered	22·55	5·03	0·7
	Patches	19·63	16·26	0·9

Table 1. The work to fracture W, the apparent stiffness E and the strength F_m of the different investigated structures in this study

and distribution of sticky sites. The results show that the work to fracture is mostly dependent on the number of SBs present in the system and does not dramatically change when the distribution of sticky sites is changed. For $\rho_s = 0\cdot08$, the work to fracture is identical within error bars for the ordered and random arrangement, while for $\rho_s = 0\cdot24$, it moderately increases from $W = 19\cdot63$ eV in the patches configuration to $23\cdot51$ eV for the random arrangement, which is a change of 20% only. Thus, it is the number of SBs that has to be broken and not their distribution that mainly determines the toughness of a material. For non-reversible bonds, it is even expected that W is constant because for the two extreme configurations of all bonds loaded in series or in parallel, the product of elongation and strength is constant. It is the reversibility of the SBs allowing bond reformation after rupture that is responsible for the slight increase in W. This situation is reversed when the behaviour of the apparent stiffness is investigated. The apparent stiffness is a measure of how much force is needed to elongate the chain. However, in contrast to the elastic modulus that is determined by the reversible elastic behaviour of a material, the apparent stiffness is a result of SB rupture, that is, plastic deformation. Nevertheless, the reversibility of the SBs allows for molecular repair and recovery of the initial mechanical parameters. The apparent stiffness for the two investigated random configurations is the same, although the number of SBs changes by a factor of 3 for the two investigated densities. Otherwise, when the number of SBs is kept constant and only their distribution is changed, the apparent stiffness changes from $E = 1\cdot84$ meV/R^2 for the random distribution to $16\cdot26$ meV/R^2 for the patches configuration, which is almost a factor of nine. The high apparent stiffness of the patches configuration is because in contrast to the other configurations, the SBs form between sticky sites that are very close along the chain. On average, there is only one non-sticky site in between, while in the ordered configuration, this distance is at least three non-sticky sites, and all distances are possible in the random arrangement. SBs between close sticky sites rupture at large elongations; thus, the patches arrangement ensures a late but high increase in the load. When comparing the strength of the different configurations, it can be observed that for the same sticky site density, the strength of the random configuration is always the smallest, while the strength of the ordered and the patches arrangement are of similar magnitude. It is the smearing of the sacrificial force peaks over

the entire length that is responsible for the reduced strength in the random distribution. The approximately twofold increase in the strength when increasing the sticky site density in the random distribution is due to the second region above $L/L_c = 0\cdot8$ in the load-displacement curve for the random arrangement and the high sticky site density that is missing in the low-density case.

The results presented in this work suggest the following guidelines for tuning behaviour of materials based on SBs via sticky site (ligand) distribution and number. To maximize the work to fracture (toughness) of the systems, the number of SBs and their ability to reform should be maximized, regardless of the specific distribution of the SBs. For an equal number of SBs, the apparent stiffness of a material can be greatly enhanced when the SBs are distributed such that it is ensured that the force rises over a small change in length of the polymer. In the present study, this was achieved by arranging SBs in patches in particular regions of the polymer, effectively reducing the distance between sticky sites. Finally, any ordered arrangement of SBs yields an elevated strength (both ordered and patches) when compared with a purely random configuration.

4.   Conclusions
The influence of the number and the distribution of SBs on the mechanical behaviour of single polymeric chains were investigated. It was shown that the work to fracture, related to the toughness of the material, is mainly determined by the number of SBs that have to be broken when the polymer is elongated, while the apparent stiffness and, to a lesser extent, the strength of the material is strongly dependent on the distribution of SBs in the system. The results presented have important implications for the development of new materials with tailored mechanical properties that employ sacrificial bonding – a concept that is masterly applied by nature to enhance the properties of biological materials.

Bioinspired, Biomimetic and Nanobiomaterials
Volume 3 Issue BBN3

**Influence of sacrificial bonds on the
mechanical behaviour of polymer chains**
Nabavi, Harrington, Fratzl and Hartmann

REFERENCES

1. Fratzl, P.; Weinkamer, R. Nature's hierarchical materials. *Progress in Materials Science* **2007**, *52*, 1263–1334.

2. Smith, B. L.; Schäffer, T. E.; Viani, M., et al. Molecular mechanistic origin of the toughness of natural adhesives, fibres and composites. *Nature* **1999**, *399*, 761–763.

3. Fantner, G. E.; Oroudjev, E.; Schitter, G., et al. Sacrificial bonds and hidden length: unraveling molecular mesostructures in tough materials. *Biophysical Journal* **2006**, *90*, 1411–1418.

4. Keckes, J.; Burgert, I.; Frühmann, K., et al. Cell-wall recovery after irreversible deformation of wood. *Nature Materials* **2003**, *2*, 810–814.

5. Thompson, J. B.; Kindt, J. H.; Drake, B., et al. Bone indentation recovery time correlates with bond reforming time. *Nature* **2001**, *414*, 773–776.

6. Fantner, G. E.; Hassenkam, T.; Kindt, J. H., et al. Sacrificial bonds and hidden length dissipate energy as mineralized fibrils separate during bone fracture. *Nature Materials* **2005**, *4*, 612–616.

7. Fantner, G. E.; Adams, J.; Turner, P., et al. Nanoscale ion mediated networks in bone: osteopontin can repeatedly dissipate large amounts of energy. *Nano Letters* **2007**, *7*, 2491–2498.

8. Becker, N.; Oroudjev, E.; Mutz, S., et al. Molecular nanosprings in spider capture-silk threads. *Nature Materials* **2003**, *2*(4), 278–283.

9. Harrington, M. J.; Wasko, S. S.; Masic, A., et al. Pseudoelastic behaviour of a natural material is achieved via reversible changes in protein backbone conformation. *Journal of the Royal Society Interface* **2012**;*9*:2911–2922.

10. Harrington, M. J.; Gupta, H. S.; Fratzl, P.; Waite, J. H. Collagen insulated from tensile damage by domains that unfold reversibly: in situ X-ray investigation of mechanical yield and damage repair in the mussel byssus. *Journal of Structural Biology* **2009**, *167*, 47–54.

11. Krauss, S.; Metzger, T. H.; Fratzl, P.; Harrington, M. J. Self-repair of a biological fiber guided by an ordered elastic framework. *Biomacromolecules* **2013**, *14*, 1520–1528.

12. Hwang, D. S.; Zeng, H.; Masic, A., et al. Protein- and metal-dependent interactions of a prominent protein in mussel adhesive plaques. *Journal of Biological Chemistry* **2010**, *285*, 25850–25858.

13. Qin, Z.; Buehler, M. J. Impact tolerance in mussel thread networks by heterogeneous material distribution. *Nature Communications* **2013**, *4*, 2187.

14. Keten, S.; Xu, Z.; Ihle, B.; Buehler, M. J. Nanoconfinement controls stiffness, strength and mechanical toughness of β-sheet crystals in silk. *Nature Materials* **2010**, *9*, 359–367.

15. Holten-Andersen, N.; Zhao, H.; Waite, J. H. Stiff coatings on compliant biofibers: the cuticle of Mytilus californianus byssal threads. *Biochemistry* **2009**, *48*, 2752–2759.

16. Holten-Andersen, N.; Fantner, G. E.; Hohlbauch, S.; Waite, J. H.; Zok, F. W. Protective coatings on extensible biofibres. *Nature Materials* **2007**, *6*, 669–672.

17. Lee, B. P.; Messersmith, P. B.; Israelachvili, J. N.; Waite, J. H. Mussel-inspired adhesives and coatings. *Annual Review of Materials Research* **2011**, *41*, 99–132.

18. Harrington, M. J.; Masic, A.; Holten-Andersen, N.; Waite, J. H.; Fratzl, P. Iron-clad fibers: a metal-based biological strategy for hard flexible coatings. *Science* **2010**, *328*, 216–220.

19. Barnes, D. S.; Pettit, L. D. Stereoselectivity in enthalpy changes accompanying the formation of metal complexes of histidine and other amino-acids. *Journal of Inorganic and Nuclear Chemistry* **1971**, *33*, 2177–2184.

20. Lee, H.; Scherer, N. F.; Messersmith, P. B. Single-molecule mechanics of mussel adhesion. *Proceedings of the National Academy of Sciences of the United States of America* **2006**, *103*, 12999–13003.

21. Mehdizadeh, M.; Weng, H.; Gyawali, D.; Tang, L.; Yang, J. Injectable citrate-based mussel-inspired tissue bioadhesives with high wet strength for sutureless wound closure. *Biomaterials* **2012**;*33*:7972–7983.

22. Kastrup, C. J.; Nahrendorf, M.; Figueiredo, J. L., et al. Painting blood vessels and atherosclerotic plaques with an adhesive drug depot. *Proceedings of the National Academy of Sciences of the United States of America* **2012**, *109*, 21444–21449.

23. Haque, M. A.; Kurokawa, T.; Gong, J. P. Super tough double network hydrogels and their application as biomaterials. *Polymer* **2012**, *53*, 1805–1822.

24. Holten-Andersen, N.; Harrington, M. J.; Birkedal, H., et al. pH-induced metal-ligand cross-links inspired by mussel yield self-healing polymer networks with near-covalent elastic moduli. *Proceedings of the National Academy of Sciences of the United States of America* **2011**, *108*, 2651–2655.

25. Fullenkamp, D. E.; He, L.; Barrett, D. G.; Burghardt, W. R.; Messersmith, P. B. Mussel-inspired histidine-based transient network metal coordination hydrogels. *Macromolecules* **2013**, *46*(3), 1167–1174.

26. Barrett, D. G.; Fullenkamp, D. E.; He, L., et al. pH-based regulation of hydrogel mechanical properties through mussel-inspired chemistry and processing. *Advanced Functional Materials* **2013**, *23*, 1111–1119.

27. Holten-Andersen, N.; Jaishankar, A.; Harrington, M. J., et al. Metal-coordination: using one of nature's tricks to control soft material mechanics. *Journal of Materials Chemistry B* **2014**, *2*, 2467–2472.

28. Xu, Z. Mechanics of metal-catecholate complexes: the roles of coordination state and metal types. *Science Reports* **2013**, *3*, 2914.

29. Lieou, C. K. C.; Elbanna, A. E.; Carlson, J. M. Sacrificial bonds and hidden length in biomaterials: a kinetic constitutive

Bioinspired, Biomimetic and Nanobiomaterials
Volume 3 Issue BBN3

Influence of sacrificial bonds on the
mechanical behaviour of polymer chains
Nabavi, Harrington, Fratzl and Hartmann

description of strength and toughness in bone. *Physical Review E* **2013**, *88*, 012703.

30. Elbanna, A. E.; Carlson, J. M. Dynamics of polymer molecules with sacrificial bond and hidden length systems: towards a physically-based mesoscopic constitutive law. *PLoS ONE* **2013**, *8*, e56118.

31. Nabavi, S. S.; Harrington, M. J.; Paris, O.; Fratzl, P.; Hartmann, M. A. The role of topology and thermal backbone fluctuations on sacrificial bond efficacy in mechanical metalloproteins. *New Journal of Physics* **2014**, *16*, 013003.

32. Hartmann, M. A.; Fratzl, P. Sacrificial ionic bonds need to be randomly distributed to provide shear deformability. *Nano Letters* **2009**, *9*, 3603–3607.

33. Harrington, M. J.; Waite, J. H. Holdfast heroics: comparing the molecular and mechanical properties of Mytilus californianus byssal threads. *Journal of Experimental Biology* **2007**, *210*, 4307–4318.

34. Knecht, S.; Ricklin, D.; Eberle, A. N.; Ernst, B. Oligohis-tags: mechanisms of binding to Ni2+-NTA surfaces. *Journal of Molecular Recognition* **2009**, *22*, 270–279.

35. Cao, Y.; Yoo, T.; Li, H. Single molecule force spectroscopy reveals engineered metal chelation is a general approach to enhance mechanical stability of proteins. *Proceedings of the National Academy of Sciences of the United States of America* **2008**, *105*, 11152–11157.

36. Manca, F.; Giordano, S.; Palla, P. L., et al. Elasticity of flexible and semiflexible polymers with extensible bonds in the Gibbs and Helmholtz ensembles. *Journal of Chemical Physics* **2012**, *136*, 154906.

37. Landau, D.; Binder, K. *A Guide to Monte Carlo Simulations in Statistical Physics*. Cambridge, UK: Cambridge University Press, 2009.

38. Marko, J. F.; Siggia, E. D. Stretching DNA. *Macromolecules* **1995**, *28*, 8759–8770.

39. Ortiz, C.; Hadziioannou, G. Entropic elasticity of single polymer chains of poly(methacrylic acid) measured by atomic force microscopy. *Macromolecules* **1999**, *32*, 780–787.

40. Gutsmann, T.; Hassenkam, T.; Cutroni, J. A.; Hansma, P. K. Sacrificial bonds in polymer brushes from rat tail tendon functioning as nanoscale velcro. *Biophysical Journal* **2005**, *89*, 536–542.

10 Appendix *III*

S. Soran Nabavi, Peter Fratzl and Markus A. Hartmann

Energy dissipation and recovery in a simple model with reversible
cross-links

Energy dissipation and recovery in a simple model with reversible cross-links

S. Soran Nabavi,[1] Peter Fratzl,[2] and Markus A. Hartmann[1, *]

[1]*Institute of Physics, Montanuniversitaet Leoben,*
Franz-Josef Strasse 18, 8700 Leoben, Austria

[2]*Max-Planck-Institute of Colloids and Interfaces, Department of Biomaterials,*
Research Campus Golm, 14424 Potsdam, Germany

(Dated: October 30, 2014)

Abstract

Reversible cross-linking is a method of enhancing the mechanical properties of polymeric materials. The inspiration for this kind of cross-linking comes from nature that uses this strategy in a large variety of biological materials to dramatically increase their toughness. Recently, first attempts have been made to transfer this principle into technological applications. In this study, Monte Carlo simulations are used to investigate the effect of the number and the topology of reversible cross-links on the mechanical performance of a simple model system. Computational cyclic loading tests are performed and the work to fracture as well as the energy dissipation per cycle are determined that both increase when the density of cross-links is increased. Furthermore, a different topology of the bonds may increase the work to fracture a factor more than two for the same density. This dependence of the mechanical properties on the topology of the bonds has important implications on the self healing properties of such systems, because only a fast return of the system to its unloaded state after release of the load ensures that the optimal topology may form.

---

*Electronic address: markus.hartmann@unileoben.ac.at

I. INTRODUCTION

Cross-linking is a common strategy used in natural as well as in technological polymeric materials to enhance their mechanical properties [1]. One of the most prominent examples is the development of vulcanization by Ch. Goodyear in 1839. Permanent cross-linking with sulfur bridges significantly improved the mechanical performance of rubber products. Since then many other applications for polymer cross-linking have been invented [2]. Recently covalent cross-linking was also suggested to improve the shear stability in carbon nanostructures like graphene and carbon nanotubes [3, 4]. In natural materials the bending properties of actin bundles of the cell cytoskeleton differ by several orders of magnitude depending on the degree of cross-linking [5–7].

Besides permanent (covalent) cross-linking nature also uses the concept of reversible cross-links that provides an efficient way of toughening the material. Different to permanent cross-links these so called sacrificial bonds (SBs) can open and close reversibly. SBs have been found in a large variety of biological materials like bone [8, 9], wood [10], and some fibrous materials such as silk [11, 12], the mussel byssus [13–15] and the whelk egg capsule [16]. The strength of individual SBs can largely differ from several 100 meV for hydrogen bridges to a value close to the strength of covalent bonds for metal coordination bonds [17, 18].

SBs are cross-links that are weaker than the covalent bonds that hold the structure together. Thus, upon loading the SBs rupture first while the covalent bonds stay intact [8, 19]. Whenever a SB fails, hidden length may be revealed by opening and unfolding of loops in the protein and, thus, energy dissipated [8]. Furthermore, SBs are often reversible, i.e. they can open and close repeatedly. Consequently, after some time the material regains its original mechanical properties when the load was released [20, 21]. These remarkable properties of reversible cross-links trigger the desire to transfer some of the underlying principles into technological applications. These attempts include the development of self-healing polymeric materials with increased stiffness and extensibility [22–24], the mechanical improvement of hydrogels [25–28], the fabrication of mussel inspired polydopamine films for use in biomedical or electrochemical applications [29–31] and the functionalization of graphene using mussel inspired chemistry [32].

Understanding the underlying structure-function relationships that allow for these ex-

traordinary mechanical performance is of utmost importance to mimic these fundamental design principles and to transfer them into novel man-made materials [33]. This understanding, nevertheless, is an extremely complicated task due to the enormous complexity and subtle interactions that are found in biological systems. Thus, simple models focusing on well defined aspects of the problem may be addressed either analytically or with the help of computer simulations and are indispensable tools making these complex systems theoretically tractable and helping the interpretation of experimental findings. Using analytical and computational modeling techniques, it was shown that confinement strongly influences the rupture of hydrogen bonds in silk like structures [34, 35], that the distribution of SBs determines the shear deformability in bone [36] and that mechanical properties of structures relying on SBs show a pronounced dependence on pulling speed [37, 38].

In the present paper we investigate a simple model of a polymer chain that can reversibly form cross-links between some of its monomers mimicking the effect of SBs. Using Monte Carlo (MC) simulations we investigate the influence of SB density and topology on the work to fracture and specifically on the amount of dissipated energy per loading cycle. Special emphasis in the discussion is put on the process of reforming ruptured SBs during unloading of the system. This reforming determines the mechanical properties after one loading cycle and is thus strongly linked to the self healing capabilities of the structures. The mechanical properties depend on the topology that SBs form when closing. The type of topology is strongly influenced by the rate at which the loaded structure returns into its native state. The approach chosen in this paper is to build an especially simple model, capturing the essentials of sacrificial bonding. The simplicity of the model gives the advantage of understanding the system completely. As a next step the basic mechanisms underlying energy dissipation and recovery identified in this model will also help to understand the much more complex situation in real systems.

II. THE MODEL

The model is inspired by the fascinating class of metalloproteins and was already presented in [39]. Thus, in the following only a short description is given focusing on the new concepts used in this paper. The model consists of a linear chain of $N = 50$ covalently bonded beads with a hard-sphere radius R (that we set as the unit of length). The covalent

bonds are described via a Morse potential

$$E(r_{ij}) = E_0\{[1 - \exp(-\beta(r_{ij} - r_0))]^2 - 1\} \tag{1}$$

$E_0 = 5$ eV is the depth of the potential, $\beta^{-1} = 0.5$ R the width of the potential, $r_0 = 3R$ the equilibrium distance and r_{ij} is the distance between the two neighboring beads. Consequently the contour length of the chain is given by $L_C = (N-1)r_0$. To account for the effect of reversible cross-links N_s of the beads are defined as sticky. The sticky sites are introduced regularly, i.e., the same number of non-sticky sites separating them. Always two of these sticky sites could form a SB. The energetics of the SBs are described with an identical potential as the covalent bonds but with a reduced binding energy $E_0^{SB} = 1.25$ eV. The cross-links were allowed to open and close reversibly and cross-link updating was performed using a standard Metropolis algorithm [40]. Updating the position of the inner beads of the chain was also performed using the Metropolis algorithm. Simulations were performed in the Helmholtz ensemble by pinning the first and last bead defining the end-to-end distance $L = |r_1 - r_N|$ of the chain [41]. Simulations mimicking cyclic loading experiments were performed by starting from a small end-to-end distance that was gradually increased until $L/L_C = 1$. Then the loading was reversed, i.e. L was slowly decreased, until the initial end-to-end distance was recovered. Eventually the chain was then stretched a second time. During each simulation step the force on the outer beads was recorded and averaged. For each length up to 3 million Monte Carlo steps (MCS), i.e. jump trials per bead and per sticky site, were performed. The results shown in this paper are the averages of 20 independent runs for stretching and 10 independent runs for unloading of the chain. In the simulations the temperature was set to the ambient value of $k_B T = 25$ meV.

III.   RESULTS

A.   Influence of the sticky site density

Independent starting configurations with small end-to-end distances were prepared by slowly unloading a fully stretched chain without sticky sites to the starting length $L/L_C = 0.04$. Then the sticky sites were introduced corresponding to densities $\rho_s = N_s/N = 0.08$, 0.24 and 0.48, respectively, and the SBs were allowed to form. Figure 1 shows the average number of closed SBs as a function of time measured in units of MCS and the two densities
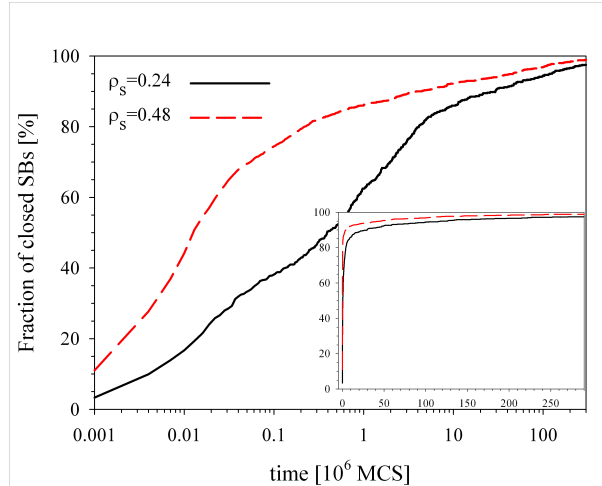
4

FIG. 1: The number of closed SBs as a function of time for the two high SB densities. The data are the average of 100 independent runs for each sticky site density. Note, the logarithmic scaling of the time axis. The inset shows the same data with a linear time axis.

of sticky sites. At both densities there is an initial steep increase in sticky site number that is subsequently slowed down at longer times. This behavior is similar to what was shown in experiments that report an initially fast recovery of the mechanical properties reaching approximately 70 % after waiting times of one hour, but considerably slowing down to a recovery of only 95 % after 168 hours [13].

Figure 2 shows load-displacement curves for cyclic loading and the three investigated sticky site densities obtained after the SBs have formed. The black symbols show the behavior during loading, while red symbols denote unloading of the structure. The bottom row of the same figure shows the corresponding number of intact SBs. The lowest density corresponds to $N_s = 4$ sticky sites in the system that are separated by 10 monomers. When this structure is stretched a discrete rupture of SBs can be observed (see Fig. 2A). The position of the observed force peaks is determined by the topology of the involved SBs, while its height is intimately tied to the thermal fluctuations of the protein backbone and is considerable smaller than the theoretical strength of one SB given by $F_{max} = \beta E_0^{SB}/2 = 1.25$ eV/R [39]. Each single peak can be fitted with the worm-like-chain model [1, 42] that has been shown to reasonably well describe such entropic loads [43, 44]. When ρ_s is increased (corresponding to $N_s = 12$ and 24 sticky sites, respectively) the distinct peaks corresponding to SB rupture merge into one large plateau and the force does not drop to zero between
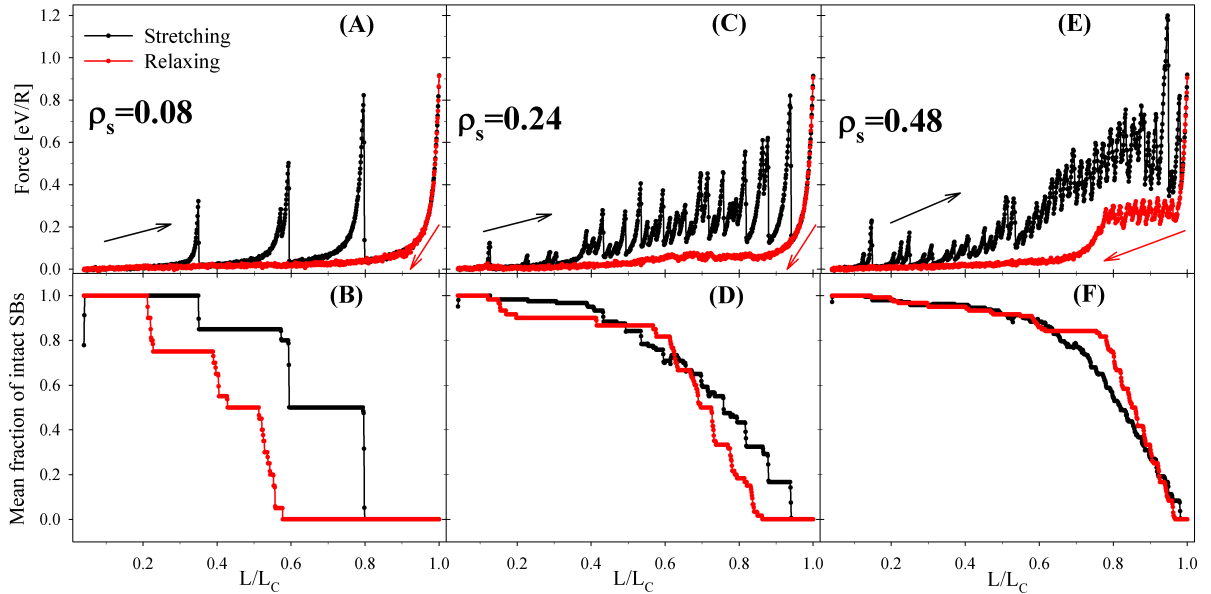
5

FIG. 2: (A), (C), (E): Cyclic loading curves for $N = 50$ at $k_BT = 25$ meV and three different sticky site densities. (B), (D), (F): The corresponding mean number of closed SBs as a function of the end-to-end distance. Black symbols denote loading, red the unloading branches. The presented curves are the averages of 20 runs of stretching and 10 runs of unloading.

discrete rupture events (see Fig. 2(C and E)). The height of this plateau is comparable to the height of the distinct force peaks seen in Fig. 2(A), in particular the plateau is also lower than the theoretical strength of one SB. Thus, entropic effects continue to largely influence the effective strength of SBs also for high sticky site densities.

As soon as the polymer is stretched to its contour length L_C, the direction of loading is reversed and the structures are unloaded. For all three sticky site densities the load-displacement curves show a pronounced asymmetry between loading and unloading—more energy is needed to elongate the polymer, than is restored when it is unloaded. The difference in the area of the two curves is a measure of the dissipated energy per loading cycle $\Delta E = E_1 - E_2$, with E_1 and E_2 the area under the loading and unloading curve, respectively. The work to fracture is given by $W = E_1 + E_C$ with $E_C = 25$ eV the energy needed to finally rupture the fully elongated polymer. Because all SBs are open for a fully elongated polymer, E_C is a constant for all investigated structures. Thus, in the following, E_C will be omitted and the energy to elongate the polymer E_1 and the work to fracture will be used interchangeably. For the three investigated densities the dissipated energy was found to be

6

$\Delta E = 5.5 \pm 0.2$ eV, 15.1 ± 0.5 eV and 23.8 ± 1.4 eV, respectively. The corresponding relative amount of dissipated energy was given by $\Delta E / E_1 = 0.49$, 0.67 and 0.65, respectively (see also Table I). The lower part of Figure 2 shows that all SBs are open when the chains are stretched to their contour lengths. Upon unloading of the chain with $\rho_s = 0.08$ the SBs reform, but at end-to-end distances smaller than the distance corresponding to bond breaking (see Figure 2(B)). At these smaller distances the chain has already enough conformational freedom that the formed SBs can relax and, thus, do not experience an elevated force. The reason for delayed bond formation is that two sticky sites have to come into close spatial vicinity that a stable SB may form. At large end-to-end distances it is highly improbable that in a fluctuating chain sticky sites find each other.

Unloading of the chain with $\rho_s = 0.24$ is similar to the low density case $\rho_s = 0.08$. Mostly, the bonds reform at distances lower than when they were broken. At higher sticky site density the distance between neighboring sites is smaller and the force is slightly increased compared to the unloading for the case $\rho_s = 0.08$ (see Fig. 2). The small region around $L/L_C = 0.6$, where sticky sites reform earlier than they were broken, is due to SBs that have been originally formed between sticky sites separated a long distance along the chain and that reform between closer sticky sites.

This effect is even more pronounced for the highest sticky site density $\rho_s = 0.48$, whose unloading behavior can be described as a three stage process (Fig. 2(E) and (F)): first, for an end-to-end distance still close to the contour length the number of intact SBs increases considerably due to bond formation between sticky sites that are in close vicinity along the chain. This different behavior compared to the low density case is explained by, first, the higher number of sticky sites and, second, their closer distance along the chain, which both increase the probability of SB formation. In contrast to the low density case, due to the elevated length of the chain these bonds have not yet the conformational freedom to relax. Thus, the SBs are still strained resulting in the plateau in the unloading part of the load-displacement curve. Second, for intermediate end-to-end distances no new bonds are formed, but the existing bonds relax. This can be seen as a sharp drop in the force in the load-displacement curve (Fig. 2(E)) and a constant number of the intact bonds (Fig. 2(F)). Third, for small end-to-end distances the chain is relaxed enough that the remaining sticky sites that are far apart along the chain can form SBs. Thus, the number of intact SBs slowly increases again, while the force is slowly decaying to zero. For low ρ_s all sticky sites are well
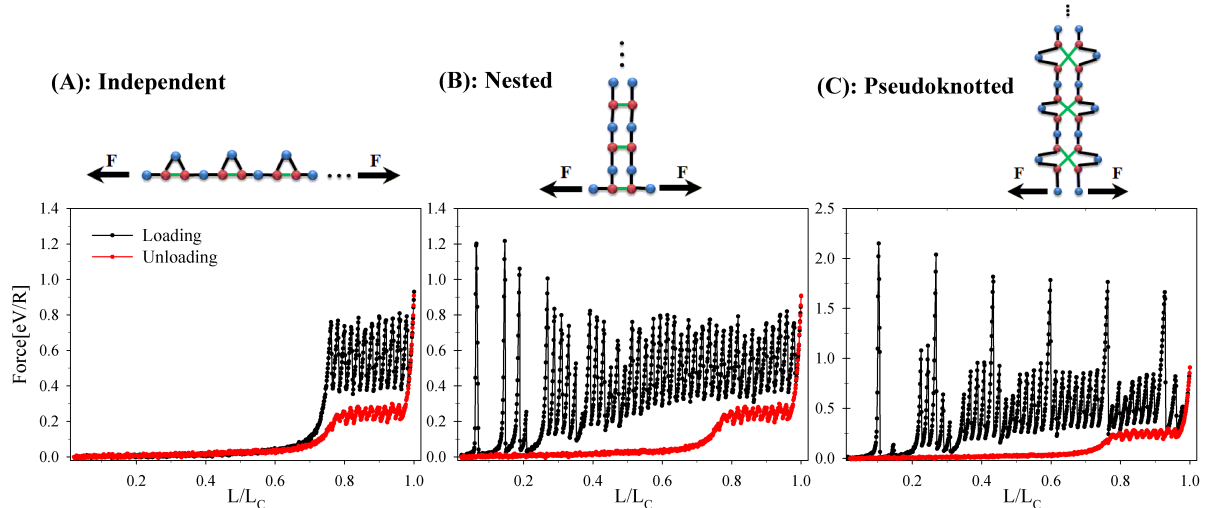
FIG. 3: Starting configurations (top) and load-displacement curves (bottom) for three different topologies of SBs: independent (A), nested (B) and pseudoknotted (C). The black line shows stretching of the different starting configurations until the contour length, the red line shows subsequent (quasi static) unloading. Note, that this curve is identical for all structures. The length of the chains was $N = 50$ and the sticky site density $\rho_s = 0.48$.

separated along the chain and unloading of the chain is described by the third stage only (see Fig. 2A).

B.   Influence of the topology of bonds

Previous work has shown that the topology of bonds has a large influence on the mechanical behavior of the polymer and its capability of dissipating energy [39, 45–47]. To test the influence of the topology on E_1 and the dissipated energy ΔE a new set of simulations with special starting configurations were performed. Instead of introducing the sticky sites in the crumpled starting state of the polymer and allowing the formation of SBs without any bias, in these new starting configurations the topology of the SBs was predefined at the beginning: the independent, nested and pseudoknotted configuration (see the top row of Figure 3 for a sketch of the starting configurations and corresponding topologies) [45]. The bottom row of Figure 3 shows the resulting load-displacement curves. The black symbols denote loading of the different starting configurations. Although the number of sticky sites and thus the initial number of SBs is equal for all three structures ($\rho_s = 0.48$), the stretching part of

8

the load-displacement curves shows a considerable different behavior. For the independent configuration the force starts rising at the largest elongations compared to the other two topologies. The first SB starts stretching when the length of the structure is increased to $L/L_C = 1 - N_s/2(N-1) \approx 1 - \rho_s/2 = 0.76$ (see Figure 3(A)), while the much lower values $L/L_C \approx 3/(N-1) = 0.06$ and $L/L_C \approx 5/(N-1) = 0.10$ are found for the nested and the pseudoknotted configuration, respectively. Another difference between the topologies can be seen in the number of single rupture events characterized by the force peaks in the load-displacement curves. There are exactly 12 rupture events for the independent configuration, while for the nested and pseudoknotted configuration the number of rupture events increases by a factor more than three. In all the different configurations there are 24 sticky sites, giving a maximum number of 12 simultaneously closed SBs. The number of 12 SB ruptures for the independent configuration shows that after SB rupture the now open sticky sites do not reform. This is different for the nested and pseudoknotted configurations. The number of SB ruptures is much larger than 12, indicating that in this case after rupture the open sticky sites recombine leading to the formation of new SBs. It is clear that reforming of SBs increases the work under the stretching curve. On the other hand, the lack of SB reforming leads to a reduction of more than 50% in E_1 for the independent topology compared to the other two cases (see Table I). Another point that can be observed concerns the height of the force peaks corresponding to individual SB rupture events. Although in the simulations all SBs are identical, the height of the observed force peaks shows significant variations. In [39] it was shown that the effective strength of SBs is reduced by thermal backbone fluctuations and, thus, crucially depends on the effective length of the chain defined by the SB. This effect can be clearly seen in the presented figure. For the independent configuration SB rupture starts at a large effective length of $L/L_C \approx 0.75$ and all the force peaks show a height of ≈ 0.8 eV/R which is a reduction of one third compared to the theoretical strength of one SB of $F_{max} = 1.25$ eV/R (see Figure 3(A)). The first rupture in the nested configuration occurs at a small effective length of $L/L_C \approx 0.06$. Due to this small length the effective strength of the SB is close to its theoretical value F_{max}. When the chain is further stretched its effective length increases and the effective strength of SBs decreases attaining the same value of ≈ 0.8 eV/R as in the independent configuration for large elongations (see Figure 3(B)). The rupture of the six pseudoknotted loops in Figure 3(C) results in force peaks approximately twice the size of the single SBs. Also here the reduction of effective strength

9

	E_1	E_2	ΔE	$\Delta E / E_1$
	[eV]	[eV]	[eV]	[-]
Crumpled starting configuration				
$\rho_s = 0.08$	11.4 ± 0.2	5.90 ± 0.02	5.5 ± 0.2	0.48 ± 0.02
$\rho_s = 0.24$	22.6 ± 0.5	7.42 ± 0.06	15.1 ± 0.5	0.67 ± 0.03
$\rho_s = 0.48$	36.7 ± 1.3	12.84 ± 0.14	23.9 ± 1.3	0.65 ± 0.04
Predefined topologies				
Independent	24.2 ± 0.1	12.84 ± 0.14	11.3 ± 0.2	0.47 ± 0.01
Nested	54.6 ± 0.5	12.84 ± 0.14	41.7 ± 0.6	0.76 ± 0.01
Pseudoknotted	63.0 ± 0.7	12.84 ± 0.14	50.1 ± 0.7	0.80 ± 0.01
Second stretching	30.0 ± 1.2	12.84 ± 0.14	17.2 ± 1.2	0.57 ± 0.05

TABLE I: The energy needed to stretch the molecule to its contour length E_1 (up to an additive constant this is corresponding to the work to fracture), the energy gained during unloading E_2, the corresponding energy dissipation $\Delta E = E_1 - E_2$ and the amount of dissipated energy $\Delta E / E_1$ for the different investigated structures.

with increasing elongation is clearly visible.

When the chains were stretched to $L/L_C = 1$ the loading was reversed and the chains unloaded. At this point all SBs were open. Thus, the starting configuration, and consequently the behavior upon unloading, is the same for all cases with the same sticky site density (especially it is also identical to the unloading already discussed and shown in Figure 2(E).

IV. DISCUSSION

The simple model presented here can not claim to describe the microscopic details of enormous complexity characterizing load bearing structures in real materials. The polymer itself is described by a simple bead model, the monomer interactions are excluded volume only, backbone elasticity is given solely by bond stretching contributions and the solvent is totally neglected. SBs are described phenomenologically with an effective potential connecting always to beads, whereas in natural and technological materials SBs are often formed between three partners [14]. Despite these massive simplifications that are necessary to

make the situation computationally tractable many characteristics found in the mechanical behavior of biological materials can also be found in the model presented. The sawtooth pattern characteristic for single SB rupture for low sticky site densities (see fig. 2A) closely resembles experimentally found loading curves reported in nacre [19] or in single molecule measurements [48–53]. Furthermore, experimental investigations of the mussel byssus show an energy dissipation of $\Delta E/E_1 \approx 0.7$ [54] that is similar to the values found during cyclic loading for the two high sticky site densities investigated in this paper.

One of the most remarkable properties of biological materials is their ability to repair and self heal. One concept of nature to achieve this, is to use reversible sacrificial bonds. It is the reversibility of these bonds that allows for repair after the load was released. Nevertheless, the repair takes some time and healing does not occur instantaneous. Whenever the structure is re-loaded immediately after unloading the mechanical properties characterizing second stretching are strongly deteriorated compared to the first, while the mechanical properties recover after some waiting time in between consecutive loading cycles [55]. This effect is attributed to the time needed for the sticky sites (that are mostly open after loading) to find and reform stable SBs. Experiments showed that this process speeds up when the temperature is increased, thus indicating that SB formation is a random, thermally activated process [13]. The rate of bond formation obtained with the present model resembles the experimental finding of an initially fast formation that subsequently slows down (see Fig. 1) giving further indication that the recovery is a stochastic, thermally activated process. Nevertheless, one should keep in mind that the self healing process in reality is much more complicated than can be captured with the simple model presented, depending e.g. on the pH [56, 57] and the pI value [58].

Not only reforming of SBs rather all relevant mechanical parameters depend on time, i.e. stretching speed [38, 59]. Energy dissipation becomes larger if the structure is unloaded faster than the SBs can form, i.e. $\Delta t_{Unload} \ll \tau_{SB}$. No elevated force would be seen on the unloading branch, effectively increasing the area between the curves. On the other hand, the energy dissipation would decrease when stretching is faster than the relaxation time of the polymer, such that it is not the SBs but rather the covalent bonds that fail. Although MC simulations do not allow to directly determine time dependent properties it is still possible to gain some insights on the two limiting cases of infinitely fast and infinitely slow (quasi static) loading. The load-displacement curves presented in Figs. 2 and 3 correspond to quasi-static

deformation, i.e. the polymer was stretched so slowly that the structure was given enough time to equilibrate at each loading step. When these quasi statically unloaded structures are stretched a second time, this second stretching is different to the first. This is due to the different preparation of the starting state. The starting configuration for the first stretching was prepared such that SB formation was allowed only when the polymer was fully unloaded. This corresponds to a unloading much faster than the SBs can form, i.e. the limiting case of infinitely fast unloading $\Delta t_{Unload} \ll \tau_{SB}$. In contrast the starting configuration for the second stretching was obtained by a quasi static unloading of the polymer allowing for SB formation already at large elongations. Fig. 4 shows the difference of the first and second stretching cycle $\Delta F = F_1 - F_2$ calculated from the averaged load-displacement curves as a function of elongation. Clearly, on average $\Delta F > 0$ showing that the load of the second stretching is reduced compared to the first. This leads to a 20 % reduction of the area under the stretching curve from 36.7 to 30 eV (see Table I). The different mechanical behavior of the second stretching cycle can be attributed to a changed topology of the SBs induced by the different methods of preparation of the starting configuration. On average 72 ± 3.4 % independent, 14.5 ± 2.4 % nested and 13.5 ± 2.1 % pseudoknotted SBs are formed for the fast unloading. In contrast, quasi-static unloading favors the independent topology (SBs are formed between neighboring sticky sites) on cost of the pseudoknotted structure (SBs are formed between non-neighboring sticky sites). A detailed analysis showed that during quasi static unloading 83 ± 3 % of the SBs show the independent topology. The remaining 17 ± 3 % of SBs are of the nested type, while not a single pseudoknotted configuration was created in any unloading simulation run. It is this decrease in the number of pseudoknotted SBs that is responsible for the roughly 20 % decrease in E_1 for the second stretching cycle after a quasi static return. Thus, in the investigated model a fast unloading is essential to achieve a complete recovery of the initial material properties, i.e. the unloading has to be much faster than the time scale of SB reformation. A similar mechanism might explain why the mussel byssus possesses a highly ordered elastic framework that ensure a very fast return of the stretched structure upon release of the load [60]. An analogous situation is found for cyclic loading of titin where the second stretching cycles are characterized by a lower number of the characteristic sawtooth peaks compared to the first [49].

As discussed above for random polymers a fast return of the structure into its unstrained state can give an approximately 20 % increase in the work to fracture. This increase can
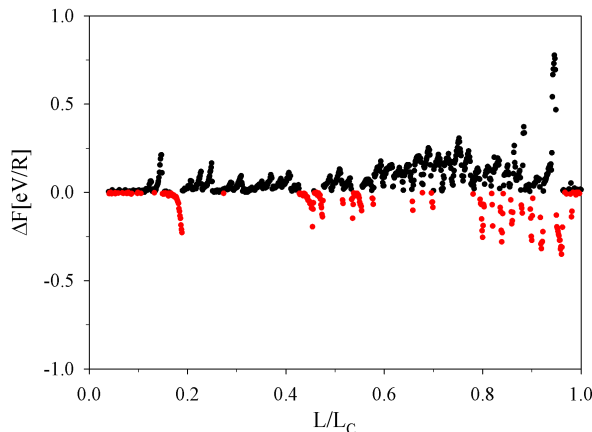
12

FIG. 4: The difference $\Delta F = F_1 - F_2$ of the load-displacement curves for the first and second stretching. Black points denote $\Delta F > 0$ and red points $\Delta F < 0$, respectively. Clearly, on average $\Delta F > 0$ showing that the first stretching cycle shows on average a higher load than the second. This results in an approximately 20 % decrease in E_s - see also Table I.

be enhanced to almost 100 % if it is possible to favor the nested or pseudoknotted over the independent topology (see Table I). This can be achieved if the polymer shows a certain folding pattern. While random polymers have to rely on thermally induced formation of SBs governed by the fluctuations of the backbone, the advantage of folding is that it is possible to bring selected sticky sites into close spatial vicinity that can form SBs of a chosen topology. While proteins control their folding pattern via the mutual interaction of the sidechains and of the sidechains with water, one of the most important factors determining the shape of polymers in general is backbone elasticity. When additional bending terms are included in the description of the backbone elasticity of the polymers, depending on the magnitude of the bending constant and the temperature a broad range of equilibrium shapes of the polymers, including hair pin structures, can be observed [61]. Naturally these hair pin structures favor the formation of the nested topology. Another example are SBs based on hydrogen bridges in beta-sheets that are responsible for the remarkable mechanical properties of silk [34, 35]. The parallel strands allow for the pseudoknotted topology. The resulting cooperative failure of the SBs maximize the force to unfold the polymer [59, 62]. Furthermore, due to the cooperative loading of the SBs in these structures the rather weak hydrogen bridges can provide considerable forces. On the other hand, to provide sufficient mechanical stability

13

SBs in random coil polymers like the metal coordination bonds investigated in this paper are much stronger, because they normally fail sequentially.

V. SUMMARY AND CONCLUSIONS

Using a simple model the influence of the number and topology of SBs on the mechanical behavior of polymeric chains during cyclic loading was investigated. In general both, the work to fracture E_1 and the energy dissipation ΔE, increase with increasing sticky site density. While for low sticky site densities a discrete rupture of single SBs can be observed, for high sticky site densities these single peaks merge into one large plateau. Computational cyclic loading experiments showed a pronounced asymmetry between the stretching and unloading branch for all sticky site densities. This hysteresis is due to two different reasons: first, the SBs reform at elongations smaller than they rupture and, second, the SBs reform between sticky sites with a smaller distance along the chain than they have been originally formed. Consequently upon quasi static unloading the topology of the SBs changes. In general, the amount of SBs of the independent type increases on cost of the pseudoknotted type.

It was shown that the nested and pseudoknotted topology possess superior mechanical properties compared to the independent configuration. The work to fracture and the dissipated energy are increased a factor more than two from a purely independent to the pseudoknotted topology. This large increase is due to a pronounced reforming of the bonds ruptured during loading. After a quasi-static unloading the formation of SBs of independent type are favored on cost of the pseudoknotted behavior. Thus, the mechanical performance of the polymer is deteriorated when it is stretched a second time. It can be concluded that after release of the load a fast return to its initial state is essential for the polymer to maintain its mechanical performance.

Although simple, the model presented captures several aspects of sacrificial bonding also found in real systems. These are, first, the characteristic sawtooth patterns found for low sticky site densities, second, the pronounced hysteresis in cyclic loading with an energy dissipation of ≈ 70 % for high sticky site densities, third, the characteristic time scale of reformation of SBs after unloading with an initial fast and a subsequent slow recovery, and fourth, the deterioration of mechanical properties during second loading depending on

14

unloading speed. This resemblance might indicate that the mechanisms of energy dissipation and recovery identified in this simple model have also some importance in real systems.

VI.   ACKNOWLEDGEMENT

[1] M. Rubinstein and R. H. Colby, *Polymer Physics* (Oxford University Press, 2003).

[2] A. Abe, K. Dusek, and S. Kobayashi, eds., *Crosslinking in Materials Science*, vol. 184 of *Advances in Polymer Science* (Springer, 2005).

[3] R. H. Telling, C. P. Ewels, A. A. El-Barbary, and M. I. Heggie, Nat. Mater. **2**, 333 (2003).

[4] A. Kis, G. Csányi, J.-P. Salvetat, T.-N. Lee, E. Couteau, A. J. Kulik, W. Benoit, J. Brugger, and L. Forró, Nat. Mater. **3**, 153 (2004).

[5] M. M. A. E. Claessens, M. Bathe, E. Frey, and A. R. Bausch, Nat. Mater. **5**, 748 (2006).

[6] S. Ulrich, A. Zippelius, and P. Benetatos, Phys. Rev. E **81**, 021802 (2010).

[7] P. Benetatos, S. Ulrich, and A. Zippelius, New J. Phys. **14**, 115011 (2012).

[8] G. E. Fantner, T. Hassenkam, J. H. Kindt, J. C. Weaver, H. Birkedal, L. Pechenik, J. A. Cutroni, G. A. G. Cidade, G. D. Stucky, D. E. Morse, et al., Nat. Mater. **4**, 612 (2005).

[9] H. S. Gupta, P. Fratzl, M. Kerschnitzki, G. Benecke, W. Wagermaier, and H. O. K. Kirchner, J. R. Soc. Interface **4**, 277 (2007).

[10] J. Keckes, I. Burgert, K. Frühmann, M. Müller, K. Kölln, M. Hamilton, M. Burghammer, S. V. Roth, S. Stanzl-Tschegg, and P. Fratzl, Nat. Mater. **2**, 810 (2003).

[11] E. Oroudjev, J. Soares, S. Arcidiacono, J. B. Thompson, S. A. Fossey, and H. G. Hansma, Proc. Natl. Acad. Sci. USA **99**, 6460 (2002).

[12] N. Becker, E. Oroudjev, S. Mutz, J. P. Cleveland, P. K. Hansma, C. Y. Hayashi, D. E. Makarov, and H. G. Hansma, Nat Mater **2**, 278 (2003).

[13] M. J. Harrington, H. S. Gupta, P. Fratzl, and J. H. Waite, J. Struct. Biol. **167**, 47 (2009).

[14] M. J. Harrington, A. Masic, N. Holten-Andersen, J. H. Waite, and P. Fratzl, Science **328**, 216 (2010).

[15] D. S. Hwang, H. Zeng, A. Masic, M. J. Harrington, J. N. Israelachvili, and J. H. Waite, J. Biol. Chem. **285**, 25850 (2010).

[16] M. J. Harrington, S. S. Wasko, A. Masic, F. D. Fischer, H. S. Gupta, and P. Fratzl, J. R. Soc. Interface **9**, 2911 (2012).

[17] D. S. Barnes and L. D. Pettit, J. Inorg. Nucl. Chem. **33**, 2177 (1971).

[18] Z. Xu, Sci. Rep. **3**, 2914 (2013).

[19] B. L. Smith, T. E. Schäffer, M. Viani, J. B. Thompson, N. A. Frederick, J. Kindt, A. Belcher, G. D. Stucky, D. E. Morse, and P. K. Hansma, Nature **399**, 761 (1999).

[20] W. C. Yount, D. M. Loveless, and S. L. Craig, Angew. Chem. Int. Ed. **44**, 2746 (2005).

[21] L. Schmitt, M. Ludwig, H. E. Gaub, and R. Tampe, Biophys. J. **78**, 3275 (2000).

[22] A. M. Kushner, V. Gabuchian, E. G. Johnson, and Z. Guan, J. Am. Chem. Soc. **129**, 14110 (2007).

[23] P. Cordier, F. Tournilhac, C. Soulié-Ziakovic, and L. Leibler, Nature **451**, 977 (2008).

[24] Y. Yang and M. W. Urban, Chem. Soc. Rev. **42**, 7446 (2013).

[25] M. A. Haque, T. Kurokawa, G. Kamita, and J. P. Gong, Macromolecules **44**, 8916 (2011).

[26] M. A. Haque, T. Kurokawa, and J. P. Gong, Polymer **53**, 1805 (2012).

[27] J. Hu, T. Kurokawa, T. Nakajima, T. L. Sun, T. Suekama, Z. L. Wu, S. M. Liang, and J. P. Gong, Macromolecules **45**, 9445 (2012).

[28] D. E. Fullenkamp, L. He, D. G. Barrett, W. R. Burghardt, and P. B. Messersmith, Macromolecules **46**, 1167 (2013).

[29] S. H. Ku, J. S. Lee, and C. B. Park, Langmuir **26**, 15104 (2010).

[30] M.-H. Ryou, Y. M. Lee, J.-K. Park, and J. W. Choi, Adv. Mater. **23**, 3066 (2011).

[31] S. Lin, C.-T. Chen, I. Bdikin, V. Ball, J. Gracio, and M. J. Buehler, Soft Matter **10**, 457 (2014).

[32] S. M. Kang, S. Park, D. Kim, S. Y. Park, R. S. Ruoff, and H. Lee, Adv. Funct. Mater. **21**, 108 (2011).

[33] P. Fratzl, J. R. Soc. Interface **4**, 637 (2007).

[34] S. Keten and M. J. Buehler, Nano Lett. **8**, 743 (2008).

[35] S. Keten, Z. Xu, B. Ihle, and M. J. Buehler, Nature Mater. **9**, 359 (2010).

[36] M. A. Hartmann and P. Fratzl, Nano Lett. **9**, 3603 (2009).

[37] A. E. Elbanna and J. M. Carlson, PLOS one **8**, e56118 (2013).

[38] C. K. C. Lieou, A. E. Elbanna, and J. M. Carlson, Phys. Rev. E **88**, 012703 (2013).

[39] S. S. Nabavi, M. J. Harrington, O. Paris, P. Fratzl, and M. A. Hartmann, New J. Phys. **16**, 013003 (2014).

[40] D. Landau and K. Binder, *A Guide to Monte Carlo Simulations in Statistical Physics* (Cambridge University Press, 2009).

[41] F. Manca, S. Giordano, P. L. Palla, R. Zucca, F. Cleri, and L. Colombo, J. Chem. Phys. **136**, 154906 (2012).

[42] J. F. Marko and E. D. Siggia, Macromolecules **28**, 8759 (1995).

[43] C. Ortiz and G. Hadziioannou, Macromolecules **32**, 780 (1999).

[44] T. Gutsmann, T. Hassenkam, J. A. Cutroni, and P. K. Hansma, Biophys. J. **89**, 536 (2005).

[45] D. E. Makarov and G. J. Rodin, Phys. Rev. E **66**, 011908 (2002).

[46] G. E. Fantner, E. Oroudjev, G. Schitter, L. S. Golde, P. Thurner, M. M. Finch, P. Turner, T. Gutsmann, D. E. Morse, H. Hansma, et al., Biophys. J. **90**, 1411 (2006).

[47] S. S. Nabavi, M. J. Harrington, P. Fratzl, and M. A. Hartmann, Bioinspired, Biomimetic and Nanobiomaterials **3**, 139 (2014).

[48] H. Lee, N. F. Scherer, and P. B. Messersmith, Proc. Natl. Acad. Sci. USA **103**, 12999 (2006).

[49] M. Rief, M. Gautel, F. Oesterhelt, J. M. Fernandez, and H. E. Gaub, Science **276**, 1109 (1997).

[50] A. F. Oberhauser, P. E. Marszalek, H. P. Erickson, and J. M. Fernandez, Nature **393**, 181 (1998).

[51] T. E. Fisher, P. E. Marszalek, and J. M. Fernandez, Nat. Struct. Biol. **7**, 719 (2000).

[52] T. M. Dugdale, R. Dagastine, A. Chiovitti, P. Mulvaney, and R. Wetherbee, Biophys. J. **89**, 4252 (2005).

[53] T. M. Dugdale, R. Dagastine, A. Chiovitti, and R. Wetherbee, Biophys. J. **90**, 2987 (2006).

[54] M. J. Harrington and J. H. Waite, *Fibrous Proteins* (Landes Bioscience, 2008), chap. Short-Order Tendons: Liquid Crystal Mesophases, Metal-Complexation and Protein Gradients in the Externalized Collagens of Mussel Byssal Threads, p. 30.

[55] S. L. Brazee and E. Carrington, Biol. Bull. **211**, 263 (2006).

[56] M. J. Harrington and J. H. Waite, J. Exp. Biol. **210**, 4307 (2007).

[57] N. Holten-Andersen, M. J. Harrington, H. Birkedal, B. P. Lee, P. B. Messersmith, K. Y. C. Lee, and J. H. Waite, Proc. Natl. Acad. Sci. USA **108**, 2651 (2011).

[58] M. Krogsgaard, M. A. Behrens, J. S. Pedersen, and H. Birkedal, Biomacromolecules **14**, 297 (2013).

[59] K. Eom, D. E. Makarov, and G. J. Rodin, PHYSICAL REVIEW E **71**, 021904 (2005).

[60] S. Krauss, T. H. Metzger, P. Fratzl, and M. J. Harrington, Biomacromolecules **14**, 1520 (2013).

[61] D. T. Seaton, S. Schnabel, D. P. Landau, and M. Bachmann, Phys. Rev. Lett. **110**, 028103 (2013).

[62] K. Eom, P.-C. Li, D. E. Makarov, and G. J. Rodin, J. Phys. Chem. B **107**, 8730 (2003).

11 Acknowledgment

I am using this opportunity to express my gratitude to everyone who supported me throughout the three years that I spend for my PhD.

First of all, I would like to express my sincere gratitude to my supervisor Prof. Oskar Paris giving me the opportunity to join his research group. I am very grateful for his scientific advices and many insightful discussions and suggestions. I am pretty sure, a better boss and group leader can hardly be found.

I would like to express my special appreciation and thanks to my friendly boss Dr. Markus Hartmann. Markus has been a tremendous advisor for me. It has been an honor to be his first PhD student. I appreciate all his contributions of time, ideas, and funding to make my Ph.D experience productive. Without leading and helping of him writing this thesis would not be possible. I had a great time with Markus also as a friend, going out for launch and speaking about daily life. Definitely his sweet little daughter, Judith, will be proud of him.

I am deeply grateful to Prof. Peter Fratzl and Dr. Matthew J. Harrington from department of Biomaterials in Max-Planck-Institute of Colloids and interfaces in Potsdam for the many insightful discussions and great collaboration.

Working in such a group with friendly environment made a fruitful period of my life. I am deeply thankful for all my colleagues in the group, Dr. Rainer Lechner, Dr. Gerhard Popovski, Christian Prehal and Roland Morak for all great times we had. Needless to say I want to thank Dr. Parvin Sharifi and Dr. Maxim Erko which were helping me a lot during their stay in Leoben.

I also want to thank the entire institute of Physics including Prof. Oswald, Prof. Meisels and the colleagues from the working group of Prof. Teichert. I would like to thank also Heinz Pirker for the technical support. I am grateful for the secretary office Magdalena Ottrin and specially Heide Kirchberger for their helps and specially Frau Kirchberger who always motivated me to talk in German.

A special thanks to my family. Words cannot express how grateful I am to my parents for all of the sacrifices that you have made on my behalf. I also want to thank my beloved wife, Shirin, who was my greatest support and tried to make things easier for me during the stay in Austria.

Thank you very much

Curriculum Vitae

Personal data

Name: Seyed Soran Nabavi
Date of birth: 14 May 1981
Place of birth: Mahabad, Iran

Academic Qualifications

1999-2004	Bachelor of Science in Physics, Urmia University, Urmia- Iran
2004- 2007	Master of Physics, K.N.Toosi University of Technology, Tehran- Iran
Master Thesis	Electrical and magnetic properties of Gd-Bi intermetallic compounds
Oct. 2011- present	Ph.D. student, Montanuniversität Leoben, Leoben- Austria

Attended Conferences and workshops

March 2014	Oral Presentation- DPG Spring Meeting, Dresden-Germany
March 2014	Oral Presentation- Bio-inspired Materials, Potsdam-Germany
November 2013	Oral Presentation- Werkstoffkongress, Leoben-Austria
September 2013	Poster Presentation-Annual Meeting ÖPG, Linz-Austria
March 2013	Oral Presentation- DPG Spring Meeting, Regensburg-Germany
September 2012	Poster Presentation- Annual Meeting ÖPG, Graz-Austria
June 2012	Materiomics workshop; CISM course, Udine-Italy
March 2012	Poster Presentation- Bio-inspired Materials, Potsdam-Germany
February 2007	Poster Presentation- 8th Annual Iranian condensed matter physics conference, Mashhad-Iran
August 2006	Poster Presentation- 11th Annual Iranian physics conference, Shahrud-Iran

Teaching Experience

Montanuniversität Leoben (2012-2013)	Exercises for Physics I
Dadeh Pardazi && Rahyaft A.S.Uni. (2008-2011)	Electromagnetism Physics and Lab.
Imam Ali Uni. (2008-2011)	General Physics and Lab. (Military service)
Pakdasht P.N.Uni. (2008-2010)	Foundation of Electromagnetic Theory && Mathematical Methods for Physicists
K.N.Toosi Uni. (2006-2008)	TA for the course of Electromagnetism Physics